DEVELOPMENT OF 3D TISSUE-ENGINEERED LARYNX USING NANOCOMPOSITE POSS-PCU MATERIAL AND STEM CELLS

Thesis submitted for the degree of Doctor of Philosophy (Ph.D.) by

Mr. Poramate Klanrit

Centre for Nanotechnology & Regenerative Medicine

Division of Surgery and Interventional Science

University College London

May 2016

Declaration

I hereby, certify that the work presented in this thesis is the result of my own investigations carried out at the Centre for Nanotechnology and Regenerative Medicine at University College London and the Royal Free during the period of 2011-2015. Where information has been derived from other sources, I confirm that this has been indicated in the thesis.

Poramate Klanrit

May 2016

Acknowledgements

I would like to express my honest gratitude to my supervisory team, Dr. Brian G. Cousins, Professor Martin Birchall, and Professor Alexander M. Seifalian for their wonderful guidance and kind support throughout my incredible journey. You have been an inspiration and I cannot thank you enough for your patience and encouragement.

I would also like to acknowledge the following persons:

- Mr Arnold Darbyshire for teaching me everything about polymer chemistry
- Dr. Bala Ramesh for teaching me all the essentials on confocal microscope
- Mr Gary Wood for his kind support on all the voice analysis
- Dr. Achala De Mel for guiding me on the basis of epithelial cell culture

I wish to acknowledge the Royal Thai Government Scholarship for their financial contributions throughout my PhD study.

My love and gratitude also goes out to each of my friends and colleagues at Division of Surgery and Interventional Science, especially Claire Crowley, Peggy Lange, Carla Carvalho, Maria Menikou, Stephanie Bogan, Samar Hamad, Victor Lopez-Davila, Lara Yildimir, Ryan Dee, Guizhen Teoh, Safaa Fallatah, Weiguang Loh, Rhea Saksena, Wai I Ho, Jun Hong Pang, Li Yutong, and Linxiao Wu for your cares, supports and making my Ph.D. an unforgettable experience.

Most of all, I would like to thank my grandmother, Lumyai, my parents, Manot and Prayong and my sisters, Poramaporn and Preekamol for their endless love and supports. You are my fundamental pillars and the also the wind beneath my wings. Without you, I wouldn't have achieved my goals and dreams.

Abstracts

Background: Loss of laryngeal function severely affects the quality of life. To date, there are no optimised implants for laryngeal replacement or reconstruction; hence, it is still considered an unmet clinical need. The aim of this research is to develop a 3D scaffold made from POSS-PCU materials. This scaffold could then be assessed the biocompatibility with human primary bronchial epithelial cells (HBEC) and bone-marrow mesenchymal stem cells (BM-MSC) to produce tissue-engineered artificial larynx.

Methods: 3D laryngeal scaffolds were fabricated from polyhedral oligomeric silsesquioxane – poly(carbonate-urea)urethane (POSS-PCU). The scaffolds were designed to be microporous with sodium bicarbonate ($NaHCO_3$) particle size of 25 - 40 μm at different concentrations. This procedure created an interconnected microporous network and can be coated on the outer surface of casted POSS-PCU to create the 3D laryngeal frameworks. The materials were fully characterised and optimised for biocompatibility and voice function. HBEC and BM-MSC were seeded onto scaffolds and observed the viability as well as the characteristics after differentiation on the material such as morphology, and specific protein expressions via staining.

Results: Comparison studies of mechanical strength showed no significant difference between porcine epithelial tissue and microporous POSS-PCU ($P > 0.05$), while the mechanical strength of the non-porous POSS-PCU was higher than the microporous samples and native epithelial tissue and cartilage ($P < 0.05$). The microporous POSS-PCU also responded to the air flow and generated the oscillating sound wave with the energy and fundamental frequency similar to the human range. Wettability analysis demonstrated the significant reduction in contact angle (θ^o) of the material after ethanol rinse ($P < 0.05$) which was similar to the commercial tissue-culture treated plastics (74°±3.32, $P > 0.05$). The

material also showed the significant protein adsorption and enhanced cell attachment and growth in all samples with ethanol rinse. Primary HBEC and BM-MSC had significant growth on 3D porous scaffolds over 14 days ($P < 0.05$). Furthermore, the scaffold supported the differentiation of primary HBECs using air-liquid interface culture to develop mature epithelial cells with pseudostratified layer and migration into the POSS-PCU materials. SEM and immunofluorescence staining revealed the specific epithelial characteristics which were keratin 5 in the basal layer, keratin 18 on the top layer, epithelial tight junction, ciliated cells and mucin5AC production. BM-MSC also presented the growth and the differentiation on the material. Chondrogenic lineage properties had been observed through the change in cell morphology and the increased production of cartilaginous-like ECM such as sulphated-glycosaminoglycan (sGAG) and collagen.

Conclusion: It had been demonstrated that the 3D scaffold made from POSS-PCU promotes cell adhesion, proliferation and differentiation with mature epithelial features as well as chondrogenic properties. This scaffold holds great promise to develop a tissue-engineer-based larynx for laryngotracheal replacements.

Table of contents

List of figures

List of tables

List of abbreviations

Ø	Diameter
θ	Contact angle
µL	microliter
µm	micrometre
AC-tubulin	Acetylated alpha-tubulin
AFM	Atomic force microscopy
ALI	Air-liquid interphase culture
BCA assay	Bicinchoninic acid assay
BEpiCM	Bronchial epithelial cell culture medium
BM-MSC	Bone marrow-derived mesenchymal stem cell
BSA	Bovine Serum Albumins
DNA	Deoxyribonucleic acid
Em	Emission
EtOH	Ethanol
Ex	Excitation
FBS	Foetal bovine serum
GAG	Glycosaminoglycans
GF	Growth factors
h	hour
HBEC	Human bronchial epithelial cell
H&E	haematoxylin and eosin staining
Hz	Hertz
M70% $NaHCO_3$	Modified 70% sodium bicarbonate
MCDM	Mesenchymal stemm cell chondrogenic differentiation medium

min	minute
mL	millilitre
MSCM	Messenchymal stem cell culture medium
N	sample number
$NaHCO_3$	Sodium bicarbonate
nm	nanometre
NS, ns	Non-significant
P	*P*-value
PBS	Phosphate buffer saline
PFA	Paraformaldehyde
POSS-PCU	Polyoligomeric silesquioxane poly-(carbonate)urea urethane
P/S	Penicillin and streptomycin
PU	Polyurethane
sec	second
SEM	Scanning electron microscopy
sGAG	Sulfated glycosaminoglycans
TCP	Tissue culture polystyrene
TGF-β3	Transforming growth factor β3
w/w	weight by weight
w/v	weight by volume
v/v	volume by volume
VFFs	Vocal fold fibroblast

Chapter 1 Introduction

Currently, there is no ideal surgical or prosthetic solution for patients with the irreversible laryngeal disease. Total laryngectomy is still the most common surgical option available for serious trauma which negatively impacts the patient's quality of life[1,2]. The impacts were not so much because of the loss of voice and speech capabilities, but rather the exposed tracheostomy, that influences social consequences and quality of life[3–5]. The most significant impacts are the change of patient's self-image, a deteriorated relationship with their partners, reduced sexuality, and increased social isolation[2]. Moreover, some reports conclude that a tracheostomy has a destructive influence on postoperative modification and it may have more impact on quality of life than loss of voice[6]. To date, laryngectomy is the only possible therapeutic option available for patients with advanced laryngeal trauma[7].

The treatment for patients with total laryngectomies has not been changed for decades. Laryngeal replacement with donor's organ was done successfully. However, the risk of chronically immunogenic rejection may present later on[8,9]. Many approaches are employed to develop substitute materials to improve the treatment, especially the biomaterial manufacture and tissue engineering. Because the architecture of the larynx is complicated, which consists of epithelium, muscles and cartilages as a framework, the main issue is how to construct the larynx with the bioartificial 3D structures with low immunogenicity[10]. Thus, the development of total laryngeal replacement devices is aiming at the functional prosthesis with tissue regeneration, and the considerable increasing quality of life of patients.

1.1 Anatomy and the physiology of the larynx

The human respiratory system lines across the digestive tract in the area known as the pharynx. By sharing a common passageway with the upper digestive system, the larynx serves three importantly major functions, 1) respiration, 2) protection and 3) phonation[11–13]. The larynx connects to the upper (pharynx and nose) and lower airways (trachea and lungs) essential for respiration. The protective mechanism is initiated when the larynx is elevated, and the flap-like epiglottis closes the airway, which results in food travelling into the oesophagus during swallowing. The larynx also provides the basic phonatory sounds upon the adduction of the vocal cords. When the air passes from the lungs to the pharynx, the vocal folds consequently move together to close the glottis (adduction) and cause the rise in subglottic pressure that push the vocal folds to vibrate. This cycle is repeated to produce vibrations and hence a multitude of different sound frequencies[14–16].

The larynx (Figure 1.1) is composed of cartilaginous structures that protect the glottis, which is the small opening that lets in the air as it passes through in to the lungs. The structure is divided into three unpaired cartilage tissues; namely, the thyroid cartilage, cricoid cartilage and epiglottis, which forms the structure of the lateral wall of the larynx. It also consists of smaller paired cartilage structures namely the arytenoid, corniculate and cuneiform cartilages. The smaller cartilages together with the ligaments mostly involve the opening and closure of the vocal folds. The biomechanical properties of the vocal folds depend on its unique layers of squamous epithelium, the lamina propria and the vocalis muscle[17]. The superficial layer of lamina propria combined with epithelium is also known as the mucosa. The lamina propria is composed of extracellular components, which consist of elastic and collagen fibres, glycosaminoglycans, glycoproteins, minerals and water[17,18].

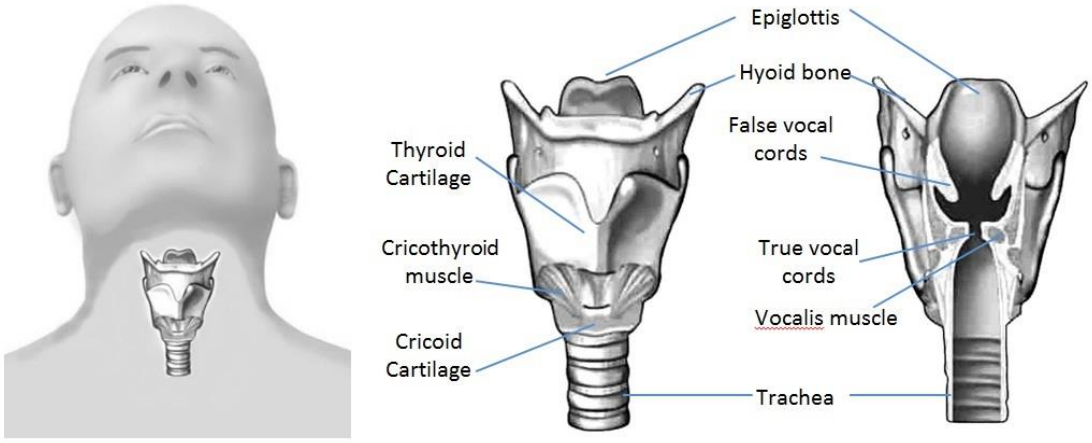

Figure 1.1 Anatomy of human larynx, showing the structure of cartilage, muscle, and vocal cords.

1.2 Laryngeal diseases and treatment

Many stimuli can lead to the larynx malfunction and damage, including excessive mechanical stress, smoke inhalation, vital accidents and cancers[19]. The larynx is the second most common site for head and neck cancer which is globally the sixth most common cancer[20,21]. In 2008, an estimated 635,000 new patients with head and neck cancers were diagnosed, including 47,500 cases in the United States and 95,500 in Europe[22]. In 2012, 13,510 new cases of pharyngeal cancer and 12,360 new cases of laryngeal cancer were diagnosed in the United States (http://www.cancer.gov).

Total Laryngectomy is the surgical procedure of removing the larynx and separating the airway from the mouth, nose and oesophagus, and still plays an important role in primary therapy for advanced stage laryngeal cancer[23]. Subsequently, the laryngectomee will breathe through an opening in the neck known as a stoma[24]. This procedure is usually performed in cases of laryngeal cancer and also on individuals with other types of head and neck cancer[25].

Apart from laryngeal damage, the congenital disorder is one of the reasons that require later laryngeal reconstruction. Most of the cases could be treated with microsurgery; however, in some cases require the material postoperatively to maintain or reconstruct the laryngotracheal cavity[26]. Reports have shown patients with laryngotracheal stenoses went through the laser surgery[27] and were usually reconstructed and dilated their airways with Montgomery silicone tube[28]. Recently, advanced materials have played an important role and pave the way for the development of laryngotracheal replacements in the clinic, especially for the case that has high complications. These include stem-cell-based decellularised tissues[29], stem-cell-seeded nanocomposite POSS-PCU[30], Marlex-mesh tube coated with collagen sponge[31], and titanium tube with solid and porous parts[2]. The objectives of these developed materials are using the regenerative medicine approach to improving the efficacy and sustainable healing with restoration of organ's function.

1.3 Regenerative medicine approaches for laryngotracheal applications

Regenerative medicine is currently the research field combining tissue engineering and stem cells to create improved personalised treatment for patients. The immense progress of these studies is advanced and some of them have gone to clinical trials. The two main fields being developed for laryngotracheal tissue engineering application include biomaterials, act as a scaffold for tissue regeneration, and stem cell mediation, for improved tissue regeneration and wound healing process. The concept for laryngotracheal regenerative medicine is shown in **Figure 1.2**.

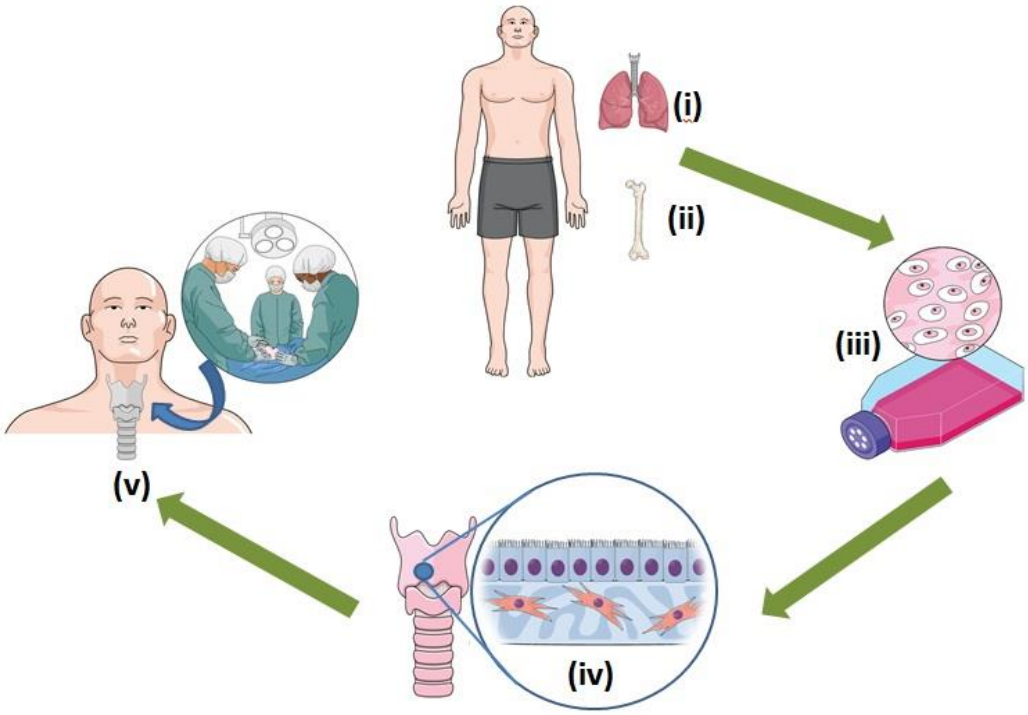

Figure 1.2 A schematic shows laryngotracheal regenerative medicine concept. The primary bronchial epithelial cells (i) and stem cells, e.g., BM-MSCs (ii) are extracted from the patient. Cells are expanded with induced growth supplement in a laboratory (iii). Cells are seeded onto biomaterial scaffold (iv), and the cell-scaffold construct is implanted back to the patient with functionality (v).

1.3.1 Biomaterials for tissue engineering

In recent years, there has been the considerable progress of research based on tissue-engineering approach including finding new materials, incorporation of growth factors, and particular cell seeding, to enhance the survival of the graft. Regarding the materials, they are usually divided into two types, natural-derived scaffolds (i.e., autologous, allogeneic, or xenogeneic donor tissue source) and synthetic scaffolds (i.e., metal or plastic polymer). Much debate surrounds whether to use natural- derived scaffolds, which aim to preserve the major components of the extracellular matrix (ECM) through a process known as decellularisation, or synthetic scaffolds which are easier to control the manufacture. The main differences between natural and synthetic scaffolds are summarised in **Table 1.1**.

Table 1.1 Differences between natural and synthetic scaffolds for laryngotracheal applications, published by Fishman, *et al*[32].

Natural	Synthetic
Biological scaffolds composed of ECM, mimics native tissue and can accommodate cell growth	Artificial material
Contain donor antigens: decellularisation makes them non-immunogenic	More likely to cause a foreign body reaction when implanted into the body
Better biocompatibility	Biocompatibility depends on material
Excellent tissue microarchitecture	Microarchitecture does not resemble tissue it is being used to replace
Excellent bioactivity if ECM components and growth factors preserved	Bioactivity depends on material
Preserved microvasculature	Absent vasculature
Less control over biodegradation properties	Biodegradation and porosity can be controlled to some extent
Biomecahnical properties depend on material	Biomechanical properties can be controlled
Possibility of microbial contamination during preparation and storage	Contamination less likely
Requires times for harvesting and preparation (weeks). Supply depends on donor tissue availability	Off-the-shelf availability
Cheaper to manufacture	More expensive to manufacture

1.3.1.1 Natural-derived scaffolds

In recent years, decellularised tissues obtained with the detergent-enzymatic method, have increased the evidence that they are non-immunogenic, and can be used as scaffolds to promote *in vivo* in-growth of host cells and tissue[33,34]. Scaffolds derived from decellualrised tissues have been used successfully in both pre-clinical animal studies and human clinical trials, without the formation of anti-HLA antibodies[35–37].

The donated tissues are usually degraded by cellular enzymatic activity through proteolysis, hence releasing growth factors and peptides that could stimulate constructive tissue remodelling are now in great demand[7]. These proteins serve many functions, namely structural supports, development of angiogenesis and vascularisation, cell migration, proliferation and subsequent tissue growth[38].

Natural ECM from donor tissues can be processed using surfactants and enzyme degradation steps that get rid of native cells, and antigens to leave 3D scaffolds composed of

natural ECM tissue for new cell growth and create adequate compatibility, and a minimal tissue response with the recipients' host immune system. The material could be obtained from various sources, such as decellularised autogenic, allergenic or xenogenic grafts. Porcine urinary-bladder submucosa-layer was used as decellularised ECM for laryngeal reconstruction in canine models[39]. The vocal cords were removed and thyroid cartilage was replaced with urinary bladder submucosa ECM, and presented a simple squamous epithelial lining, organised glandular structure within the submucosa and thyroid cartilage and bundles of skeletal muscle three months after surgery.

An acellular xenogenic ECM substitution was developed using the vocal fold lamina propria from bovine sources and seeded with human vocal fold fibroblasts to examine the biochemical properties and biocompatibility[40]. The results showed that the scaffold was repopulated with cells with greatly improved biomechanical properties of the 3D structure and production of active proteins such as hyaluronic acid and decorin. Further research was carried out in a rat model using the same material[41]. The results demonstrated significant cellular infiltration into the scaffold following implantation in the acute stages of wound repair (day 3 to 10 post surgery). Also, the key ECM proteins were higher in the acute stage than those of the controls, indicating ECM remodelling by the host fibroblasts. However, the implanted scaffolds were found to be completely degraded by Month 3. Moreover, a whole laryngeal allograft was also performed in rabbits in 2011[42]. The larynges connected to the upper part of trachea was removed and perfused with enzymatic reagents through the carotid arteries. The larynges were then recellularised with mesenchymal stem cells (MSCs) from bone marrow from rabbits and implanted in the greater omentum. After 8 weeks of implantation, the recellularised larynx was dissected and the laryngeal framework remained intact and well integrated with muscle tissue and vascularisation was also apparent.

The potential replacement by decellularised larynx has become feasible when human cadaveric larynges were used in decellularisation of 25 consecutive cycles of the detergent-enzymatic method (DEM)[7]. The study revealed the success of decellularisation removing all cells, nuclear debris and materials from the ECM. The procedure preserved not only ECM structural components necessary for cell proliferation, but also ECM proteins that have an impact on angiogenesis. Although natural scaffolds tend to facilitate tissue repair, the method of its preparation can dramatically alter the biomechanical properties of the resulting scaffold, compromising its ability to provide mechanical support during the remodelling process, as well as, affecting the host remodelling response of the tissues.

Long-segment congenital tracheal stenosis and pulmonary sling in a 12-year-old boy had been replaced with a decellularised cadaveric donor tracheal scaffold seeded with BM-MSCs and patches of autologous epithelium[43]. The graft vascularised within 1 week after surgery but the cytological indication of epithelium restoration did not present until 1 year. The graft did not have mechanical strength focally until 18 months; however, the patient did not need any further medical intervention. Eighteen months after surgery, he had a regular chest CT scan and ventilation-perfusion scan. At 2 years follow-up, he had a functional airway and had returned to school.

1.3.1.2 Synthetic scaffolds

Several synthetic scaffolds have been investigated for larynx reconstruction over the past decade. The following are examples of scaffolds made of effective materials developed so far, which have been mainly applied to pre-clinical studies. A clinical challenge has remained in the development of the materials with few reliable options available. Laryngotracheal treatments have been focused on injectable fillers, implantable 3D

materials, or cell therapy with the aim of restoring the normal biomechanical function of the organ[44].

1.3.1.2.1 Hydrogels

The lamina propria of vocal folds is a multi-layered connective tissue, which is mainly composed of fibroblasts, and their ECM structures containing elastin, collagen, hyaluronic acid, and proteoglycans[45]. When the composition of ECM of the lamina propria changed, the vocal fold vibratory function can be severely impaired and interrupted due to modifications in tissue viscoelasticity[46]. Hydrogels have become promising materials to treat specific symptoms like vocal fold scar and fibrosis since the materials are known to influence cell-cell and cell-matrix interactions[47]. Human vocal fold fibroblasts (VFFs) encapsulated within the hydrogel matrices expressed genes related to several ECM proteins[19]. Biocompatibility was evaluated in human VFFs cultured in 3D Carbylan GSX (A disulphide cross-linked hydrogel of hyaluronan and gelatin, used as an extracellular matrix), and was compared with commercially available Matrigel™ (Corning, Massachusetts, USA). There was no significant difference regarding viability, and marker protein expression of human VFFs cultured with Carbylan GSX compared to Matrigel™ after 1 week. Also, cytokine IL6 and IL8, ECM (COL1) and hyaluronic acid synthase 3 gene expression levels decreased when cultured in Carbylan GSX demonstrating that Carbylan GSX may be suitable for tissue engineering and reconstruction of human vocal folds[46]. Five different hydrogels (hyaluronic acid, collagen, fibrin, and co-hydrogels composed of fibrin-collagen and fibrin-HA) were used under defined experiment conditions, which controlled the differentiation of adipose-derived stem cells into the functional equivalent of VFFs. The cells cultured in the co-hydrogels show stellate and elongated morphology, expressed decorin and elastin and produced glycosaminoglycan, thus enhancing

proliferation, differentiation and gene expression[48]. Thibeault *et al*. studied the utilisation of injectable hyaluronan hydrogels via vocal fold injection against normal saline as controls in a rabbit model in 2011, and found the treated vocal folds were found to be significantly less fibrotic than the saline controls with significantly improved viscosity and tissue elasticity[49].

1.3.1.2.2 Collagen coated polypropylene mesh

Collagen coated polypropylene mesh has been used for laryngeal and tracheal reconstruction and tissue engineering applications in 2004[50]. Polypropylene mesh (Marlex™) was employed as a 3D scaffold or framework for larynx, which was coated with collagen type I and III and cross-linked to the surface before implantation *in vivo*[50] or human patients[51]. The collagen scaffold was further investigated by culturing with bone-marrow stromal cells (BMSCs). The material was found to support cell growth, adhesion and proliferation. The cell surface markers for mesodermal tissue were also positively identified[52]. In a canine model, regeneration of the epithelium and sub-epithelial tissue was also apparent[53], and also, the incorporation of the fascia lata by the wrapping of the scaffold around the defect was found to repair the tissue and reduce infection. In 2012, this material was used to create a prosthesis for cricoid repair and regeneration. The collagen scaffold incorporated fibroblasts to regenerate the tissue and enhance wound healing. It was found that after 14 days of implantation, epithelialisation and cartilage formation was observed throughout the scaffold[54].

1.3.1.2.3 Porous titanium

Most attempts to reconstruct an artificial trachea have hardly accomplished long-term success[55]. Tissue integration as a result of the biomaterial itself and mechanical properties[56] were the main difficulties caused the rejection of the prosthesis. Titanium is a

metal known to be chemically resistant to the corrosive and oxidative activity of various agents[57]. These characteristics make titanium a widely used metal for implants, and especially in odontology[58].

Porous titanium was also developed and used as an artificial tracheal prosthesis for short-term study in rats[59]. Eleven of seventeen animals were survived throughout the experiment and the histologic analysis revealed fibroblast colonisation in titanium pores, a ciliary cylindrical epithelial layer developed on the luminal side of the prosthesis, and the inflammatory reaction was minimal[59]. Another study with the same material in mice and rabbits also showed the regeneration of mucosa with the submucosal layer on top of the titanium, multiple blood vessels extending from the muscle layer through the titanium, and expression of cytokeratin in the basal layer of the mucosal epithelium[60]. This porous titanium was also included in the design of artificial titanium larynx used in the clinical trial, with the aim of assisting the integration of patient's proximal trachea[2].

1.3.1.2.4 POSS-PCU nanocomposite material

A novel nanocomposite material has been developed at the Centre for Nanotechnology and Regenerative Medicine, University College London. POSS-PCU is a hybrid co-polymer, consisting of a crystalline hard segment and soft elastomeric segments in which polyhedral oligomeric silsesquioxanes (POSS) nanoparticles are attached as pendant chain functional groups to the backbone of poly(carbonate-urea) urethane (PCU)[61]. The POSS nanoparticle is one of the most promising nanomaterials for medical applications[62],[63,64], consisting of a nanocage structure with an inner silicon frameworks and oxygen atoms, and the outer part of organic functional groups.

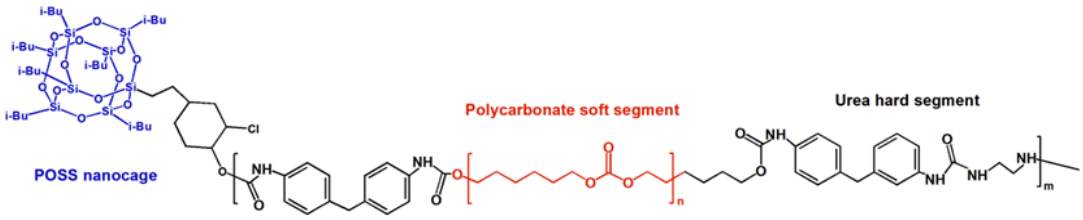

Figure 1.3 Schematic diagram of POSS-PCU molecular structure. The POSS nanocage with the size approximately of 1.5 nm with an inner silicon and oxygen frameworks, externally covered by organic functional groups, which are covalently bonded to PCU. The incorporation of POSS into PCU has resulted in an advanced nanocomposite polymer with unique characteristics for larynx applications. I-Bu=R, Isobutyl tertiary groups.

The addition of the POSS-nanocage to the PCU backbone has caused an improvement in the construct's overall resistance to oxidative degradation when compared to PCU alone, as demonstrated in a previous study where POSS-PCU was exposed to in vitro accelerate degradation[65]. The POSS nanoparticle was shown to enhance the PCU's mechanical strength while maintaining its elasticity, making it ideal for use in vascular prostheses, particularly at low flow states[65],[66],[67].

POSS-PCU has been demonstrated to possess superior mechanical and viscoelastic behaviour compared to conventional polyurethane-based (PU) polymers and the heterograft tissues. It has shown a comparable hardness and tear strength to commercially available polymers such as Estane®, Chronoflex C®, and Elasteon™[68]. POSS-PCU has been used to develop surgical implants following extensive *in vitro* and *in vivo* studies to show enhanced degradation resistance[65], *in vivo* biocompatibility, and biological stability over a 3 year period in an ovine model[69]. POSS-PCU is currently undergoing pre-clinical studies as heart valve replacements[68] and has been used for first-in-man studies as compassionate cases as a lower limb bypass graft[70] and lachrymal duct conduit[71]. The material was

used to develop the first synthetic trachea by incorporating the patient's own stem cells and implanted successfully into a patient suffering from cancer[30].

Table 1.2 Summary of materials being developed for laryngotracheal reconstruction

Year	Material	Method	Experiment	Outcome	Reference
2012	Decellualised trachea	The trachea was using detergent-enzymetic method (DEM) previously published[72].	Clinical trial	The graft revascularised with epithelial restoration after 1 year. The mechanical strength of the graft did not present until 18 months, but the patient did not need any medical intervention since then. Eighteen months after the operation, he had a normal chest CT scan and ventilation-perfusion ratio. At 2 years follow-up, he had a functional airway.	Elliott et al.[43]
2011	Decellularised larynx	Larynges were decellularised with a total of 25 consecutive DEM cycles.	*In vitro*	Decellularisation procedure preserved not only ECM structural component necessary for cell proliferation but also ECM proteins that have an impact on angiogenesis.	Baiguera et al.[7]
2011	Decellularised larynx	Perfusion-decellularised larynges were obtained from 20 rabbits by perfusion of the carotid arteries with decellularised solution. The larynges were seeded with myogenic-induced MSCs from eight receptor rabbits. The constructs were implanted into greater omentums of receptor rabbits after cell adherence *in vitro*.	Rabbit	Larynges perfused by sodium dodecyl sulphate became clear after 2 h of perfusion. Histology and SEM indicated almost no intact cells or nuclei were found while pores and collagen fibres were maintained in the decellularised matrix. Vascularization was clearly seen after 4 weeks and integrated cartilage frameworks remained by 8 weeks. Histological and immunohistochemical revealed muscles and vessels.	Hou et al.[42]
2010	Decellularised bovine vocal fold lamina propria	Decellularised bovine lamina propria scaffold	Rat	After implantation of the acellular scaffold, the remodelling process occurred during the wound healing. Collagen I, Collagen III and glycosaminoglycans was significantly higher than those of the control after 3 days. Scaffold was degraded by 3 months with no fibrotic tissue formation or calcification.	Xu et al.[41]
2007	Decellularised bovine vocal fold lamina propria	Human vocal fold fibroblast seeded in decellularised bovine lamina propria scaffold	*In vitro*	Bovine vocal fold lamina propria can utilized as a biodegradable scaffold via decellularisation. Human vocal fold fibroblast demonstrated well attachment to the scaffold, biocompatibility, and active protein synthesis, especially hyaluronic acid and decorin.	Xu et al.[40]
2003	Porcine-urinary bladder submucosa ECM	Canine hemilaryngectomy – vocalfold was replaced with 1 sheet UBS-ECM - 4 sheet and 8-sheet fort hyroid cartilage in each study group.	Canine	Presence of a simple squamous epithelial lining, organized gradular structures within the submucosa, reconstructed thyroid cartilages and bundle of skeletal muscle by 3 months after surgery.	Huber et al.[39]

Year	Material	Method	Experiment	Outcome	Reference
2010	Hydrogels	Primary vocal fold fibroblast from porcine's larynx encapsulated in hydrogels	*In vitro*	The collagen HA composite hydrogels, when properly formulated, are attractive candidate for prolonged 3D culture for PVFF.	Farran et al.[19]
2010	Hydrogel – Carbylan GSX	Human vocal fold fibroblast (hVFF) seeded in transwell for 2D and 3D culture	*In vitro*	Carbylan GSX does not induce significant toxicity or inflammation. After 7 day-period, hVFFs were able to produce m-RNA for ECM constituents found in lmina propria tissue.	Chen et al.[46]
2010	Hydrogel	Human female adipose-derived stem cell (ASCs) embedded in hydrogels consisted of 1)Fibrin, 2)Collagen, 3)HA, 4)Fibrin-collagen or 5)fibrin-HA	*In vitro*	Cells grown in the co-gels showed preferable morphology, expressed Decorin, and synthesised glycosaminoglycan, which indicate differentiation of ASC. Cogels of HA or collagen with fibrin enhanced cell proliferation and differentiation.	Park et al.[48]
2010	Hydrogel	Isolated mouse bone-marrow messenchymal stemcell (BM-MSC) embedded in Extracel hydrogel, vocal fold injected	Mouse	BM-MSC grown in vitro within sECM expressed Sca-1, was positive for hyaluronan receptor CD44 and proliferated. Embedded BM-MSC in sECM presented an increase of pro-collagen III, fibronectin and TGF-β1, downregulated SMA, but upregulated HYAL3 and no change in HAS3.	Johnson et al.[73]
2011	Injectable Hyaluronan derivative (Extracel)	Inject directly to the vocal fold compared to saline	Rabbit	Vocal folds treated with Extracel significantly improve viscoelastic properties and healing with less fibrosis on ECM.	Thibeault et al.[74]
2009	Fibrin hydrogels	Human adipose-derived stem cells embedded in air-gel matrix in transwell with EGF 10ng/mL or FGF10ng/mL	*In vitro*	Cells survived, attached and populated three dimensional fibrin matrices. Epidermal Growth Factor and air interface were required to produce epithelial differentiation.	Long et al.[44]
2006	Collagen-alginate and collagen-hyaluronan (HA) hydrogel	Collagen-alginate and collagen-hyaluronan (HA) hydrogel seeded with pig vocal fold fibroblasts	*In vitro*	Collagen-alginate and collagen-HA hydrogel enhanced vocal fold fibroblasts to proliferate and synthesize GAG; however, collagen-alginate hydrogel was more stabilized and provided longer mass augmentation.	Hahn et al.[75]

Year	Material	Method	Experiment	Outcome	Reference
2010	Pre-clotted polypropylene mesh coated with collagen	Material was wrapped with autologous fascia lata	Canine	Favourable vocal fold contour was found in 4 of 5 cases. Histologic data revealed the regeneration of lined epithelium, subepithelial tissue and muscle structure in both groups.	Yamashita et al.[53]
2009	Terudermis, an atelocollagen sponge derived from calf dermis	Bone marrow-derived stromal cells were obtained from GFP (green fluorescent protein) mouse femurs. The cells were seeded into Terudermis and incubated for 5 days. Their survival, proliferation, and expression of extracellular matrix were examined.	*In vitro*	Bone marrow-derived stromal cells adhered to Terudermis and underwent significant proliferation. Immunohistochemistry demonstrated that cells were positive for vimentin, desmin, and fibronectin, and negative for beta III tubulin. These findings indicated that these cells were mesodermal cells and attached to the atelocollagen fibres biologically.	Ohno et al.[52]
2008	Marlex mesh tube covered by collagen sponge	*In situ* tissue engineering with a scaffold implant was applied to repair the larynx and trachea in 4 patients.	Clinical trial	A patient with subglottic stenosis and 3 patients with thyroid cancer and cricoid-tracheal tumour invasion were replaced with the scaffold implants. Postoperative endoscopy in a period of 8 to 34 months presented a well-epithelialised airway lumen without any obstruction.	Omori et al.[31]
2004	Marlex mesh tube coated by collagen sponge	Marlex mesh tube coated by collagen sponge was used for a rigid airway framework and for tissue regrowth around the tube.	Canine	By endoscopic investigation at 3 to 7 months, no airway obstruction was found in any of the dogs. There was a good confluent regeneration of the epithelium layer over the scaffold and incorporation of the scaffold mesh into the host tissue.	Omori et al.[50]
2014	Artificial larynx with porous titanium ring	The prosthesis was formed of 2 parts of a tracheal prosthesis with a porous titanium connected with the trachea, which was implanted in the first step to ensuring tissue integration and a removable part composed of valves that enable breathing. The implant was observed with a nasofibroscopy of the lumen and CT scans.	Clinical trial	The laryngeal function of the patient in the postoperative has significantly improved, such as breathing and swallowing. The patient was able to talk with a whispering voice while the tracheostomy was temporarily closed. The implant's porous part was colonised by the proximal tissue and no fistulas were found as evidenced by barium swallow.	Debry et al.[2]

Year	Material	Method	Experiment	Outcome	Reference
2009	Porous titanium	The defects were reconstructed with porous titanium implants and mucosa using a 2-step procedure. The implants were investigated on angiogenesis and mucosal survival.	Rabbit	All animals survived after the reconstruction. The titanium implants were integrated to the proximal tracheal cartilage and surrounding tissues, supporting the regeneration of the mucosa.	Janssen et al.[60]
2002	Porous titanium tracheal prosthesis	Seventeen rats had a partial tracheal reconstruction made of porous titanium. The histological analysis of the tissue was performed in 11 surviving animals.	Rat	Fibroblast colonisation into titanium pores and a ciliation of the cylindrical epithelial layer were observed on the endoluminal side of the graft. The inflammatory reaction of the rats was minimal.	Schultz et al.[59]
2011	POSS-PCU	A 36-year-old male patient presented a primary cancer of the distal trachea and main bronchi. After complete tumour resection, the airway was replaced with nanocomposite tracheal scaffold previously seeded with autologous bone-marrow mononuclear cells via a bioreactor for 36 h.	Clinical trial	After cell reseeding and bioreactor process, there was an extracellular matrix-like coating and proliferating cells with a CD105+ subpopulation. No major complications were observed and the patient no complicated symptom and tumour free 5 months after transplantation. The nanocomposite scaffold integrated to anastomosis, with a vascularised neomucosa. These findings suggest wound repair and neovascularisation of the graft.	Jungebluth et al.[30]
2009	POSS-PCU	The peptide was cross-linked to POSS-PCU material. The contact angle was analysed and specificity tests were performed with the peptide RAD. Progenitor cells were extracted from peripheral blood and cultured on the porous biofunctionalised material under static conditions.	*In vitro*	Endothelialization was confirmed by SEM and immunostaining for endothelial cell markers. Contact angle indicated that biofunctionalisation had increased the hydrophilicity of the nanocomposite polymer. Alamar Blue assay indicated cells on nanocomposite scaffold and the relative increase in cell viability was specific to RGD samples.	De Mel et al.[70]

1.3.2 Stem-cell-mediated therapy

Many types of reseach have currently paid attention towards the potential of stem cells for laryngotracheal applications. The main goals are usually for 1) assisting in the extracellular matrix (ECM) remodelling for vocal fold scar and fibrosis, and 2) differentiating stem cell to substitute the primary cell sources, e.g., epithelial cells, due to its limited expansion ability.

Vocal fold scarring demonstrates therapeutic challenges by using cell therapy with stem cells which have become a promising approach. Treatment of adipose-derived stem cells (ASC) and bone marrow-derived stem cells (BM-MSC) in rats showed improved ECM of the vocal fold with significantly increased hyaluronic acid (HA) and reduced dense collagen deposition in ASC and BM-MSC groups compared to sham controls up to 3 months after treatment[76]. Mechanosensitivity of MSC may also respond to the dynamic mechanical environment of the larynx. A vibratory-strain bioreactor and gene expression study (cDNA microarray) were used to investigate the similarity of ASC and BM-MSC to the native cell source (VFF). The results demonstrated that VFF shared more gene ontology (GO) terms related to epithelial differentiation, ECM remodelling, growth factor activity, and immune response with BM-MSC than with ASC. However, GO terms relating to differentiation toward osteogenic, adipogenic, and chondrogenic lineages were fewer and tended to lose osteogenic potential in the vibrated conditions compared to the non-vibrated one[77]. Treatment of vocal fold scarring in rats with the injection of BM-MSC in the sECM hydrogel (Glycosan BioSystems, Inc., Utah, USA) presented the positive outcomes in ECM production, hyaluronan metabolism, myofibroblast differentiation, and production of TGF-β1 with no detectable cytotoxicity[78].

Epithelial cells are crucial for airway lumen as they form the barrier, produce the mucus by Clara cells to trap pathogenic substance, and remove the mucus away by the harmonic waving of ciliated cells[79],[80]. Due to their limitations in isolation and expansion, induced

pluripotent stem cell (iPS), is the alternative researchers are interested with aiming to cope with these difficulties. Imaizumi *et al*. had shown human iPS cultivated on hydrogel with human VFFs or with EGF had significantly decreased levels of pluripotency marker (Oct 3/4). However, the epithelial-associated proteins (cytokeratin 13 and 14) expressed at 4 weeks after cultivation with a degree of nuclear polarity, suggested that cells had changed to the epithelial phenotype[81]. The method to generate functional human respiratory epithelial cells from human iPSCs has been well established by Firth *et al*. using multi-step differntiations[82]. The differentiated cells presented relevant gene expressions, protein expressions and phenotype of epithelial cells.This results can provide not only unlimited source of cells but also the opportunity for using the cells in disease modelling or tissue engineering, incorporation with biomaterial scaffolds.

1.4 Conclusion

Unmet clinical needs of organ transplantation and shortage of organ donors required the world to seek for the optional treatment for patients. Many biomaterials with patient's cell seeded are viable plans and had been widely in trials around the world to use in tissue reconstructions and organ replacements. Among them, the synthetic material has offered the potential in many ways to develop using tissue-engineering techniques; however, some issues still needs more investigation such as biocompatibility and long-term effect after implantation. POSS-PCU has been developed and studied on biocompatibility, *in vivo* implantation and a clinical trial in human for many applications such as bypass graft, lacrimal duct, and trachea. Over 10 years of extensive research on POSS-PCU material makes it a potential candidate to develop for laryngotracheal applications. The versatility of POSS-PCU fabrications make it useful in many ways, from making a 3D macro-scale of organ, to the interaction with cells in micro- and nano-scales. This has been the inspiration to use one material to serve different purposes by developing a 3D laryngeal scaffold to serve the transplantation of the total larynx with functionalisation including organ structure/stent,

voice production, and cellular mediation/regeneration. Also, the better epithelialisation and cartilage formation on the material might help the implant integrates to the proximal trachea with less chance of extrusion. Therefore, the aim of this thesis is to optimise and develop a manufacture of POSS-PCU 3D scaffold for laryngotracheal reconstruction with a focus on *in vitro* epithelialisation and chondrogenesis on the material.

Chapter 2 Aims of thesis

The complications of laryngotracheal reconstruction with both biologic and synthetic implants have previously been discussed. The important aim of this thesis is to design and develop a clinically feasible replacement that improves upon the current available laryngeal implants, which have not yet fully served laryngeal functions. Multiple challenges need to be overcome to assist the development of such an implant. The laryngeal implant should mimic the mechanical properties of the human larynx, be readily available (off-the-shelf). Moreover, the implant also needs to interact well with the surrounding tissue (epithelium or cartilage), promote tissue integration and angiogenesis, and heal the inflammatory effects. The hypothesis of this study is that the new nanocomposite biomaterial based on POSS-PCU can be used as an alternative for a synthetic implant for laryngeal reconstruction. To support this hypothesis POSS-PCU scaffold has been used in optimization of a 3D scaffold, and evaluated the capability to generate epithelialisation and chondrogenesis in vitro.

The work in this thesis can be broken down into a number of specific aims:

1. To design and develop personalised laryngeal scaffolds based on the POSS-PCU material.

- To create a novel custom-made thyroid shape scaffold
- To investigate the using of the solvent evaporation and phase inversion(coagulation)/particulate leaching techniques for 3D scaffold fabrication
- To evaluate the mechanical properties of the material, matching to the porcine larynx (for future in vivo work)
- To set up the test rig and examine the capability of microporous POSS-PCU material on air-flow induced voice

2. To characterise and optimise POSS-PCU material to provide the suitable environment for in vitro cell culture

- To evaluate the surface properties based on non-porous POSS-PCU material under different sterilisation technique
- To investigate the microenvironment of microporous POSS-PCUs at different porosities
- To study the protein adsorption pattern on microporous POSS-PCUs at different porosities using BSA as a model

3. To evaluate HBECs growth and differentiation on microporous POSS-PCUs

- To determine optimal protein level that enhances HBECs proliferative ability
- To compare HBECs growth on microporous POSS-PCUs at different porosities
- To differentiate HBECs on microporous POSS-PCUs at different porosities under ALI condition
- To evaluate the characteristic of differentiated epithelium including stratification, intercellular tight junction, mucin production and ciliation

4. To evaluate BM-MSCs growth and chondrogenic differentiation on microporous POSS-PCUs

- To compare BM-MSCs growth on microporous POSS-PCUs at different porosities
- To differentiate BM-MSCs on microporous POSS-PCUs at different porosities under chondrogenic differentiation condition
- To evaluate the characteristic of chondrogenic-like ECM and cell including sGAG and collagen

Chapter 3 General materials and methods

3.1 Synthesis and fabrication of POSS-PCU scaffold materials

3.1.1 Synthesis of POSS-PCU (Prep 9 formula)

The POSS-PCU was prepared and manufacturing controlled by laboratory technician (Mr Arnold Darbyshire). The procedures were described previously elsewhere in detail[83]. In brief, 76g of polycarbonate polyol (2000 mwt), and 2g of trans-cyclohexanechloroydrinisobutyl-silsesquioxane (POSS) (Hybrid plastics Inc, Mississippi, USA) were placed in a 500 mL reaction flask equipped with mechanical stirrer and nitrogen inlet. The mixture was heated to 135°C to dissolve the POSS cage into the polycarbonate polyol and then cooled to 70°C. 20g of Flake 4,4'-Methylenebis(phenyl isocyanate), (MDI), was added to the polyol blend and then reacted, under nitrogen, at 70°C - 80°C for 2 h to form a pre-polymer. Dimethylacetamide (DMAC) was added slowly to the pre-polymer to form a solution; the solution was cooled to 40°C. Chain extension of the pre-polymer was carried out by an addition of 2g Ethylenediamine (EDA) in Dimethylacetamide (DMAC) to form a solution of POSS modified Polycarbonate urea-urethane in DMAC (Prep9). All chemicals and reagents, except POSS, were purchased from Sigma-Aldrich (Gillingham, UK).

3.1.2 Casted (non-porous) POSS-PCU sheet

Non-porous POSS-PCU was fabricated via the solvent evaporation technique using an 18 cm Ø stainless steel plate stainless steel plate or a 9 cm Ø glass Petri dish. Required amount (mass) of Prep9, 18% (w/w) POSS-PCU in DMAC was calculated from desired thickness of the sheet to obtain the required mass using the equation below.

Required Mass (g) = Area of the mould (cm^2) X Desired thickness (cm^2) X 1.15 (g/cm^3)X (100/18)

Where 1.15 (g/cm^3) is solid POSS-PCU density and 100/18 is the correction factor when DMAC is fully evaporated away.

After that the pre-calculated amount of Prep9 POSS-PCU was poured onto the mould on the scale (Mettler-Toledo, Leicester, UK). The mould was transferred to 65^o C incubator with a balanced stage to equalise the POSS-PCU thickness. POSS-PCU was left overnight to let the DMAC fully evaporate and obtain the non-porous POSS-PCU sheet.

3.1.3 Microporous POSS-PCU sheet

The microporous scaffolds were fabricated using phase inversion/particulate leaching technique with the pre-sieved $NaHCO_3$ size of 25 - 53 µm at the different percentage (0). A mixture of POSS-PCU and 70% $NaHCO_3$ had a very high viscosity that couldn't place in a mould or dip-coated, and a modified version M70% was used instead. By adding more DMAC while maintaining the concentration of porogen, the porosity was similar to the 70% $NaHCO_3$. The compositions were mixed in the ARE-250 planetary centrifugal mixer (ThinkyUSA, Inc., California, USA) at 2,000 rpm mixing step and 1,500 rpm defoaming step. This mixture was then poured onto the glass mould while tapping around the edges with autoclave tape to obtain the thickness of 500 µm (4 layers X 125 µm). A metal rod was used to remove excess mixture and remove air bubbles. Finally, the mould was transferred into the deionised water to initiate the phase inversion/particulate-leaching to allow the solvent exchange and let DMAC and $NaHCO_3$ micro-particles slowly dissolved to form microporous sheets. The water was changed regularly up to 5 times over a 2-day period to wash away excess solvent and $NaHCO_3$.

Table 3.1 Composition of different percentage (w/w) for microporous POSS-PCU shown in every 100 g

Chemicals	30% $NaHCO_3$	50% $NaHCO_3$	70% $NaHCO_3$*	Modified 70% (M70%$NaHCO_3$)
18% POSS-PCU in DMAC (Prep9)	68 g	48 g	28 g	24 g
Tween 20	2 g	2 g	2 g	2 g
$NaHCO_3$ 25-53 µm	30 g	50 g	70 g	60 g
DMAC	-	-	-	14 g
POSS-PCU : $NaHCO_3$	**1 : 2.45**	**1 : 5.79**	**1 : 13.89**	**1 : 13.89**

* cannot be used in dip-coating

3.2 Manufacture of microporous POSS-PCU samples for cell culture

The POSS-PCU sheet was manufactured into the different shape such as dumbbell for mechanical testing or, into 16mm Ø circular discs for cell culture, and performed using pulsed CO_2 laser ablation. Briefly, POSS-PCU sheets were placed on a flatbed of the Trotec Speedy 100R (Trotec Laser, Guildford, UK). The shape was designed using CorelDRAW® Graphics Suite version X7 (Corel Corporation, Ottawa, Canada) to match the laser software. The samples were cut was performed using the laser condition at 6% of 30W Power, 0.6 cm/s speed and 1,000 frequency for non-porous POSS-PCU and 10.00 power unit, 0.50 volt and 9,000 pulses for microporous POSS-PCU.

3.3 Mechanical properties of POSS-PCU materials

Mechanical testing of the POSS-PCU materials or laryngeal tissues (n = 6 per condition) were performed using a uniaxial tension on the Instron 5565 testing system (Instron Corporation, High Wycombe, UK). Specimens were cut into a flat dumbbell shape (according to 3.2), mounted onto the grips with a 20 mm path length, and thickness of specimens measured using a digital electronic micrometer (UKAS Calibration Ltd, Middlesex, UK) for four cross-sectional areas across the dumbbell and were used to

calculate mean values and standard deviations. The mean values were input into the programme before processing of the mechanical testing software ready for testing. The data was plotted and analysed using Bluehill software version 2.9 (Instron Corporation, High Wycombe, UK). The maximum stress, strain at break and Young's modulus were obtained.

3.4 Surface morphology via scanning electron microscopy (SEM)

Scanning electron microscopy was performed by SEM Unit (Royal Free Hospital, London, UK) Basically, POSS-PCU samples were attached to aluminium stubs with double sided sticky tape and coated with gold using an SC500 sputter coater (EMScope, Sussex, UK) with a gold target before being imaged at high resolution and analysed using a Philips (FEI) 501 scanning electron microscope (Philips, Eindhoven, the Netherlands).

3.5 Sterilisation of POSS-PCU

3.5.1 Steam sterilisation (autoclave)

POSS-PCU samples were placed in the glass bottle filled with deionised water. The bottle cap was released a little bit and the autoclave indicator tape was attached. The bottle was placed in autoclave machine and sterilised at 121^{o} C, 15 psi for 15 minutes.

3.5.2 Ethanol cleanse

POSS-PCU samples were submerged in absolute ethanol (Sigma-Aldrich, Gillingham, UK) for 5 min. After that, POSS-PCU scaffolds were transferred into 50 mL tubes filled with 20 mL of 70% ethanol to rinse the surface. The tube was placed onto a roller shaker for 30 min. Then, the ethanol was removed from the tube washing steps were performed by adding 20 mL of PBS and placed on the roller for 15 min. The washing steps were then repeated 3 times.

3.6 Quantification of total protein concentration

The total protein content was quantified using the bicinchoninic acid (BCA) assay (Pierce Biotechnology, Illinois, USA). The BCA Protein Assay combines the well-known reduction of Cu^{2+} to Cu^{1+} by protein in an alkaline medium with the highly sensitive and selective colorimetric detection of the cuprous cation (Cu^{1+}) by bicinchoninic acid.

The first step is the chelation of copper with protein in an alkaline environment to form a blue coloured complex. In this reaction, known as the biuret reaction, peptides containing three or more amino acid residues form a coloured chelate complex with cupric ions in an alkaline environment containing sodium potassium tartrate.

In the second step of the colour development reaction, BCA Reagent, a highly sensitive and selective colorimetric detection reagent reacts with the cuprous cation (Cu^{1+}) that was formed in step 1. The purple coloured reaction product is formed by the chelation of two molecules of BCA Reagent with one cuprous ion. The BCA/Copper Complex is water-soluble and exhibits a strong linear absorbance at 562 nm with increasing protein concentrations.

In 96-well, 25 µL of standard or unknown samples were mixed with 200 µL of working reagent prepared by mixing 50:1, BCA reagent A: BCA reagent B. The plate was incubated at 37^{o}C for 30 minutes, cooled to room temperature and measured the absorbance at 562 nm. The standard curve of protein concentration was generated using standard bovine serum albumin (BSA) provided with the kit.

3.7 Cell culture and maintenance

3.7.1 Primary human bronchial epithelial cell (HBECs)

Human bronchial epithelial cells (HBECs) were purchased from ScienCell Research Laboratories (California, USA). The cells were isolated from human bronchi and was cryopreserved at Passage 0 to be delivered frozen at >5 x 10^5 cells in 1 ml volume. The cells

were tested by the company and were positive for keratin-18, keratin-19, and vimentin, but negative for HIV-1, HBV, HCV, mycoplasma, bacteria, yeast and fungi. HBECs were expanded in T75 cm^2 flasks with bronchial epithelial cell medium (BEpiCM) (Sciencell, California, USA). At passage 1-4 was cryopreserved in BEpiCM with 10% (v/v) DMSO (Sigma-Aldrich, Gillingham, UK) in liquid nitrogen storage (-196°C) as a stock concentration.

Cryopreservation vial was removed from liquid nitrogen storage, quickly thawed at 37^o C and the cells were transferred to a pre-warmed BEpiCM supplemented with growth factors (instead of foetal bovine serum), and 1% penicillin/streptomycin. The cells were pelleted at 1,200 rpm and re-suspended in new fresh media before putting in a T-75 cm^2 flask. The cells were placed in the CO_2 incubator (Binder GmbH, Tuttlingen, Germany) with the condition of 37^o C and 5% CO_2/Air with humidity. The medium of 15 mL was changed every 2 days to complete cell feeding. HBECs were sub-cultured and used between passages 2-9 for all cell culture experiments.

3.7.2 Human bone marrow-derived mesenchymal stem cell (BM-MSCs)

Human bone marrow-derived mesenchymal stem cells (BM-MSCs) were purchased from ScienCell Research Laboratories (California, USA). Cells were isolated from human bone marrow, cryopreserved at passage 1 and delivered frozen at >5 x 10^5 cells in 1 ml volume. BM-MSCs were previously characterised by the company using antibodies specific to CD73, CD90, CD105 and positive lipid staining after induced differentiation. BM-MSCs were also negative for HIV-1, HBV, HCV, mycoplasma, bacteria, yeast and fungi. BM-MSCs were expanded in T75 cm^2 flasks with mesenchymal stem cell medium (MSCM) (Sciencell, California, USA). Passage 1-4 was cryopreserved in MSCM with 20% fetal bovine serum and 10% (v/v) DMSO in liquid nitrogen storage (-196°C) as stock.

Stocked vial was removed from liquid nitrogen storage, quickly thawed and placed into a pre-warmed MSCM supplemented with MSC growth supplement, 10% foetal bovine serum,

and 1% penicillin/streptomycin. Cells were spun at 1,200 rpm, re-suspended in new fresh media and plated on a T-75 flask. The cells were placed in the CO_2 incubator (Binder GmbH, Tuttlingen, Germany) with the condition of 37^o C and 5% CO_2/Air with humidity. The medium was changed every 2 days to complete cell feeding. BM-MSCs were sub-cultured and used between passages 2-9 for all cell culture experiments.

3.7.3 Cell expansion and seeding on materials

The cells were allowed to grow up to confluence (80-90%) and were detached by first washing with warm 10 mL phosphate buffer saline (PBS). After washing, PBS was aspirated, and approximately 3 mL of 0.25% trypsin-EDTA was added and allowed to incubate at 37^o C for 3 min. Then, 3 mL of trypsin was allowed to neutralise by adding 7 mL of medium, and cell suspension which was collected in a 15 ml centrifuge tube and spun at 1,200 rpm to concentrate the cell population. The supernatant was discarded and the cells were re-suspended in 1-2 mL of fresh medium. 50 µL of sample was stained with an equal amount of 0.4% Trypan Blue (Sigma-Aldrich, Gillingham, UK) to determine the amount of live and dead cell using the improved Neubauer haemocytometer (VWR International, Leicestershire, UK), and the trypan blue exclusion assay. The cell suspension was diluted with different amounts of media to obtain cell concentrations for each application such as 5 x 10^5 cells/flask for further cell expansion, or 5 x 10^4 cells/scaffold for the *in vitro* experiment.

Pre-sterilised 1.6 mm Ø POSS-PCU discs, were placed into each well of a 24-well tissue-culture polystyrene (TCP) plate. Culture medium (1 mL) was added in to each well to incubate the discs in an incubator with 95% humidified air, 5% CO_2, and 37^o C for 24h before the experiment to ensure the medium had infiltrated though out the material, as well as, completed the adsorption of proteins. The initial cell number at 5 x 10^4 cells per scaffold/well (determined from the optimal growth phase of HBECs on TCP, Appendix C) was plated on to each scaffold and cultured for 14-35 days according to experiment conditions at 37^o C with 5% CO_2 /95% air. The medium (1 or 2 mL) was changed every 2

days and cells on TCP were employed as a positive control for comparison with POSS-PCU materials

3.8 Cell-based assay

3.8.1 Assessment of cell viability on POSS-PCU

Alamar Blue™ (AbD Serotec, Oxford, UK) was used to measure metabolic activity of cells on TCP and POSS-PCU scaffolds at each time point. Upon entering cells, the blue dye composed of resazurin is oxidised to a red coloured dye resorufin, which could be quantitatively detected using a fluorescent reader. Viable cells continuously convert resazurin to resorufin, increasing the overall fluorescence and colour of the media surrounding cells. Alamar Blue™ stock solutions were diluted with cell culture medium at the concentration of 10% (v/v). At each time point, the scaffolds were washed with 1 mL of media, and then, 10% (v/v) Alamar Blue™ in culture media was added to each well with minimal light exposure during aspiration. The 24-well plate was wrapped with aluminium foil and incubated at 37^{o} C with 5% CO2/95% air for 4 h. After completion of incubation, 100 µL solutions of each well was transferred into a black 96 well plate (Thermo-Fisher Scientific,

Massachusetts, USA), and the fluorescence was measured with 530 nm excitation and 620 nm emission using a Fluoroskan Ascent FL (Thermo-Fisher Scientific, Massachusetts, USA).

$$\% \text{ Reduction of Alamar Blue®} = \left(\frac{F_{Test} - F_{control}}{F_{100\% \text{ reduction}} - F_{control}} \right) X \ 100$$

Where $F_{control}$ is the fluorescence from Alamar Blue® in media without cells, F_{test} is fluorescence from samples, and $F_{100\% \text{ reduction}}$ is a complete reduction of Alamar Blue® generated by autoclaving Alamar Blue® in media (according to company's instruction).

After measurement, the scaffolds in each 24 well plate were washed once with 1 mL of fresh culture media. Finally, another 1 mL of fresh culture medium was added to each well and followed the "regular cell culture scheme".

3.8.2 Cell proliferation on POSS-PCU

Cell proliferation was determined by measuring the amount of total DNA in a given population. Briefly, the culture medium was removed from samples and washed with PBS. Then, 100 µL of deionised water was added into each scaffold. The scaffold was subjected to x3 freeze-thaw cycles by placing in -70^{o}C and then room temperature for 3 times to lyse the cells to release DNA. The fluorescent dye solution was prepared by dilution to 1 µg/mL Hoechst 33258 in buffer solution according to the company's instruction (Sigma-Aldrich, Gillingham, UK). After performing 3 freeze-thaw cycles, the whole supernatant (100 µL) was transferred to black 96-well plate pre-added with 100 µL of the dye solution. The solution in each well was mixed using a pipette and the plate was then subjected to fluorescent readings at 380 nm excitation and 420 nm emission using Fluoroskan Ascent FL (Thermo Fischer Scientific, Massachusetts, USA). A DNA standard curve was generated using standard calf thymus DNA provided with the kit. The mean fluorescence reading of each sample was then compared to the blank. If there was no significant difference ($P > 0.05$), the sample was interpreted as DNA not detected. However, if there was significant ($P < 0.05$), the fluorescence was then quantified referring to DNA standard curve and was presented in the graph.

Chapter 4 Design and development of a 3D POSS-PCU scaffold for laryngeal implants

4.1 Introduction

Loss of laryngeal function severely affects the quality of life of those effected breathing, speaking, swallowing, and other basic functions, are all compromised. Conventional voice restoration as well as breathing after laryngectomy requires constant maintenance and delivers suboptimal phonation at best[84]. Where the laryngeal structures remain in place, but remain damaged through scarring leads to distortion of the vocal fold edge, as well as, the alteration of lamina propria, viscosity and stiffness[85] of the tissue leading to vocal impairment[86]. Speech restoration also is a vital part for functional rehabilitation of patients undergoing partial or total laryngectomy[87]. Voice rehabilitation in the latter patients is usually accomplished by employing esophageal speech, an artificial larynx, or most recently the construction of a tracheoesophageal fistula and use of valve voice prostheses[88].

The field of laryngeal tissue engineering aims to reconstitute structurally and restoring the function of the organ using regenerative medicine approaches[89]. To date, laryngeal implants have developed in divergent designs for different applications. Most implants are primarily used for glottic insufficiencies[90]. These implants have a variety of forms including injectable implants consisting of micro-particles for vocal fold augmentation[91] and solid implants from titanium[92] and silastic[93] for more permanent vocal fold medialisation in patients with vocal cord paralysis. Silicone stents (e.g. Montgomery T-tubes, Eliachar stents) are applied to prevent or by-pass life-threatening laryngeal stenosis[94], whilst most recently a titanium-based artificial larynx implant is being developed to replace oral breathing and speech for laryngectomees[2].

Synthetic materials have many advantageous properties over natural materials; for example, the manufacturing and developmental procedure can be easily controlled, and the materials can be sterilised in various ways prior to clinical use such as steam sterilisation (autoclave), gamma irradiation and ethylene oxide (EtO) gas exposure. Polyhedral oligomeric silsesquioxane – poly (carbonate urea) urethane (POSS-PCU) has been shown to possess ideal characteristics for 3D scaffolds, such as anti-thrombogenicity[95], degradation resistance[65], and extensive biocompatibility testing over a 3 year period in vivo[69]. In terms of sterilisation, it also showed resistance to autoclaving with no cytotoxicity side effect[96], which is a very promising property to use for sterilisation of medical device according to ISO standards in clinical usage.

In this study, two different fabrication methods were examined using nanocomposite POSS-PCU materials to optimise 1) the 3D structure of laryngeal implants using a combination of solvent casting and particulate-leaching/phase inversion coagulation techniques and 2) voice simulation of particulate-leaching/phase inversion coagulation POSS-PCU material.

4.2 Materials and methods

4.2.1 Synthesis of POSS-PCU nanocomposite materials

The production of polymer has been prepared by Mr Arnold Darbyshire and the process was described previously elsewhere in detail[65]. In brief, polycarbonate polyol, and trans-cyclohexanechloroydrinisobutyl-silsesquioxane were placed in a reaction flask equipped with mechanical stirrer and nitrogen inlet. The mixture was heated to 135°C to dissolve the POSS cage into the polyol and then cooled to 70°C. Flake 4,4'-Methylenebis(phenyl isocyanate), (MDI), was added to the polyol blend and then reacted, under nitrogen, at 70°C - 80°C for 2 h to form a pre-polymer. Dimethylacetamide (DMAC) was added slowly to the pre-polymer to form a solution; the solution was cooled to 40°C. Chain extension of the pre-

polymer was carried out by addition of Ethylenediamine in Dimethylacetamide to form a solution of POSS modified Polycarbonate urea-urethane in DMAC. All chemicals and reagents were purchased from Sigma-Aldrich (Gillingham, UK).

4.2.2 Fabrication of 3D laryngeal implant structures

The laryngeal framework was fabricated using a multiple step approach. Non-porous POSS-PCU was fabricated using solvent-evaporation techniques at temperature of 65^{o}C overnight (18h) in metal mould to obtain the desirable thickness (5 mm). The non-porous POSS-PCU sheets was cut according to porcine cartilage shape in 2D, and was reshaped to form a 3D tubular structure by heating at 140^{o}C for 1h. Non-porous larynx structures including larynx, and the upper part of trachea were cross-linked using DMAC, and formed the 3D larynx and upper airway scaffold. The whole structure was dip-coated in a mixture of porogen (25 – 53 µm $NaHCO_3$) and POSS-PCU mixture (50 mL). Particulate-leaching/coagulation was performed in sterile water to let solvent and $NaHCO_3$ microparticles slowly dissolved and formed an outer microporous layer.

4.2.3 Surface morphology using scanning electron microscopy (SEM)

The fabricated materials were sectioned using scalpel to obtain thin sections containing non-porous POSS-PCU in the centre and microporous POSS-PCU coated on both sides. The porous section was analysed to examine the surface morphology. The samples sent to SEM unit (Royal Free Hospital, London UK) were attached to aluminium stubs with double sided sticky tape and coated with gold using (SC500) sputter coater (EMScope, Sussex, UK) with a gold target before being imaged and analysed using a Philips (FEI) 501 scanning electron microscope (Philips, Eindhoven, the Netherlands).

4.2.4 Effect of heat aging on mechanical properties of non-porous POSS-PCU

Non-porous POSS-PCU with thickness of 500 µm was cut into dumbbell shaped, specimens were subjected to processing using the heating at 140^{o}C at different time points

(1h, 3h and 6h)(n = 6 per condition), and at a room temperature at 25^{o} C (n = 6). All samples were then subjected to testing the mechanical properties using the Instron 5565 testing system (Instron Corporation, High Wycombe, UK) as previously described in section 3.3.

4.2.5 Mechanical properties of POSS-PCU vs. native porcine tissue

Mechanical testing of porous and non-porous POSS-PCU, and laryngeal tissues from a porcine model (n = 6 per condition) were performed with a uniaxial tension on the Instron 5565 testing system (Instron Corporation, High Wycombe, UK). Specimens were cut into a flat dumbbell shape with 20 mm path length and the thickness of specimens were measured using a digital electronic micrometer (UKAS Calibration Ltd, Middlesex, UK) form four cross-sectional areas across the dumbbell specimen, and were used to calculate standard deviations and mean values. Porcine larynxes were purchased from Orchard Farm (Essex, UK). All mechanical properties were measured on the day of organ retrieval. Different areas of the organ were sampled to test the supraglottic epithelium, vocal cord, subglottic epithelium and thyroid cartilage (Figure 4.1). The mean thickness values of thickness were input to the software program before processing of the mechanical tests. Data was plotted and analysed using Bluehill software version 2.9 (2010) (Instron Corporation, High Wycombe, UK). The maximum stress, strain at break and Young's modulus were obtained for each of the specimens and their respective locations.

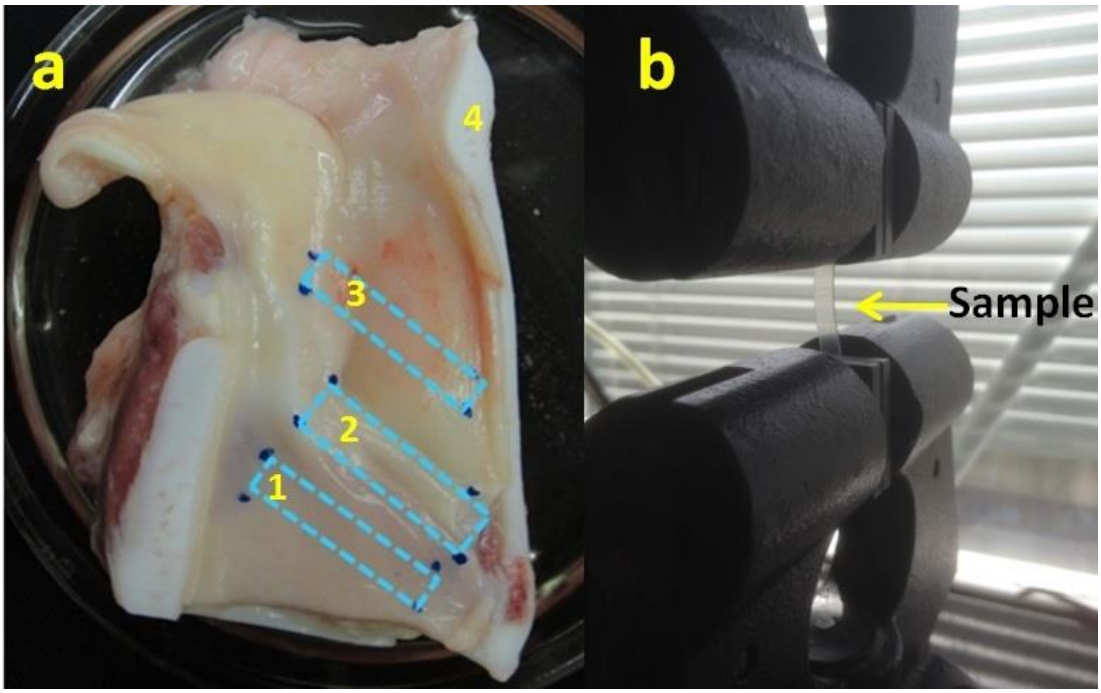

Figure 4.1 Pictures showing selective tissue region (a), 1 = subglottis, 2 = glottis, 3 = supraglottis, and 4 = thyroid catilage, and samples were attached to Instron's grips for tensile testing (b).

4.2.6 Oscillatory response of coagulated POSS-PCU

Custom made acrylic tube was designed for the voice test rig (Figure 4.2). Briefly, silicone tubing was connected to the air supplier with a reading gauge (L/min). Another end of the tube was connected to the Y-shape connector with tubes which led to a pressure metre (Comark, Northampton, UK) and a testing chamber with a wetted paper towel to keep moisture in the air flow. Microporous POSS-PCU membranes comprised of 50% NaHCO3, 25-53 µm, were tested with n = 4 per condition at different thickness values (e.g. 0.5 mm, 1.0 mm, 2.5 mm. 3.0 mm, and 5.0 mm) and were attached to the square stage on the top of the tube. The different levels of strain applied across the membrane was created by marking of two positions with a distance of 2.0 cm. Then the membranes were stretched equally to 2.1 cm and 2.2 cm (5% and 10% strain)(Figure 4.3-a) and no stretch at all for 0% strain.

Finally, around the membrane was sealed using sticky tape to prevent the air leakage (Figure 4.3-b).

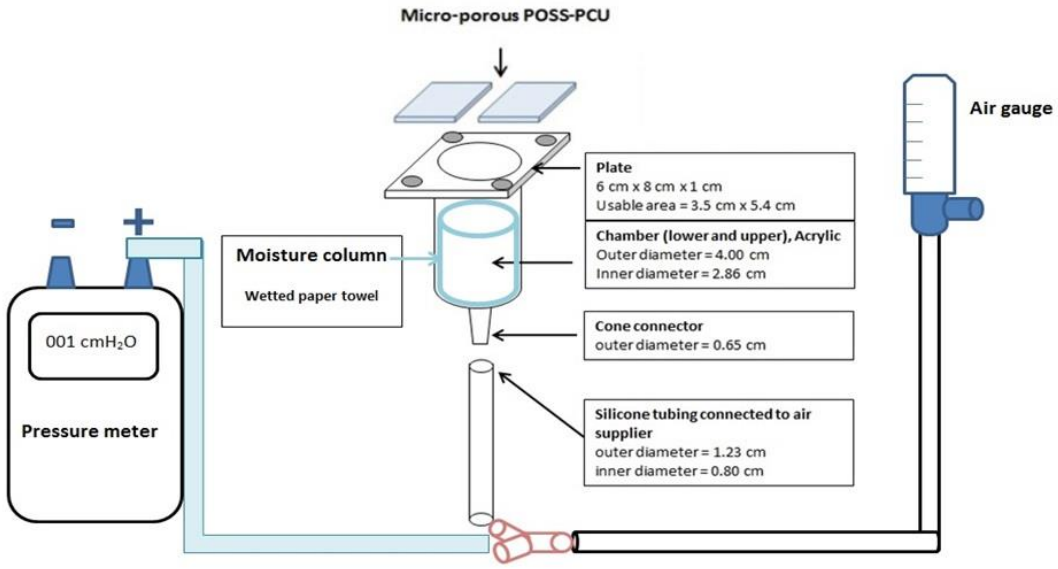

Figure 4.2 Schematic diagram presenting the voice test rig.

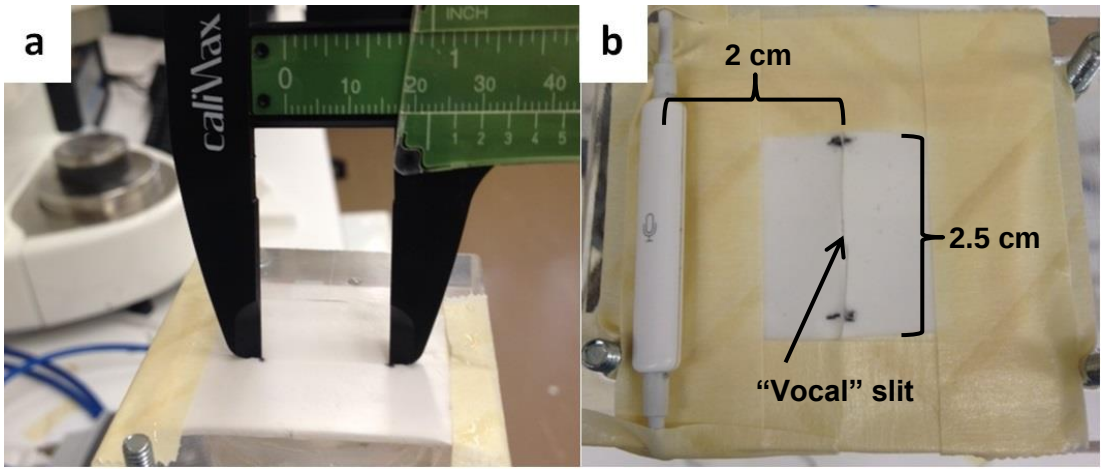

Figure 4.3 a) strain applied on to POSS-PCU membranes to achieve 10% at 2.2 cm and b) sticky tape was sealed around the membrane and microphone was placed at the side to record the sound (2 cm, same position in all samples). The arrow show where the "vocal" slit vibrated and generated the sound.

When the air flow gauge was open, a vibration at response was recorded in the parameters of the air flow rate, differential pressure, and sound. The air flow rate for this experiment was fixed at 5, 10, and 15 L/min plus an initial response if lower or higher than

5L/min. The sound from each sample was recorded for 10 seconds at the same position (2 cm away from the sound source) using an iPhone and microphone (Apple, California, USA). The files (.wav) were analysed for average fundamental frequency (F0) and average sound energy using Analysis of Dysphonia in Speech and Voice programming software (ADSV™)(KayPENTAX, New Jersey, USA).

4.2.7 Statistics

The data are compared using a two-way ANOVA with Bonferroni's multiple comparisons test in mechanical testing experiment. Linear regression was analysed using a differential pressure, sound energy, and F_0. Non-parametric correlation was used to analyse the sound energy. All statistical analyses were performed on the data sets using GraphPad Prism version 5.01. (2007) *P* – values < 0.05 were considered to be statistical significance.

4.3 Results

4.3.1 3D laryngeal implant structure

The fabricated laryngeal framework replica is shown in Figure 4.4. After casted POSS-PCU sheet was cut into thyroid shape in 2D (Figure 4.4, 1), it was heat aged at 140^{o} C to form a 3D tubular structure similar to the native cartilage (Figure 4.4, 2). Non-porous larynx structures including the larynx and the upper part of trachea were cross-linked using DMAC solvent and formed the 3D larynx scaffold (Figure 4.4, 3). The whole structure was dip-coated in sodium bicarbonate ($NaHCO_3$) and POSS-PCU mixture, and particle-leaching/coagulation was performed in sterile water to let solvents and $NaHCO_3$ micro-particles slowly dissolve to form an outer microporous layer. The fabrication technique revealed the full tubular structure was composed of non-porous rigid structures inside and soft microporous structure fully covering the outer layer (Figure 4.4, 4).

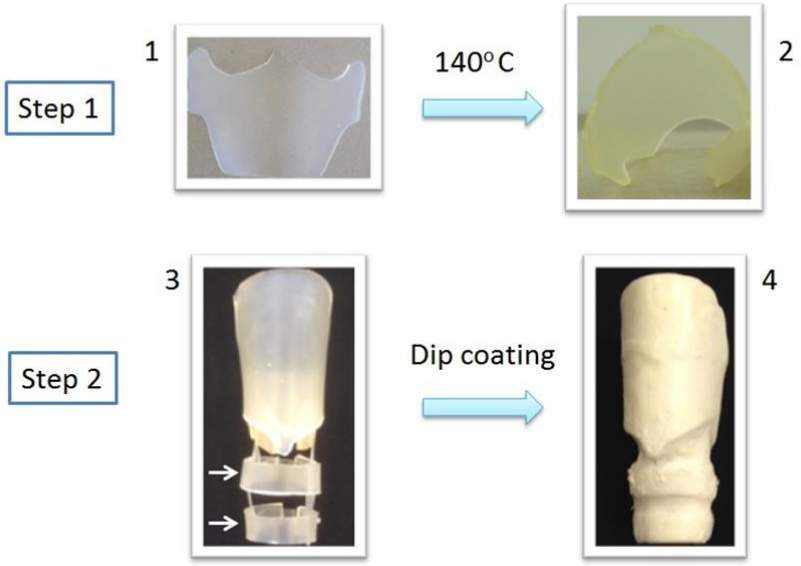

Figure 4.4 Development of 3D scaffold is demonstrated on the schematic diagram. Step 1, casted POSS-PCU was cut in to thyroid cartilage shape (1). The casted thyroid structure was heated to 140^{o} C to form a tubular structure (2). Step 2, the thyroid structure was glued together with casted tracheal rings (arrow) using DMAC, forming a complete internal rigid structure (3). The whole structure was dip-coated the outer layer with porous coagulated POSS-PCU (4), revealed the complete tube with porous structure covered the entire surface.

The hemilarynx was fabricated using a similar technique to create a semi-tubular structure (Figure 4.5, A) showing the difference of inner lumen (IL) without or with the vocal fold structures (VF) which was similar to the native porcine thyroid cartilage (Figure 4.5, B). A cross-section sample was examined under SEM to identify the microstructures of the scaffold. The scaffold presented a complete outer layer of porous structures with an internal rigid structure (Figure 4.5, C). The outer layer of coagulated POSS-PCU scaffolds with 25 - 53 µm NaHCO3 presented microporous structures with an open network throughout the surface (Figure 4.5, D).

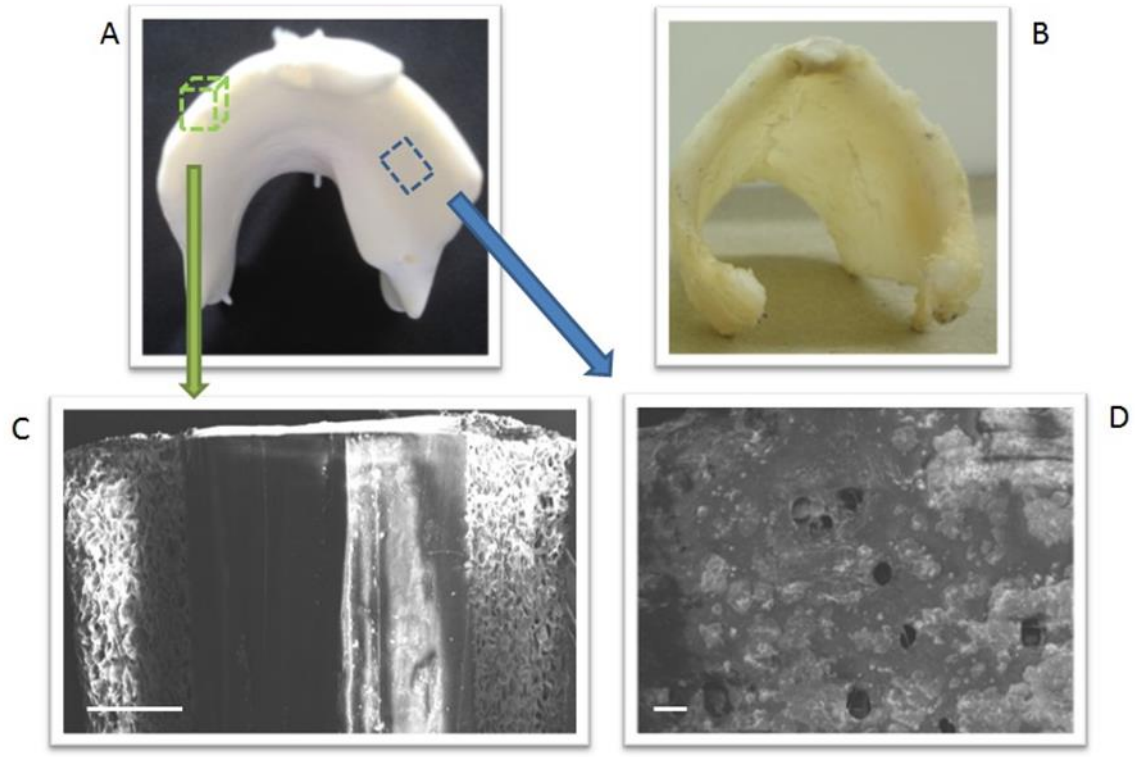

Figure 4.5 POSS-PCU thyroid shape (A) demonstrates a similar structure to the native porcine cartilage (B). High magnification of the cross-section revealed a uniform porous structure with rigid casted POSS-PCU in the middle (C), bar = 1 mm. The outer layer also demonstrates pores across the surface (D), bar = 30 µm.

4.3.2 Effect of heat aging on mechanical properties of casted POSS-PCU

Mechanical testing showed that there was no significant difference in terms of maximum stress and Young's modulus among the casted samples, which were incubated at 140^{o} C for 1, 3 and 6 h, respectively, when compared with controls (Figure 4.6).

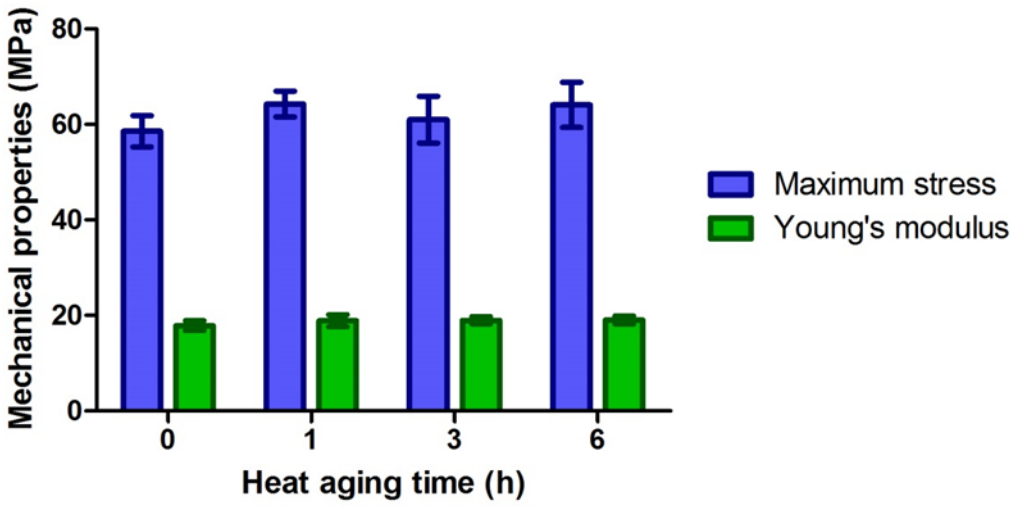

Figure 4.6 The mechanical properties of casted POSS-PCU when exposed to heating at different time (n=6).

4.3.3 Mechanical properties of POSS-PCU scaffold vs. native porcine model

Different parts of laryngeal tissue and nanocomposite scaffolds were investigated in terms of tensile properties as shown in Figure 4.7. In terms of maximum stress, casted POSS-PCU (rigid structure) exhibited the highest value at 58.56 ± 3.26 MPa, which was 11 times higher than that of thyroid cartilage at 5.09 ± 0.90 MPa. Whereas epithelial tissues from the supra glottis, vocal cord and subglottis were at 1.32 ± 0.44, 1.97 ± 0.65 and 0.90 ± 0.46 MPa, respectively, which were not statistically different from coagulated POSS-PCU (soft microporous structures) at 0.65 ± 0.02 MPa. A combination of 100:400 μm in thickness of casted – coagulated POSS-PCU was also observed in this experiment to study the properties of the combined material. Casted – coagulated POSS-PCU exhibited a maximum

stress value in between the coagulated polymer only, and the casted only at 4.50 ± 1.04 MPa, and there was no statistical difference from that of thyroid cartilage. It's maximum stress was a 7 fold increase was observed when compared with coagulated – sample of POSS-PCU.

The relationship of stress – strain or Young's modulus of different materials was also studied to determine the stiffness of material (Figure 4.7). Thyroid cartilage presented the highest stiffness at 29.42 ± 9.08 MPa while casted POSS-PCU's was at 17.02 ± 0.90 MPa. Supraglottic, vocal cord and subglottic tissues were at 4.11 ± 2.10, 6.03 ± 2.29 and 4.46 ± 1.60 MPa, respectively, whereas, coagulated POSS-PCU was at 0.40 ± 0.09 MPa. A combination of casted + coagulated POSS – PCU again exhibited the higher young's modulus at 2.88 ± 0.33 MPa compared to that of coagulated POSS – PCU.

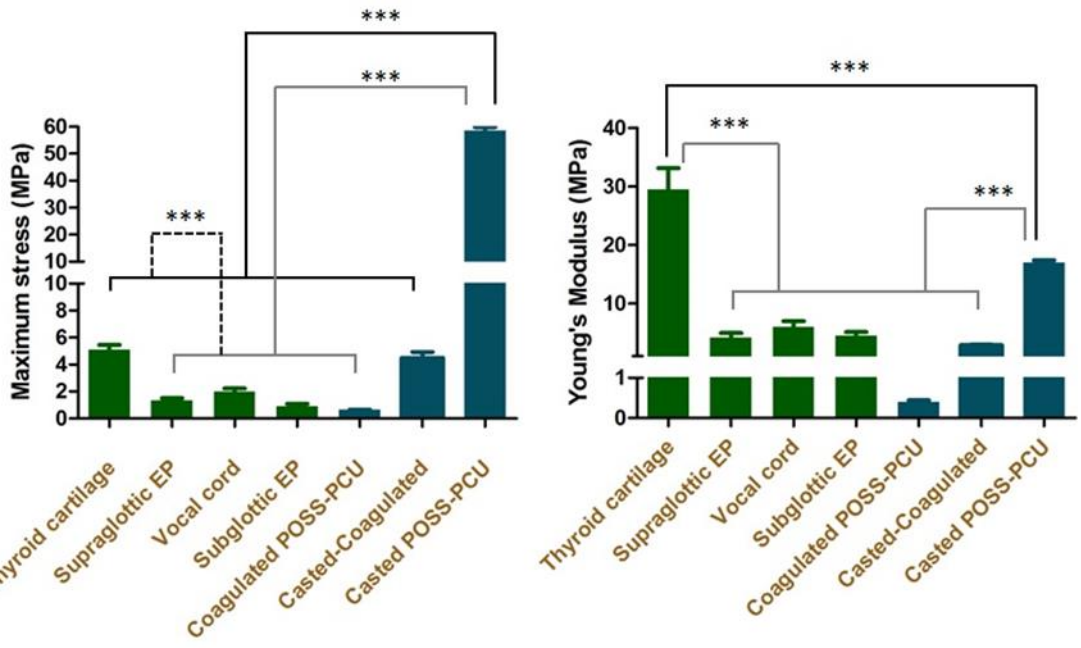

Figure 4.7 The mechanical properties of casted POSS-PCU, microporous POSS-PCU, and porcine laryngeal tissues, *** $P < 0.001$. (n=6)

4.3.4 Oscillatory vibration of coagulated POSS-PCU

The vibration and response was examined using 50% NaHCO3, (sized 25-53 μm), coagulated POSS-PCU (Table 4.1). The response was initiated by the membrane, which was elevated to be a dome shape (Figure 4.8), which started to vibrate, and generate sound in the thickness range between 0.5 mm to 2.5 mm, however; there were no vibrations at 0% strain. In 0.5 mm thickness, only 10% strain of the material was vibrating at air flow rate 7L, 10L and 15L per minute. For 1.0 mm coagulated POSS-PCU, the material vibrated at 3L, 5L, 10L and 15L per minute at 5% strain, however; the material only vibrated at 7L, 10L and 15L per minute at 10% strain. In 2.5 mm coagulated POSS-PCU, the material vibrated at 3L, 5L, 10L and 15L per minute at 5% strain whereas only vibrated at 7L, 10L and 15L per minute at 10%. Finally, 3.0 mm and 5.0 mm coagulated POSS-PCU had no response at all conditions.

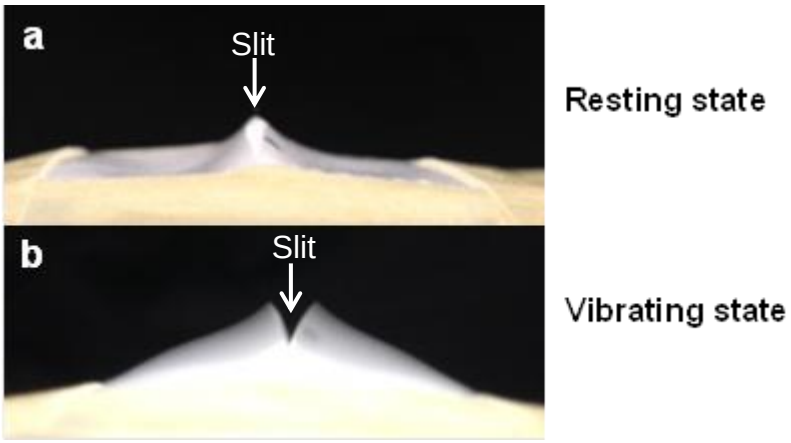

Figure 4.8 Capture images of the side view (2 cm away from the slit) of microporous membrane in resting state (a) and vibrating state while generating sound (b). White arrow shows the opened slit (2 cm in length).

Table 4.1 Overview of the vibrational response of coagulated POSS-PCU nanocomposites. (n=4)

Thickness	0% strain				5% strain				10% strain			
	Threshold	5L/min	10 L/min	15 L/min	Threshold	5L/min	10L/min	15L/ min	Thershold	5L/min	10L/min	15L/min
0.5 mm	No	No	No	No	No	No	No	No	7L/min	No	Yes	Yes
1.0 mm	No	No	No	No	3L/min	Yes	Yes	Yes	5L/min	Yes	Yes	Yes
2.5 mm	No	No	No	No	3L/min	Yes	Yes	Yes	7L/min	No	Yes	Yes
3.0 mm	No	No	No	No	No	No	No	No	No	No	No	No
5.0 mm	No	No	No	No	No	No	No	No	No	No	No	No

The differential pressure was measured and plotted against the air-flow rate to see the relationship (Figure 4.9). The mean value of the lowest and highest differential pressure detected at 1.50 cmH2O and 4.25 cmH_2O, respectively. Linear regression of all of the conditions revealed slopes that deviated from zero ($P < 0.01$) and suggested that they had or almost linear relationship. However, correlation analysis showed a significance ($\alpha = 0.05$) only in 1.0 mm thick samples, 5% strain ($P = 0.0023$) and 2.5 mm, 5% strain ($P = 0.0298$) with $R^2 = 0.9954$ and 0.9978, respectively. Other samples showed no significant correlation ($P > 0.05$).

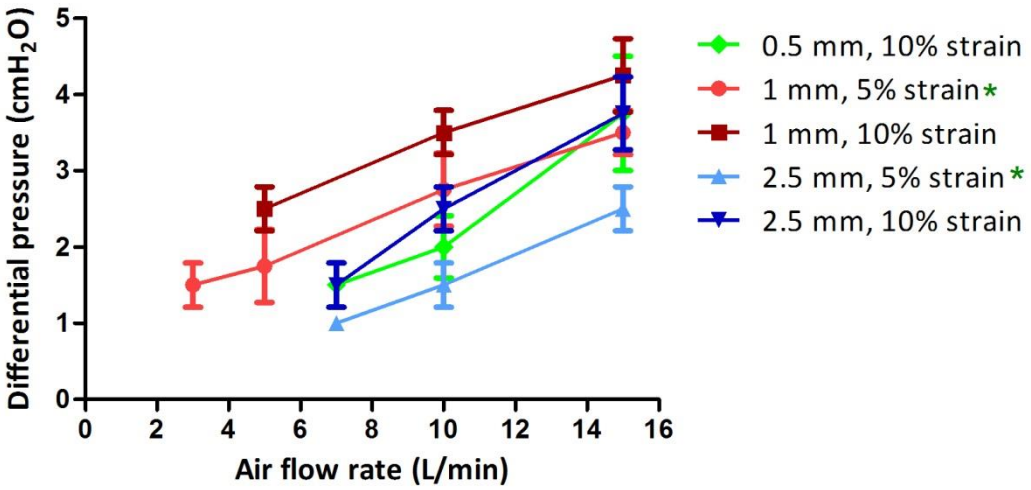

Figure 4.9 Mean value of differential pressure increased in higher air-flow rate but showed significant correlations only in 1 mm and 2.5 mm with 5% strain (*). (n=4)

The mean value of sound energy increased when the flow rate was higher at X axis with minimum at 69.53 dB and maximum at 84.77 dB (Figure 4.10). Although the trends were likely to be non-linear, linear regression test also showed significant deviation from zero in all samples ($P < 0.05$) except for 2.5 mm, 10% strain, which was non-significant ($P = 0.0572$). This suggested most of the lines could probably fit in linear correlation as well. However, when the correlations were analysed, none was significant ($P > 0.05$). With the combination results, the relationship between sound energy and air-flow rate would probably fit more with a non-linear type with a plateau.

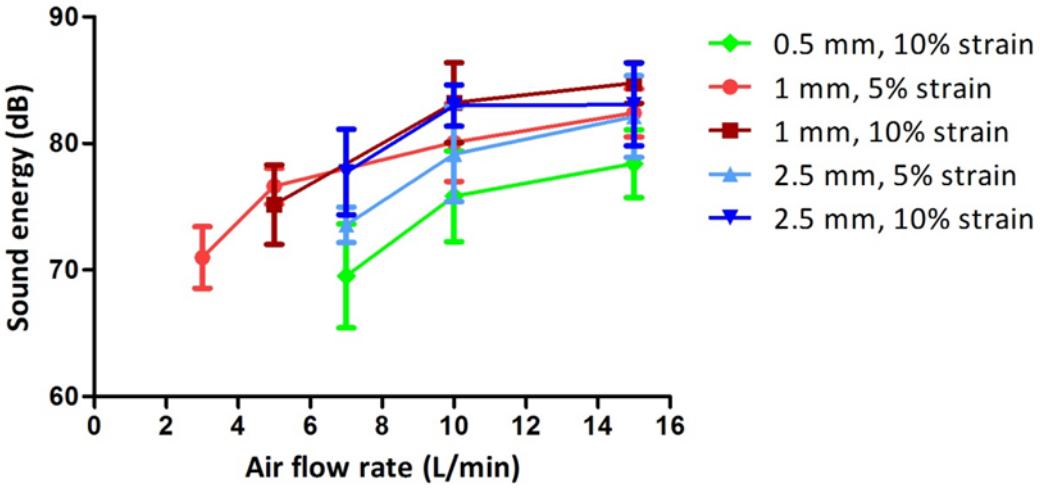

Figure 4.10 Graph exhibited the increase of sound energy when the air-flow rate was higher and in a non-linear pattern. (n=4)

Fundamental frequency (F_0) demonstrated almost a straight line fit (Figure 4.11) when the air flow rate increased with no linear regression in all conditions ($P > 0.05$). Mean comparisons of each thickness at 5% and 10% strain were made using a t-test. The results presented the significant difference between 1 mm, 5% strain vs. 1mm, 10% strain (mean F0 = 168.7 Hz and 185.0 Hz) and 2.5 mm, 5% strain vs. 2.5 mm 10% strain (mean F_0 = 161.3 Hz and 188.3 Hz). 0.5 mm, 10 % strain did not have pairs, however; its mean F_0 (184.7 Hz) is similar to 1 mm, 10% strain and 2.5 mm, 10% strain ($P < 0.05$). The higher F_0 in higher % strain were also noticed in this experiment.

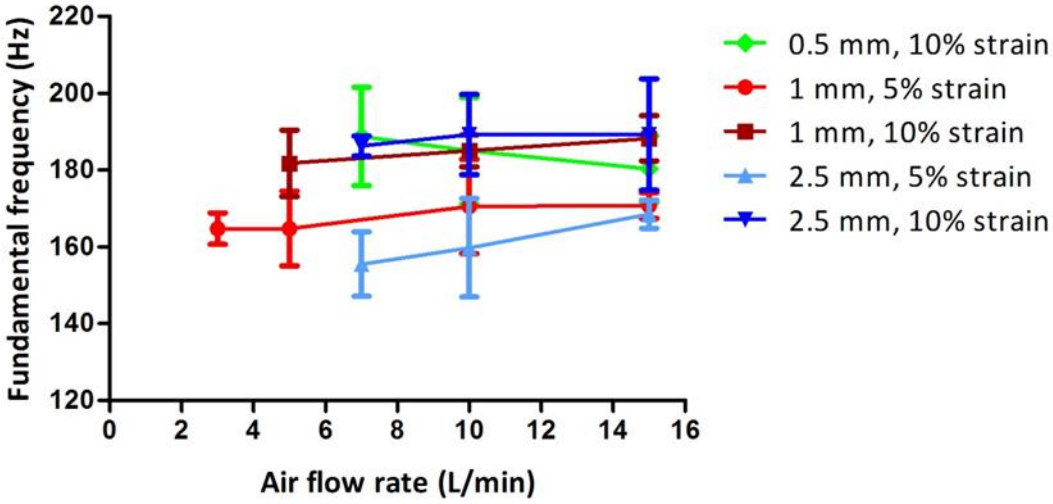

Figure 4.11 F_0 remained the same when air flow rate was higher, however; F_0 significantly increased when % strain was higher. (n=4)

4.4 Discussion

The classic paradigm of tissue engineering is three-pronged based on (a) cells acting as a guide for native tissue regeneration, (b) biomaterial scaffolds (either synthetic or biologic, and (c) regulatory factors, both biochemical and physical, that mediate cellular and material behaviour[97–99]. Our laboratory has demonstrated the advantage of nanocomposite POSS–PCU for tissue engineering applications in terms of controllable mechanical strength and elasticity, high compatibility and resistance to degradation and calcification[95]. Here we examined its specific suitability as the basis for a laryngeal scaffold for clinical use.

The solvent-casting technique provided the rigid non-porous structure, which might be suitable for supporting the whole organ structure, as well as, withstanding the environment and pressure inside the body. Our data showed that casted POSS-PCU exhibited flexibility by shaping this material from 2D to 3D tubular structure under 140°C without changes in tensile properties, and the durability with the higher overall maximum stress compared to the native thyroid cartilage. The particle-leaching and coagulation technique, in contrast, was suitable for creating the soft microporous structures underlying the epithelium with interconnected networks suitable for cell growth, which will be discussed in the following chapter. Moreover, its tensile properties were similar to those of porcine laryngeal epithelia. In addition, a ratio of 100:400 µm thickness of combined casted and coagulated POSS-PCU presented improved tensile properties, and revealed the possibility of adjusting the desirable tensile and mechanical properties for specific application.

Debry et al. recently reported a first-in-man total artificial larynx replacement[2]. The implant was made of titanium with a porous titanium rings underneath to permit better integration of tissue from the proximal trachea and a silicone stent to reduce or by pass stenosis. Valves on top of the device are intended to not only help patients swallow better, but also restore speech described as an “understandable whispering voice”, though probably rather sub-optimal compared to normal speech. Similarly, POSS-PCU has durable properties

and a porous component, which facilitates cell and tissue integration. Microporous POSS-PCU was separately examined for the oscillatory response for voice restoration applications. Because of its similar mechanical properties to laryngeal epithelia in porcine vocal cords, we hypothesised that microporous POSS-PCU would also respond to the oscillation.

We set up the voice testing rig using an in-house design acrylic tube to deliver the air flow while placing the tube upright so that the POSS-PCU membrane would be under the influence of air-flow, and gravity in a similar way to human cords. Inside the tube, the wet paper towel was wrapped around to provide the moisture during the air flow because the dryness of the material could alter the vibration result[100] while the temperature was controlled at ambient (25° C). However, the using of humidity and temperature controller is recommended for future work to monitor environment and the previously published condition was 25–30° C, at 95% relative humidity[101–103].

The thickness of microporous POSS-PCU altered the response to air flow: 0.5, 1.0, and 2.5 mm thickness generated oscillatory vibration while 3.0 and 5.0 mm did not. When strain was increased from 5% to 10%, the air-flow threshold increased from 3L/min to 5 L/min in 1 mm thickness material and 3L/min to 7L/min in 2.5 mm thickness material, possibly due to changing the viscoelastic properties of the material. In tensile testing, Young's modulus and elastic modulus of micro porous POSS-PCU reduced when higher strain was applied. This might result in "stiffer" material, which would probably require more pressure to initiate vibration and phonation.

Phonation threshold, pressure drop, or "differential pressure" (our favoured term here) is the difference between the pressure of lower glottis and upper glottis and is important to initiate vocal fold vibration in man. This experiment measures the pressure difference of inside and outside the tube to mimic that phenomenon. Titze et al. showed that vibration would require about 2-5 cmH_2O pressure drop to generate human voice[104]. Microporous

POSS-PCU material exhibited the differential pressure to be well within this range, also demonstrating linear increase with increased air-flow rate.

The membrane thickness that responded to vibration was thinner than that of normal human vocal folds (3-5 mm[75]). However, the quality of "voice" produced was quantitatively similar to that in man. In terms of energy, normal speech in daily life of 60 dB average with fundamental frequencies around 108 – 129 Hz in male and 183 – 226 Hz in female[105]. Microporous POSS-PCU exhibited the F_0 161.3 Hz to 188.3 Hz, which is between the human male and female range. At threshold pressures, the sound energy produced by microporous POSS-PCU was 69.53 dB which is quite close to that of normal speech. Furthermore, it also produced higher energy when more pressure or air-flow was applied. This suggested that the loudness of sound can be controlled from this material in the same physiological way that speech or shouting are achieved in humans. Interestingly, POSS-PCU material in the same thickness range but different level of strain could change to the higher shifting of F_0 or "pitch" after applying more strain. This is similar to the process of pitch changing in a human voice by different stretching of the vocal cords.

4.5 Conclusion

POSS-PCU material has the potential to form the basis of a 3D laryngeal implant. Mechanical properties and oscillatory response indicated how the material could be optimised to develop a "voice restoration" prosthesis responsive to human lung-generated air-flow. Particle leaching and coagulated POSS-PCU exhibited interconnected microporous networks which could be useful for cell integration and coverage. In-depth characterisation and cyto-compatibility testing are presented in subsequent chapters.

Chapter 5 Pre-optimisation of POSS-PCU properties for *in vitro* cell culture

5.1 Introduction

Polyurethane (PU) block co-polymers are the most common class of polymeric biomaterials, and are widely used in a broad application range of blood-contacting device due to their diversity, excellent mechanical properties and haem compatibility, compared to other polymeric biomaterials e.g. PTFE[106]. These block co-polymers are typically constructed from a 'soft' segment, a polyether, polyester, or a polycarbonate, and a hard segment, which contains urethane and/or urea linkages[107].

Copolymer materials like PUs are different from other non-polymer solid materials, due to its unique "microphase separation". Microphase separation often resulted in hard segment (domain) aggregates together with H-bond and therefore, separate from soft segment and could be seen in nanoscale surface using Atomic Force Microscopy (AFM) techniques[108]. Moreover, these separated features of PU affected how protein was adsorbed when Xu et al. demonstrated BSA-nano gold adsorption on polyurethane urea (PUU) and adsorbed more on the soft segment (131±36 proteins/μm^2) than on the hard segment (61±20 proteins/μm2), due to hydrophobic interactions[109].

As the soft segment is the most vulnerable component of PU[110], efforts have been made to improve resistance by varying the soft segment groups dependant on chemistry. Therefore, PUs are affected by some in vivo degradation mechanisms. For example, poly(ester)urethanes can undergo hydrolytic degradation and are no longer utilised as long-term implanted devices[111]. Our polymer employed carbonate groups instead, which have

been shown to increase the degradative resistance of PU[111], an effect due to the better hydrogen bonding between all of the segments[112].

Poly(carbonate-urea) urethane based materials were established by incorporation of silsesquioxane nanocages by core heat cross-linking to provide molecular stability and has been shown to possess anti-inflammatory and anti-thrombogenic properties[69]. These hard and soft segments properties are believed to arise from the presence of separated microphases of the hard and soft segments in the copolymers which is a result of thermodynamic immiscibility of the polar hard segments, and the nonpolar soft segments[113].

Material surface properties influence the interactions that occur at the tissue-implant interface and play a role when proteins adsorb on to the materials, and cells come into contact with the surface. When the material is implanted into the body, proteins can rapidly adsorb on the material surfaces within a short time. As protein adsorption occurs almost immediately well before cells arrive at the surface, the cells “sense and feel” primarily a protein layer rather than the actual surface of the biomedical material[114]. In addition, many factors can influence protein adsorption such as porosity, surface chemistry, energy, wettability, charge, topography, and hydrophobic interaction[115].

Micro-pore structures and porosity can maintain higher proteins adsorption (fibronectin and serum albumin) and has been shown to enhance human bone cell attachment on hydroxyapatite ceramics[116]. The higher porosity results in higher surface area than 2D non-porous materials; therefore, more chance of proteins to be adsorbed to the surface. Wettability can be determined using contact angle (θ) measurements, when a liquid droplet contacts the material surface. Wettability evaluation usually includes the measurement of contact angle (θ) measured in degrees, which indicates the level of wetting. Small contact angles (< 90°) correspond to high wettability (hydrophilic), while large contact angles (> 90°) correspond to low wettability (hydrophobic)[117],[118]. Due to low surface energy,

liquids will not wet material surfaces and the contact angle will be greater than 90°; therefore, the liquid molecules are more attracted to other liquid molecules compared to the polymer surface. θ measurement is the easy way to determine surface properties of bulk material; however, micro and nano scale study on surface of copolymer needs to be studied to explain more about this phenomenon.

A better understanding of such phenomenon may lead to the optimal material properties of POSS-PCU that could control protein adsorption, cell adhesion, and integration, which are the fundamentals. In this chapter, the material properties were examined in different aspects by bulk modification and linked all the data together to explain and optimise the microporous POSS-PCU material in order to enhance the in vitro cell culture using HBECs as a model.

5.2 Materials and methods

5.2.1 Sterilisation and effect on casted POSS-PCU bulk properties

5.2.1.1 Sterilisation of casted POSS-PCU

The sterilisation was performed on casted non-porous POSS-PCU using autoclave and ethanol cleanse previously described in section 3.5. Casted POSS-PCU sterilised from both techniques were assessed the bulk properties such as wettability, surface chemistry, SEM analysis, and mechanical properties.

5.2.1.2 Effect of sterilisation techniques on casted POSS-PCU wettability

Wettability of the scaffold surface was determined using contact angle (θ) measurement using DSA 100 drop shape analyser (Krüss GmbH, Hamburg, Germany). The sessile drop technique was used. The needle was using a droplet of 20 µl water as the solvent on to 6 different regions on the surface, and θ was measured (n = 6 per condition) and analysed by DSA program version 1.9.2.1.1 (1997-2008). The measurement was performed on normal non-porous POSS-PCU sheet, under sterilisation technique (autoclave and EtOH treated) and

under single aqueous solution (absolute ethanol, 70% ethanol, and PBS). The lower of θ resulted in higher relationship in hydrophilicity and surface wetting (Figure 5.1).

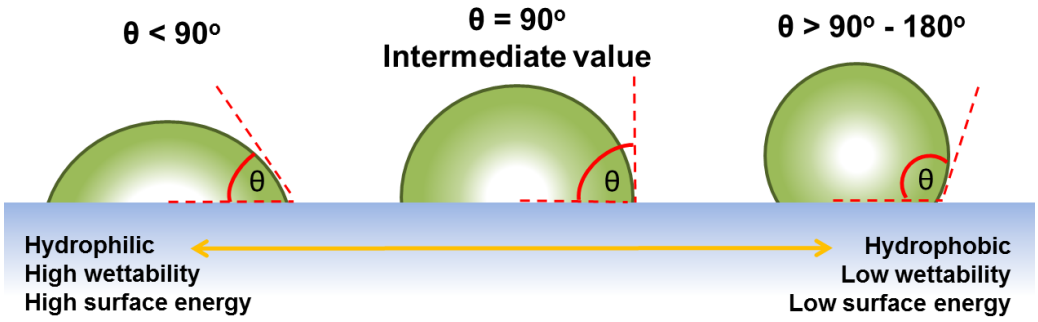

Figure 5.1 Sessile drop shape relating θ and hydrophilic/hydrophobic relationship.

5.2.1.3 Effect of sterilisation on casted POSS-PCU surface chemistry

ATR-FTIR spectroscopy (JASCO FT/IR 4200, Jasco, Tokyo, Japan) was used to analyse any alteration in the surface chemical functional groups before and after sterilisation.

Spectra were produced from an average of 20 scans at 4 cm^{-1} resolution over a range of 600 cm^{-1} to 4000 cm^{-1} wavenumbers. POSS-PCU showed absorption bands characteristic of poly(carbonate urea-urethane) with the main peaks from the soft segment at 1738 cm^{-1} (carbonate C=O stretching from carbonate) and 1242 cm^{-1} (carbonate C-O-C stretching).

The urethane/urea groups of the hard segment give rise to bands at 3323 cm^{-1} (N-H asymmetric stretching), 1525 cm^{-1}(CHN deformation) and 1065 cm^{-1}(urethane C-O stretching).

The aromatic rings of the urea/urethane hard segments show absorption bands at 1635 cm^{-1}, 1591cm^{-1} and 1465 cm^{-1} (p-substituted stretching) and also at 1017 cm-1, 957 cm^{-1} (p-substituted C-H bending) and 791cm^{-1}(p-substituted C-H deformation).

The Polyhedral Oligomeric Silsesquioxane is characterised by the absorption band at 1112 cm^{-1} (cage Si-O-Si stretching).

Alkyl groups from the carbonate soft segment and also iso-butyl POSS give absorption bands at 2938 cm^{-1} (C-H asymmetric stretching), 2802cm^{-1}(C-H symmetric stretching) and 1403cm^{-1}(C-C stretching).

The resulting spectrum represents the molecular absorption and transmission, creating a molecular fingerprint of the sample. Absorptions due to water and atmospheric air were subtracted.

5.2.1.4 Effect of sterilisation on surface topography

The sterilisation was performed on casted non-porous POSS-PCU using autoclave and ethanol cleanse previously described in section 3.5. Each sample was placed on the stub and imaged as previously described in section 3.4.

5.2.1.5 Analysis of ethanol extraction of POSS-PCU materials

In ethanol cleanse, absolute ethanol firstly came in to contact with POSS-PCU material and it was known to dissolve POSS crystal. Therefore, the trace of dissolved POSS particles was extracted and analyse (Butterworth Laboratories, Teddington, UK). Briefly, 1g of casted POSS-PCU or dried microporous (70% $NaHCO_3$) POSS-PCU was weighed into a vial to which 5 mL of absolute ethanol was added. After 5 min, the test item was removed from the solvent. A 1000ppm solution of POSS in ethanol was also prepared. Ethanol extracts/solutions were then tested for volatile and semi-volatile organic components by Gas Chromatography Mass Spectrometry (GC-MS) and trace metals by Inductively Coupled Plasma Optical Emission Spectroscopy (ICPOES).

5.2.1.6 Assessment of casted POSS-PCU mechanical properties

Mechanical testing of the casted POSS-PCU with autoclave and ethanol sterilisation (n = 4 per condition) was performed with a uniaxial tension on the Instron 5565 testing system (Instron Corporation, High Wycombe, UK) as previously described in section 3.3.

5.2.2 Material properties of microporous POSS-PCUs

5.2.2.1 Assessment of microporous POSS-PCU mechanical properties

Mechanical testing of the microporous POSS-PCU scaffolds at different % $NaHCO_3$ (n = 6 per condition) was performed with a uniaxial tension on the Instron 5565 testing system (Instron Corporation, High Wycombe, UK) as previously described in section 3.3.

5.2.2.2 Assessment of microporous POSS-PCUs porosity

Microporous POSS-PCU sheets were fabricated in to 3-mm thickness as described in section 3.1.3. They were cut in to 16 mm circle discs (n = 6 per condition), completely dried in the oven for 48 h and measured the dry weight. The porosity of each condition was calculated using the following equations previously published by Ahmed *et al.*[83]:

$$\text{Porosity (\%)} = (1 - d/d_p) \times 100$$

Where d is the density of the scaffolds and d_p is the density of non-porous polymer which is equal 1.15 g/cm3. The density of the scaffold, d, can be calculated from:

$$D = m/v$$

Where m is the mass and v is the volume of the scaffold.

5.2.2.3 Assessment of microporous POSS-PCU permeability

Water permeability of microporous POSS-PCU samples were assessed using custom designed apparatus by connected to 500 mL pressure infuser bag to a pressure metre (Figure 5.2). Briefly, the microporous POSS-PCU sheets were cut into 2 cm x 2 cm, samples with a standard thickness value of 500 µm (± 25). The membrane was inserted in to the stage. The cover was mounted across the sample and placed in to the holder followed by 4 bolts. Then, the bolts were tightened to prevent the side leakage and forced the water to pass through membrane. The water pressure was generated by 500 mL pressure infuser set to 100 mmHg using the pressure metre. Measurements were recorded over a 1 min interval. The amount of dH_2O that passed through the membrane was collected using an analytical balance (Mettler-

Toledo, Leicester, UK). Microporous POSS-PCU sheets composed of 30% $NaHCO_3$, 50% $NaHCO_3$, M70% $NaHCO_3$, coagulated POSS-PCU with no $NaHCO_3$, and non-porous casted POSS-PCU were used in this experiment. (N = 6 per condition)

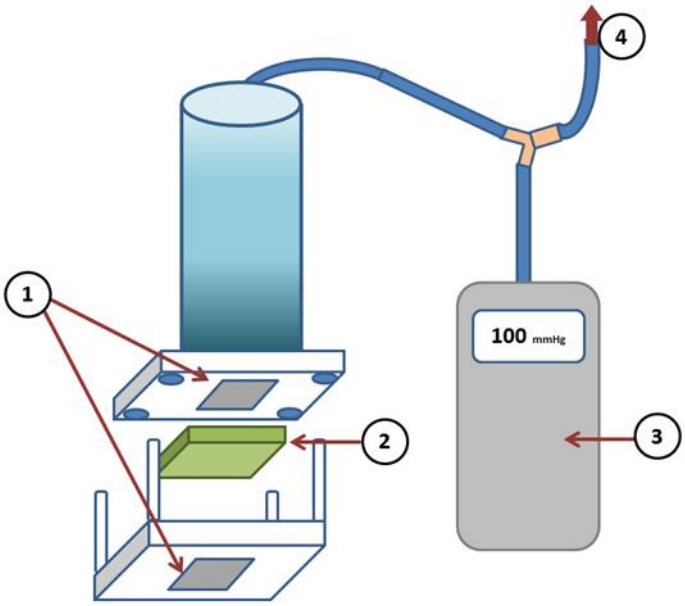

Figure 5.2 Schematic representative of a water permeability testing system. 1) stage and lid with 1cm X 1cm sample window, 2) sample sheets, 3) pressure metre, and 4) tubing connected to 500 mL pressure inducer.

5.2.2.4 Pores morphology of microporous POSS-PCU using scanning electron microscopy (SEM)

Samples were processed, placed on the stubs and imaged as previously described in section 3.4.

5.2.3 Effect of sterilisation on bovine serum albumin (BSA) adsorption of microporous POSS-PCU

Bovine serum albumin (BSA) was used as an adsorption model in this experiment to mimic the protein-material interaction when the plasma comes into contact with the material. BSA is the most abundant protein in the plasma[119], have been used in adsorption

experiment on many materials including polymer[109,120–122], and is compatible with the BCA assay protein quantification kit (Pierce Biotechnology, Illinois, USA).

Total protein adsorption was quantified using protein depletion in bulk solution method adapted from Akkas *et al*. [123]. 16 mm Ø scaffold discs with thickness of 500±25 µm were placed in 7 mL bijou tubes. Then, 1 mL of 100 µg/mL or 500 µg/mL BSA in PBS was added into each tube. Incubation of each sample was performed at 37^{o} C for 24 h. The depletion of protein (BSA) in the bulk solution was investigated using the BCA protein quantification kit previously described in section 3.5. The absorbance was read at 562 nm. The data were normalised to % adsorption using equation below.

$$\% \text{ Adsorption} = \left(\frac{\text{Absorbance}_{\text{total protein}} - \text{Absorbance}_{\text{sample}}}{\text{Absorbance}_{\text{total protein}} - \text{Absorbance}_{\text{blank}}} \right) X\ 100$$

Adsorbed protein amount was also calculated referring to BSA standard curve.

5.3 Results

5.3.1 Sterilisation and effects on casted POSS-PCU bulk properties

5.3.1.1 Effect of sterilisation techniques on casted POSS-PCU wettability

Wettability of the materials after sterilisation was determined by θ measurement to investigate the effect on surface properties. The θ quantitative measurements and qualitative images were presented in Figure 5.3. The θ of non-treated POSS-PCU was 112^{o} ±4.38 whereas the autoclaved POSS-PCU was significantly lower at 96^{o} ±3.48 ($P < 0.05$). The EtOH cleansed POSS-PCU presented significantly lower θ at 76^{o} ±3.48 ($P < 0.05$) which had no difference from gold-standard tissue-culture TCP's (74^{o} ±3.32, $P > 0.05$).

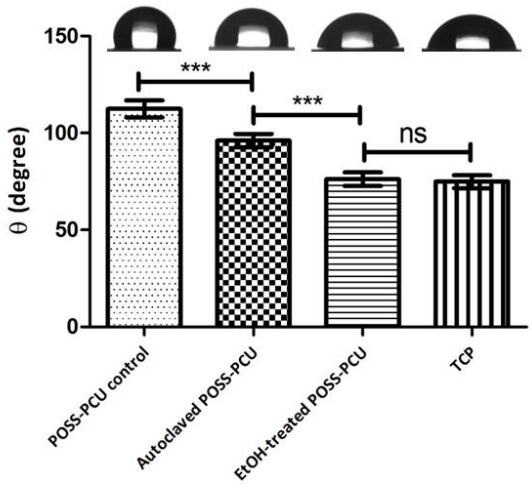

Figure 5.3 θ of casted POSS-PCU materials before and after autoclave and ethanol cleanse, comparing to gold standard tissue-culture TCP. (ns = non-significant, *** $P \leq 0.001$) (n=6)

5.3.1.2 Effect of sterilisation on casted POSS-PCU surface chemistry

Sterilisation techniques had an effect on detection of chemical groups on POSS-PCU surface. ATR-FTIR showed significant changes in the peak of C=O (1737.55 cm-1), C-O-C (1241.93 cm-1), and Si-O-Si (111.76 cm-1) (Figure 5.5). The absorbance of each peak was extracted using Microspectra Analysis software. Statistical analysis (Figure 5.4) revealed autoclave samples and EtOH treated samples had significant increase of C=O and C-O-C peaks but significant lower in Si-O-Si peak comparing to control POSS-PCU.

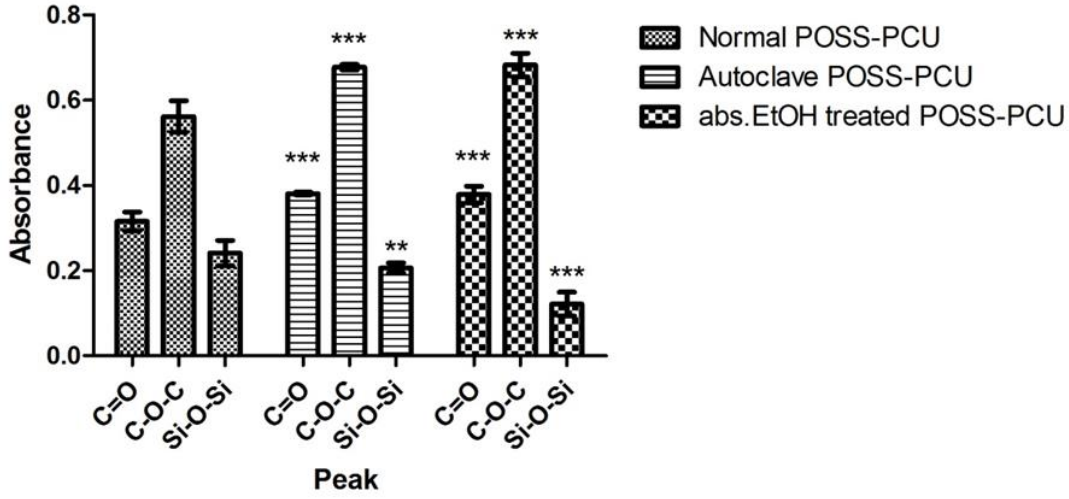

Figure 5.4 Autoclave samples and absolute EtOH treated samples had highly significant difference in these three peaks comparing to control POSS-PCU (**$P \leq 0.01$ and ***$P \leq 0.001$).(n=6)

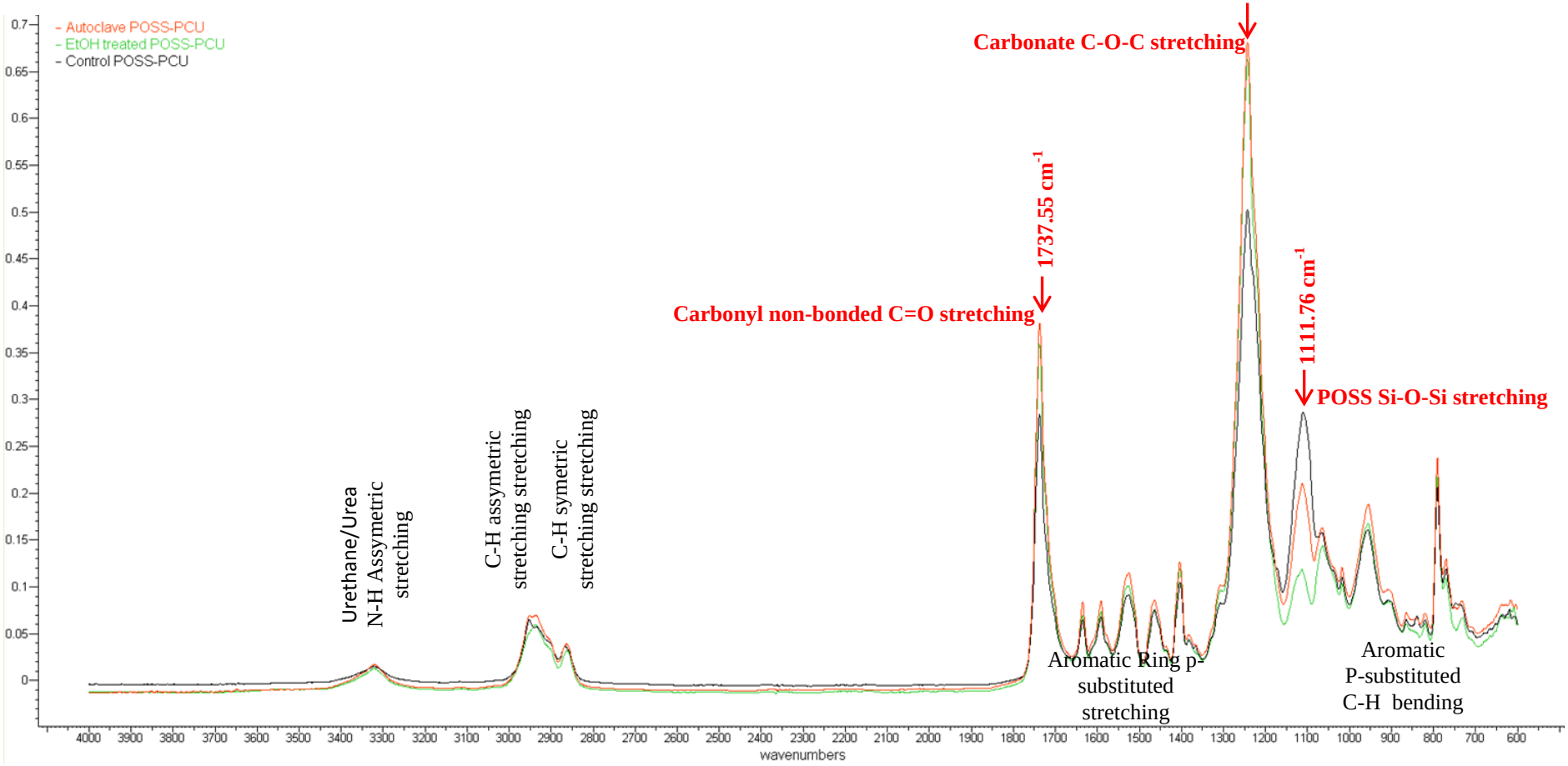

Figure 5.5 FTIR analysis showed absorbance changes in C=O, C-O-C and Si-O-Si peaks after sterilisation.

5.3.1.3 Effect of sterilisation on surface topography

Qualitative surface topography was visualised using SEM in **Figure 5.6**. POSS-PCU control presented structures similar to the cracks, or aggregation of 5 μm and larger particles covering most of the surface. However, autoclave and EtOH treated POSS-PCUs had a relatively smoother surface comparing to the control. The large particles disappeared but small particles less than 5 μm still presented and distributed slightly on the surface.

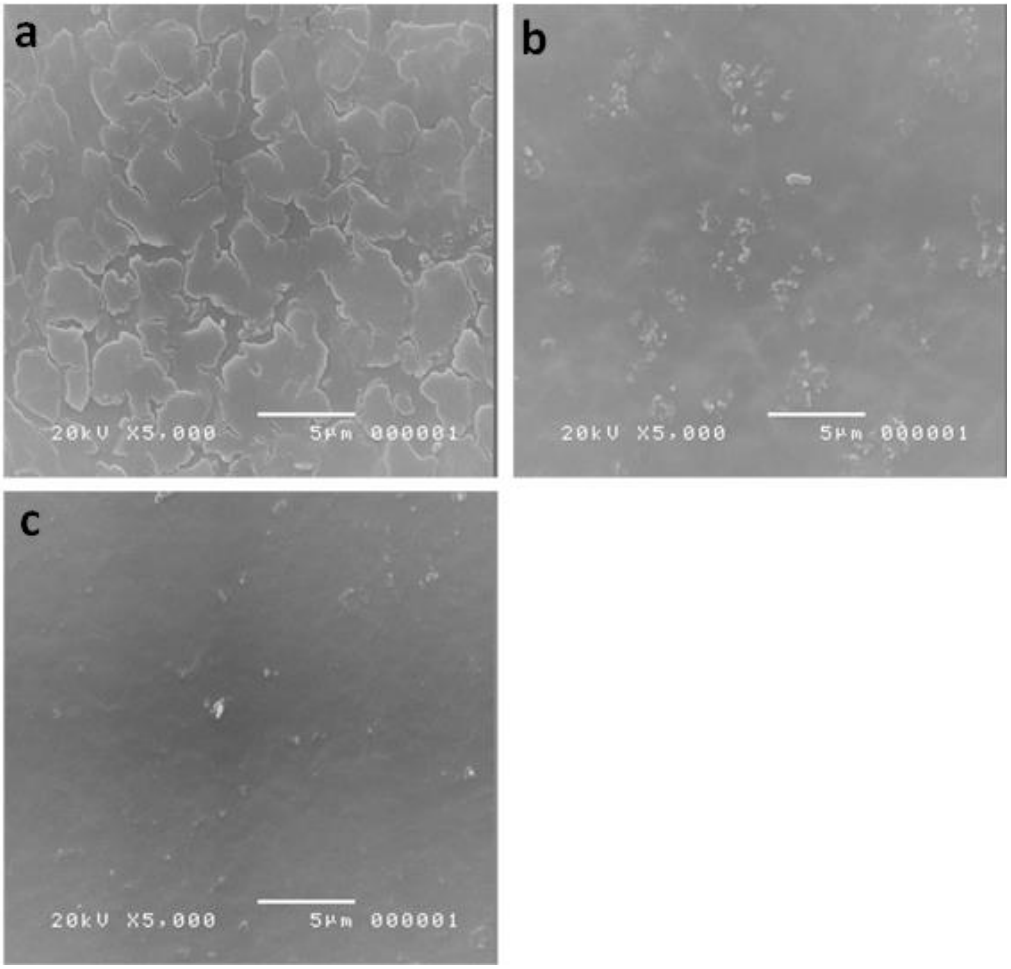

Figure 5.6 SEM images on surface of (a) control POSS-PCU, (b) autoclave POSS-PCU, and (c) EtOH treated POSS-PCU.

5.3.1.4 Analysis of ethanol extraction of POSS-PCU materials

There was no leachable organic compound detected (from hard or soft segments of POSS-PCU) other than ethanol and the internal standard observed in the GCMS analysis.

ICPOES analysis demonstrated silicon leached from casted POSS-PCU was less than 10 µg/g sample (detectable in very low amount) while the 70% $NaHCO_3$ POSS-PCU was detected at 12 µg/g sample.

5.3.1.5 Effect of sterilisation on material mechanical properties

There was no significant difference between all pairs of samples ($P > 0.05$) in terms of maximum stress and Young's modulus (Figure 5.7), suggested that sterilisation techniques did not affect the mechanical properties of the material.

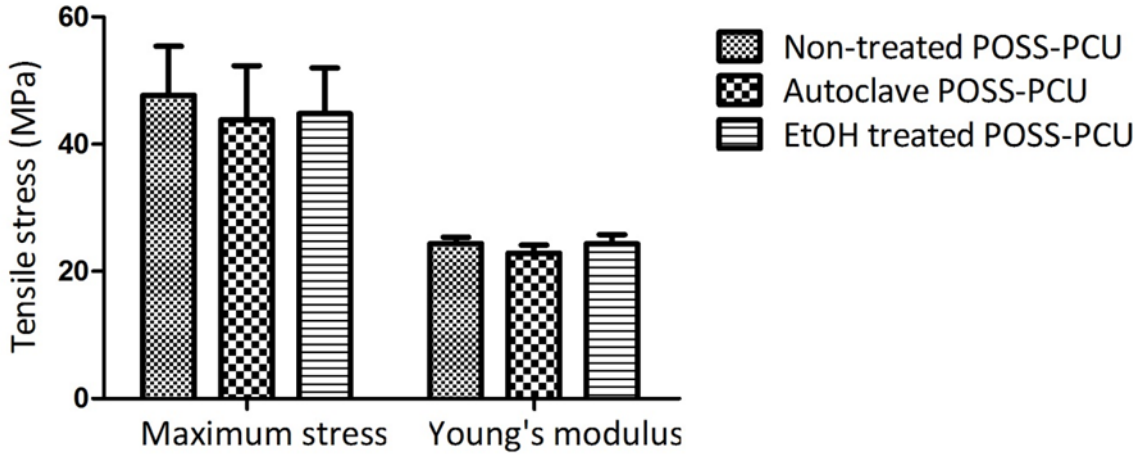

Figure 5.7 Showing mechanical properties of POSS-PCU after sterilisation comparing to non-treated control. (n=4)

5.3.2 Material properties of microporous POSS-PCUs

5.3.2.1 Assessment of microporous POSS-PCU mechanical properties

In Figure 5.8, the mechanical properties of microporous POSS-PCU materials were determined using the maximum stress and Young's modulus, which significantly decreased

in the higher % of $NaHCO_3$ ($P \leq 0.001$ in all pairs). The means of stress were 0.98±0.07, 0.63±0.06, and 0.19±0.02, for 30%, 50%, and M70% $NaHCO_3$ respectively, whereas the means of Young's modulus were 0.26±0.02, 0.19±0.01, and 0.13±0.01, respectively.

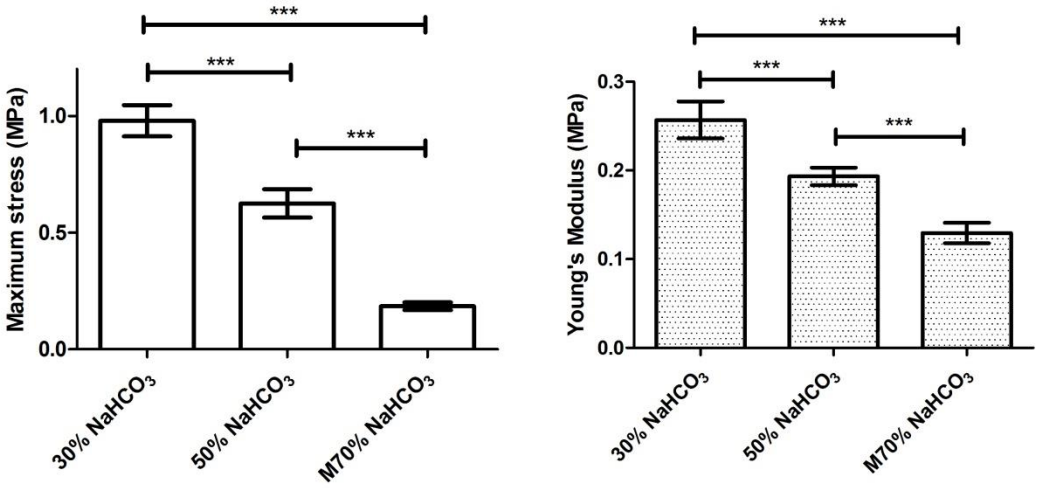

Figure 5.8 Mechanical properties of microporous POSS-PCU materials, showing the maximum stress at break point of the materials (left), and the stiffness presented in Young's modulus (right). (***$P \leq 0.001$) (n=6)

5.3.2.2 Assessment of microporous POSS-PCUs porosity

The average % porosity of microporous POSS-PCUs were 86.69%, 90.75% and 94.37% for 30%, 50% and M70% $NaHCO_3$, respectively. This indicated the porosities significantly went up ($P \leq 0.001$ in all pairs) when increasing the % $NaHCO_3$ (Figure 5.9).

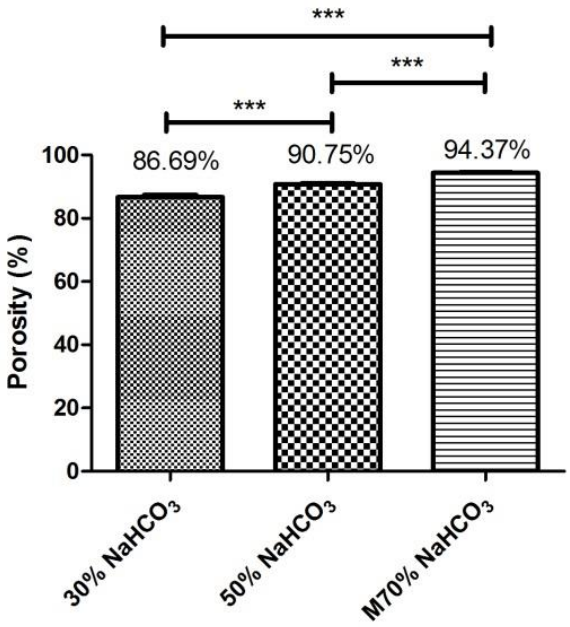

Figure 5.9 Porosities of microporous POSS-PCUs, showing the mean value of 30%, 50% and M70% $NaHCO_3$ (*** $P \leq 0.001$) (n=6)

5.3.2.3 Assessment of microporous POSS-PCU permeability

The determination of permeability was shown in Figure 5.10. The M70% presented the significantly highest water flow at 361.0 L/cm^2/min ($P \leq 0.001$). The 50% $NaHCO_3$ demonstrated the water flow at 28.85 L/cm^2/min which was significantly higher than the 30% $NaHCO_3$ at 12.17 L/cm^2/min ($P \leq 0.05$). Despite some permeability presented in the 30% $NaHCO_3$, it did not have any statistically difference from the non-porous POSS-PCU, which was the negative control and exhibited no water permeability ($P > 0.05$).

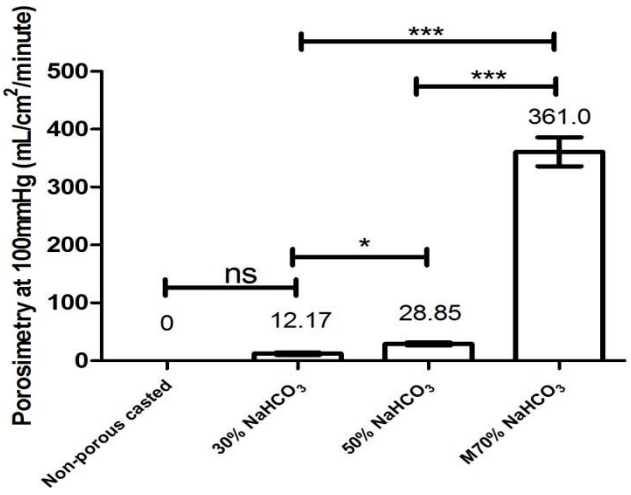

Figure 5.10 Water permeability of non-porous and microporous POSS-PCU materials. (ns = non-significant, * $P \leq 0.05$, *** $P \leq 0.001$) (n=6)

5.3.2.4 Pore morphology of microporous POSS-PCU using scanning electron microscopy (SEM)

Qualitative images from random locations of the samples were shown in Figure 5.11. The cross-sectional images showed the higher inter-connected pores and the higher open porous structure on the surface when increasing the %$NaHCO_3$.

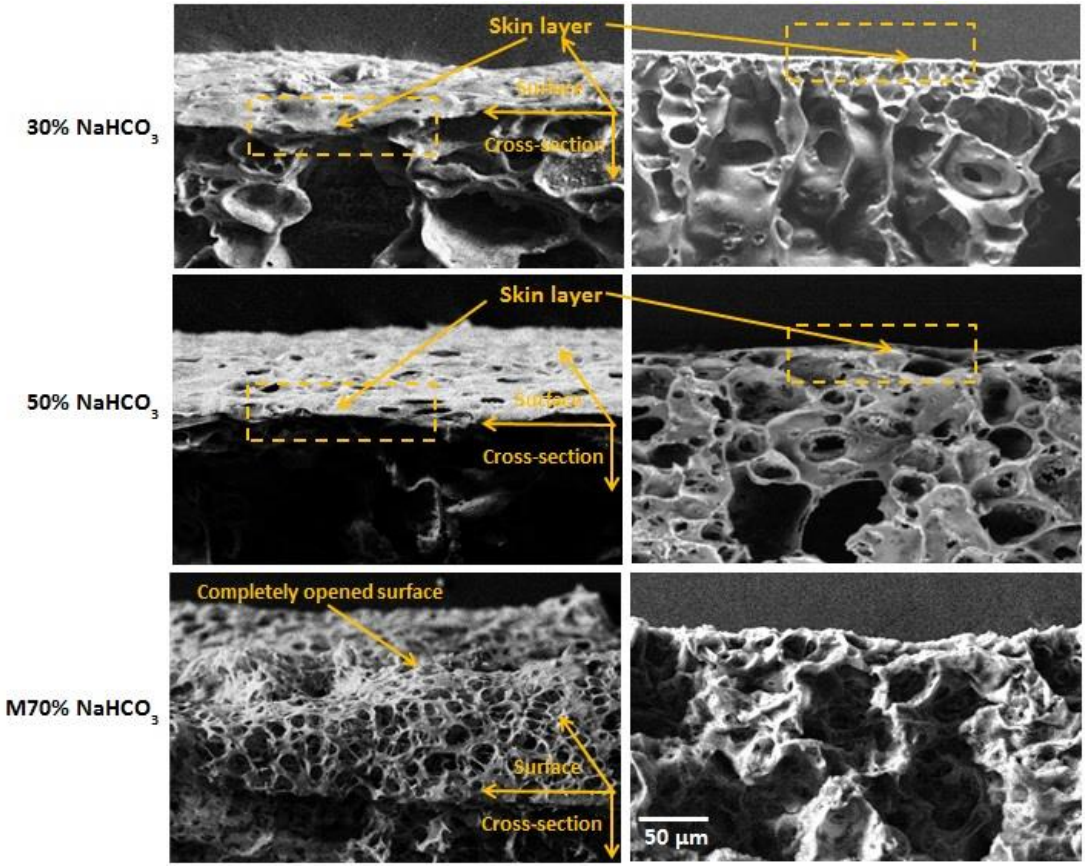

Figure 5.11 SEM images of cross-sectioned microporous POSS-PCUs in different % $NaHCO_3$

5.3.2.5 Effect of sterilisation on BSA adsorption of microporous POSS-PCUs

BCA protein assay demonstrated a linear relationship of spectrophotometric absorbance and BSA concentrations shown in Figure 5.12 ($P < 0.05$, $R^2 = 0.9827$). The depletion of total protein in the bulk solution was determined by % adsorption. Microporous POSS-PCUs with different types of sterilisation were observed the adsorption of BSA at 100 µg/mL and there were significant difference in % adsorptions between autoclaved samples and EtOH cleansed samples ($P < 0.05$). For autoclaved samples, there were no significant differences ($P > 0.05$) of % adsorption among 30%, 50% and M70% $NaHCO_3$ (average = 16.65%, 13.20%, and17.53%, respectively). However, the ethanol treated samples demonstrated significantly higher % adsorption comparing to the autoclaved samples ($P < 0.001$). The 30%, 50% and M70% $NaHCO_3$ presented the average % adsorption at 38.41%, 68.37%, and 93.68%, respectively.

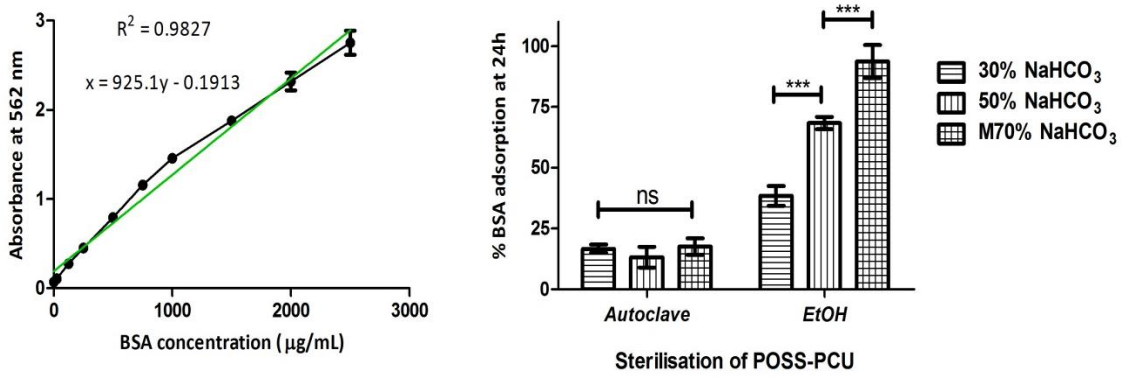

Figure 5.12 Graphs showing a linear relationship of absorbance and BSA concentration (left), and % adsorption at 100 µg/mL BSA (right). ***$P < 0.001$, ns = non-significant (n=4)

5.4 Discussion

5.4.1 Sterilisation and effect on casted POSS-PCU bulk properties

5.4.1.1 Sterilisation techniques had an effect on POSS-PCU wettability

Surface wettability was also examined for POSS-PCU material under different sterilisation techniques. Non-porous POSS-PCU was chosen in the θ experiment to reduce the effect of open pores on surface in particle-leaching/coagulation samples, which could have a top-up effect and change the θ as a result of topography changing. Our results showed the original form of non-porous POSS-PCU was relatively hydrophobic ($\theta > 90^{o}$). However, material surface became more hydrophilic after sterilisation, especially the EtOH treated, which demonstrated the θ similar to TCP's. Lower contact angle resulted in higher surface energy and wettability, therefore, the solution spreads more on the surface and proteins have more chance to interact with the surface. Regardless of the literatures, cells effectively adhere onto polymeric material surface with θ of 40-70^{o} [124],[125],[126],[127]. This led to our hypothesis that EtOH treated POSS-PCU would probably have better protein adsorptions, thus, improving of cell-material interaction in the experiment.

5.4.1.2 Sterilisation techniques altered the surface chemical groups

Polyurethane-based materials (PUs) are frequently used in a variety of blood contacting medical devices due to their desirable mechanical properties, fatigue resistance, and acceptable hemocompatibility[128],[129]. Material surface usually interacts with environment; therefore, changes of surface chemicals after sterilisation were also investigated using ATR-FTIR. Our material also showed the different characteristic of the surface after sterilisation process in aqueous solution. POSS-PCU samples were submerged in deionised water during autoclave while ethanol cleanses, samples were submerged in absolute ethanol, 70% ethanol, and PBS, respectively. After the process, they were measure chemical groups by ATR-FTIR and presented difference absorbance in the peaks of C=O, C-

O-C and Si-O-Si, comparing to the control. The samples after sterilisation increased in the peaks of C=O and C-O-C but reversely decreased in Si-O-Si. This indicated the less appearance of POSS but probably more enrichment of PCU segments and suggested there were some factors that altered the material surface.

According to ATR-FTIR profiles we had come up 2 hypotheses which were 1) the washing away of unreacted POSS on the surface and 2) the response of material surface due to aqueous environment. There were possibilities that the surface alteration was caused by either washing of POSS or surface response or a combination of these two. Our preliminary experiment on POSS particles indicated that they could be dissolved in absolute ethanol but not water (data not shown). In autoclave samples, reduction of POSS peak but presented more C=O and C-O-C peaks is probably cause by just the surface response to aqueous solution. C=O and C-O-C was presented mostly in the hard segment that was shown the schematic diagram of POSS-PCU molecular structure in Figure 1.3. When the hard segment of POSS-PCU appeared more on the surface, it probably create more negative dipole on the surface caused by C=O and C-O-C.

PUs are copolymers constructed form a mixture of soft and hard segments that form a microphase-separated structure as a result of thermodynamic immiscibility the polar hard segment and the relatively non-polar soft segment[113]. Agnihotri *et al*. had investigated the reorientation of PU's surface using topographical images from atomic force microscopy (AFM). The result demonstrated the hydrophilic hard segment of poly(urethane urea) appeared more on the surface with rougher structure after incubate the material in aqueous solution (1mM phosphate buffer) after 24h and was quite different from those of ambient conditions (air) [107]. Likewise, the hydrophilic part of POSS-PCU component might rearrange and come up to the surface as well.

5.4.1.3 Wettability results were related with chemical group changes

This result of FTIR related back to the contact angle results. When the hydrophilic part of the polymer appeared more on the surface, it could affect in the reduction of θ. There was demonstration previously that the θ of autoclave conditions reduced the contact to around 96^{o} while the ethanol treated reduced it to around 76^{o}, which was similar to TCP's at 74^{o}. When relating θ profile to the ATR-FTIR profile, the information was relevant to each other by the more appearance of C=O and C-O-C when exposed in aqueous solution (water in autoclave and ethanol/PBS after ethanol cleanse), and resulted in the more hydrophilicity (reduction in θ).

However, the ethanol treated had higher hydrophilicity than the autoclave one. This might be another effect of washing POSS away by absolute ethanol which was mentioned previously. The θ measurements of POSS-PCU treated in single type of solutions demonstrated that they did not reduce straight away to 76^{o} after treated with absolute ethanol but reduce in different degree and PBS demonstrated the most reduction of θ. This also confirmed that in ethanol cleanse technique, there might be 2 effects involved which were 1) the washing away of unreacted POSS (presented by ATR-FTIR) and 2) surface rearrangement under PBS solution (presented by contact angle profile).

5.4.1.4 Sterilisation techniques affected the surface but not the bulk mechanical properties of the material

The qualitative confirmation of surface changes had demonstrated in SEM images. Non-treated POSS-PCU had obvious rough structure on the surface which was probably caused by unreacted POSS particles aggregated on the surface, while the autoclave and EtOH-treated had changed to smoother surface. The analysis of ethanol extraction by ICPOES showed that silicon was detectable but in very low amount in ethanol extracts solution. This had confirmed that POSS leached out and was accounted for surface changing. However, GCMS results demonstrated no organic compounds were detected, especially the aromatic

compound from the hard segment which is carcinogenic. This also indicated that despite the washing away of unreacted POSS on the surface, the ethanol rinse did not break the main chemical structure of POSS-PCU. The result was also confirmed by no significant changes of mechanical properties of tested on the materials in different sterilisation techniques. Notably, the EtOH cleansed POSS-PCU had no significant difference of contact angle comparing to TCP which was commercially optimised for cell culture. Therefore, EtOH treated POSS-PCU would have the similar protein adsorption and cell viability to TCP.

5.4.2 Material properties of microporous POSS-PCUs

Tissue engineering employed scaffolds as a matrix for cell seeding. The architecture of 3D structures plays critical role in cell adhesion, proliferation, migration and organisation into specific tissue while creating extracellular matrix component[130]. There were various ways to create the microporous structures in the polymer scaffold such as gas foaming[131], freeze-drying[132], and particulate leaching[133]. The focus was on particulate-leaching technique regardless of its simplicity and cost-efficiency[134]. The fabrication of microporous POSS-PCU scaffold employing this technique had been reported by Ahmed et al. using POSS-PCU with 40 µm $NaHCO_3$ for vascular graft application[83]. Also, this fabrication technique had been used in subsequent research such as POSS-PCU scaffold with 140-150 µm NaCl for auricular reconstruction[135]. $NaHCO_3$ was employed in this study because of its advantage in commercially available in various pre-sieved particle sizes (TATA chemicals, Northwich, UK). In this study, the commercial pre-sieved $NaHCO_3$ were obtained, however; the sieving was proceeded again to obtain the range of 25-53 µm. This range was interesting because the cell size (planimetry width) is approximately 10 µm for nasal and bronchial epithelial cells[136], therefore, ideal pores should be slightly bigger to fill up couple of cells and allow them to have cellular interactions.

5.4.2.1 More porogens reduced the bulk mechanical properties

Different % $NaHCO_3$ was studied to see the effect on material properties. Mechanical properties are one of the criteria in biomaterial sciences. It demonstrated that increasing of % $NaHCO_3$ resulted in significant reduction in strength (maximum stress) and elasticity (Young's modulus). This point should be aware of when optimising % particles for making the actual 3D organ to make the scaffold integrated by new tissue and withstand the premature collapse. 3D scaffold offers the essential support for cells to proliferate and maintain their growth. The requirements for promoting cell growth into the functional tissue require the scaffold to offer several unique features such as porosity, interconnectivity, surface wettability, protein adsorption, and cytocompatibility.

5.4.2.2 More porogens increased the porosity

High porosity is one of the conditions to provide space for the cells to attach and generate extracellular matrix[137]. The porous structure also enables angiogenesis after implantation; therefore, blood vessels can develop and supply oxygen and nutrients to the construct. Our data showed scaffolds had high porosity around 86% or above and the porosity had significant increase when % $NaHCO_3$ was higher. The explanation why all scaffold had porosity greater than 80% had been revealed when looking into its mixed compositions. P9 POSS-PCU (18% w/w POSS-PCU) had already contained 82% w/w of DMAC as a solvent while % $NaHCO_3$ was varied such as 30% w/w, 50% w/w or 60% w/w for modified 70%, were mixed later to create porous structure. The major of compositions of the whole polymer were $NaHCO_3$ and DMAC (solvent) which will be dissolved away during particle-leaching/coagulation and left a lot of space in the POSS-PCU scaffold as pores.

5.4.2.3 More porogens increased opened pores on the surface, inter-connectivity, and water permeability

The porosity alone might not represent how well the pores are interconnected and this might affect insufficient water permeability. Therefore, the permeability testing was carried out using our own custom-made tube. The results showed in our study that incorporating $NaHCO_3$ particles promoted open pores to the surface as well as interconnections between pores, thus, the water could pass through, while the non-porous did not present water permeability. This indication confirmed that incorporating of porogen is necessary if water permeability is taken into account. The quantitation of water also related to how well the pores connected. M70% had presented the significantly higher water permeability than 30% and 50% $NaHCO_3$ and was confirmed by SEM images to have more interconnected pores when increasing the % $NaHCO_3$. These findings were very important for the nutrient transportation in the following experiments such as air-liquid interphase culture as well as enhancing the cell integration to the scaffold (Chapter 6).

5.4.2.4 Ethanol sterilisation promotes the protein adsorption of microporous POSS-PCU

When material is implanted in the body, it will interact with protein in seconds and result in protein adsorption on the surface. As proteins coats the material surface, the cells "see" the material as a layer of proteins and this attracts the cell and promote cell attachment or integration[138]. Colorimetric BCA assay was employed to quantified total proteins in bulk solution before and after adsorption process on microporous material. The EtOH treated samples presented significantly higher adsorption rate comparing to the autoclave samples. This might relate back to the θ profile on material surface after sterilisation (96^o for autoclave and 76^o for EtOH treated). Tamada and Ikada had reported the optimal θ that promote both maximum protein adsorption and cell adhesion was around 60-80^o and polysterene material ($\theta = 75^o \pm 2$) fell in to this category[139]. This also similar to our own

measurement ($\theta = 74^{o}\pm3.32$) of the TCP which is commercially optimised for cell culture. M70% $NaHCO_3$ had significantly more adsorption than the 30% and 50% $NaHCO_3$. This might also be the influence of interconnectivity between pores of the material. The more interconnectivity of M70% $NaHCO_3$ might lead to the higher inflow and more interaction to inner surface.

Microporous POSS-PCU had shown promising characteristics for cell culture; however, more studies need to be carried on in the future to get better understanding of this material's behaviour. Sterilisation techniques affected the surface properties of the scaffolds with changes in protein adsorption rate. The wettability of the bulk surface and chemical groups were examined. According to protein adsorption principles, many theories could be applied but the one has not been examined is the electrostatic interaction via surface charge. Sanchez-Perez et al. investigated BSA adsorption to hydrophobic polystyrene nanosphere and found it adsorbed more when the more negative charge was presented[140]. In addition, Khorasani et al. had presented O_2 plasma treated increased more negative charges on silicone and PU surface as well as enhanced fibroblasts attachment and growth[141]. However, too much force of electrostatic or hydrophobic interaction can have a negative effect and change the orientation or conformation of proteins and therefore, loosing of their function[142].

Our result showed the θ of EtOH treated POSS-PCU reduced to the similar level to the TCP and resulted in significant protein adsorption. This phenomenon cannot be clearly explained at this moment but will be the challenging study in the future regarding surface charge. Zeta potential measurement could be another interesting method to study the negative or positive charge on POSS-PCU surface related to electrostatic protein adsorption and cell attachment.

5.5 Conclusions

Incorporation of micro-particles such as $NaHCO_3$ enhances the benefit of open pores on surface as well as interconnected pores related to the water permeability. However,

increasing of porosity (% particles) might lead to the lower mechanical properties which might have to be aware of. In addition, the sterilisation techniques did affect the changes on surface properties of POSS-PCU; however, they did not affect the bulk mechanical properties or induce the destruction that may cause the harmful chemicals. The protein adsorption results show significant difference, due to the changes in surface properties. Ethanol sterilisation induced more protein adsorption of the materials than those in autoclave. This technique was chosen for the cell culture seems to be the optimal option for disinfecting the material for *in vitro* culture with more favourable cell growth. The full study on HBECs growth and differentiation will be fully presented in the following chapter.

Chapter 6 Human bronchial epithelial cell culture and *in vitro* epithelialisation on microporous POSS-PCU scaffold

6.1 Introduction

The airway system can be divided into two discrete functions, 1) the conditioning part in which the inhaled air is cleaned, moistened, and transported to the distal part of the airways, and 2) the respiratory part where the blood is oxygenated, the alveoli. The conditioning part comprises of the nasal cavities, pharynx, larynx, trachea, bronchi, and large and terminal bronchioles, and the respiratory part of respiratory bronchioles and alveolar ducts[143]. The main cell types of the airway epithelium are ciliated, goblet, and basal cells[79]. Goblet cells secrete mucus to the airway lumen which lubricates the apical surface of the epithelial layer, moistens the inhaled air and helps to trap pathogens and foreign material particles from the environment[80].

The need for a prosthetic upper airway replacement is continually modified by improved surgical techniques with primary reconstruction and interventional techniques. Synthetic prostheses such as flaps, tube constructs, and stents have been employed to maintain the structure of upper airway for the patients who have received laryngotracheal reconstructions due to disease, congenital defects or trauma. Previously, the synthetic prosthesis were usually made of rigid materials such as stainless steel[144],[145], silicone elastomers (silastic) [146],[147],[148], and silicone with a Dacron (PET) cover[149]. However, these materials did not become well integrated into the surrounding tissues. They also had problems with repeated infections, exhibited poor integration and subsequent dislodgement,

and developed granulation tissue at the anastomosis leading to airway obstruction[150],[151]. Modern implant designs have been developed and are now more sophisticated, with microstructures to allow more integration to the native tissues. Recently, microbead-based titanium implants have been developed for otorhinolaryngologeal applications[152]. The openly porous structures between the microbeads allow for better integration of the host tissue in vivo[152],[153],[60] which is a very important characteristic to sustainably keep the implant in place. This material has been subsequently studied in surgical sheep model[154] and used in a clinical trial for total laryngectomised patients to study tissue integration of an artificial larynx structure[2].

Creating a new functional laryngotracheal tissue is the ultimate goal for patients who have endured repeated surgeries. The optimal tissue repair for laryngotracheal reconstructions combining all 3 basic components, which are 1) structural support, 2) a functional mucosal lining and 3) vascular supply, has not been achieved yet despite many clinical advances in this area[155]. The nanocomposite material POSS-PCU has proven to be a good material for production of 3D hollow tubular organs, including 25mm diameter bypass grafts, about to enter clinical trials[95] and an airway replacement (trachea) in a compassionate case study[30],[156]. Also, it demonstrated that the combination of 2 fabrication techniques can successfully create a tubular structure for laryngotracheal applications, with a supporting rigid structure inside and microporous structure outside in chapter 4. This material has great potential to be further developed as a laryngeal implant for clinical applications. In this study, the microporous POSS-PCU material was optimised for in vitro epithelialisation of human bronchial epithelial cells (HBECs). In addition, the study of cell interactions with the scaffold material and examination of the gross morphology, will assist with future research in using either an acellular version of this microporous scaffold which can for example, act as a stent, or advance the tissue engineering approach to laryngeal reconstruction through the use of a cell-seeded scaffold to treat dysfunction.

6.2 Materials and methods

6.2.1 Culture media adsorption and HBECs growth on microporous POSS-PCUs

6.2.1.1 Optimisation of pre-adsorption time of cell culture media

The effect of protein adsorption was further investigated with a microporous material samples, which were pre-adsorbed with 1 mL of serum free cell culture media supplemented with artificial growth factors at different time points of 6h, 12h, 24h, and 48h. The reduction of proteins in the bulk solution was evaluated using a BCA assay protein quantification kit described in section 3.6. The optimal pre-adsorption time was determined where there was no more reduction of proteins in the bulk solution.

6.2.1.2 HBEC's growth on microporous POSS-PCUs

The seeding and culture of HBECs were performed according to section 3.8 using BEpiCM culture medium. Cell viability (n = 6) was assessed at day 1, day 4, day 7, day 11, and day 14 according to section 3.9. Cell proliferation was evaluated using total DNA (n = 4 per condition) was evaluated using the same time period as described in section 3.10. The scaffolds from day 7 were fixed and stained with phalloidin, anti-human vimentin, and anti-human ki-67 according to section 6.2.3. The total counts per field of view (560 x 420 μm) was not less than 6 frames and 250 cells per condition were recorded and analysed using ImageJ version 1.47 (National Institutes of Health, Maryland, USA).

6.2.2 Differentiation of HBECs via air-liquid interface cultures

6.2.2.1 HBEC culture and maintenance

HBECs in a T75cm^2 flasks were cultured to confluence the washed with 10ml of 20mM PBS without Ca^{2+} and Mg^{2+} . Next, 3 mL of 0.025% trypsin was added. The flask was incubated in 37^o C for 3 minutes until the cells became easily detached with gentle tapping of the side of the flask. 7 mL of fresh BEpiCM media (ScienCell, California, USA) was

added and the cell suspension was transferred into a 15 mL tube. The tube was centrifuged at 1,200 rpm for 5 minutes, after which the supernatant was discarded and the cell pellet was resuspend in 2 mL of new fresh BEpiCM media. A viable cell count was performed using the Trypan Blue exclusion assay followed by counting using a haemocytometer.

6.2.2.2 Seeding cell on polyethylene terephthalate (PET) transwell inserts

In a 24-well plate, 500 µL of BEpiCM was added to each well. A Falcon® 1.0 µm pore size polyethylene terephthalate (PET) (Becton Dickinson Labware, Claix, France) filter membrane was used as a positive control and was placed into the wells. Then, the upper chamber was filled with 200 µL of BEpiCM. 3 x 10^4 cells (1 X 10^5 cells per cm^2) were plated on to PET insert to promote cell proliferation and growth until nearly- confluent, according to the manufacturer's instructions. The PET inserts with adhered cells were cultured under Pneumacult™-ALI conditions as shown in Figure 6.1 for 3 days to promote cells attachment. After day 3, all the scaffolds were "air-lifted" by replacing 500 µL of Pneumacult™-ALI (STEMCELL technologies, Cambridge, UK) to the basal chamber only while the upper chamber was left empty to allow the cells to be exposed to the air. Nutrient levels were maintained by replacing the media in the lower chamber with fresh medium every 2 days.

6.2.2.3 Seeding cell on POSS-PCU transwell inserts

POSS-PCU scaffolds at different % $NaHCO_3$ were cut in to 16 mm Ø discs and clipped to CellCrown™ polycarbonate transwell housing for 24-well plate (Scaffdex Oy,Tampere, Finland). In new 24-well plate, 1.2 mL of BEpiCM was added into each well. POSS-PCU inserts were placed into the well and upper chamber was filled with 500 µL of Pneumacult™-ALI. 8 x 10^4 cells (1 X 10^5 cells per cm^2) were plated on to POSS-PCU inserts. POSS-PCU scaffolds with cells were cultured under BEpiCM for 3 days to promote cells attachment. After day 3, all the scaffolds were "air-lifted" by replacing 1.2 mL of

Pneumacult™-ALI to the basal chamber only while upper chamber was empty to let cells exposed to the air. Finally, the lower chamber was replaced with new medium every 2 days (Figure 6.1).

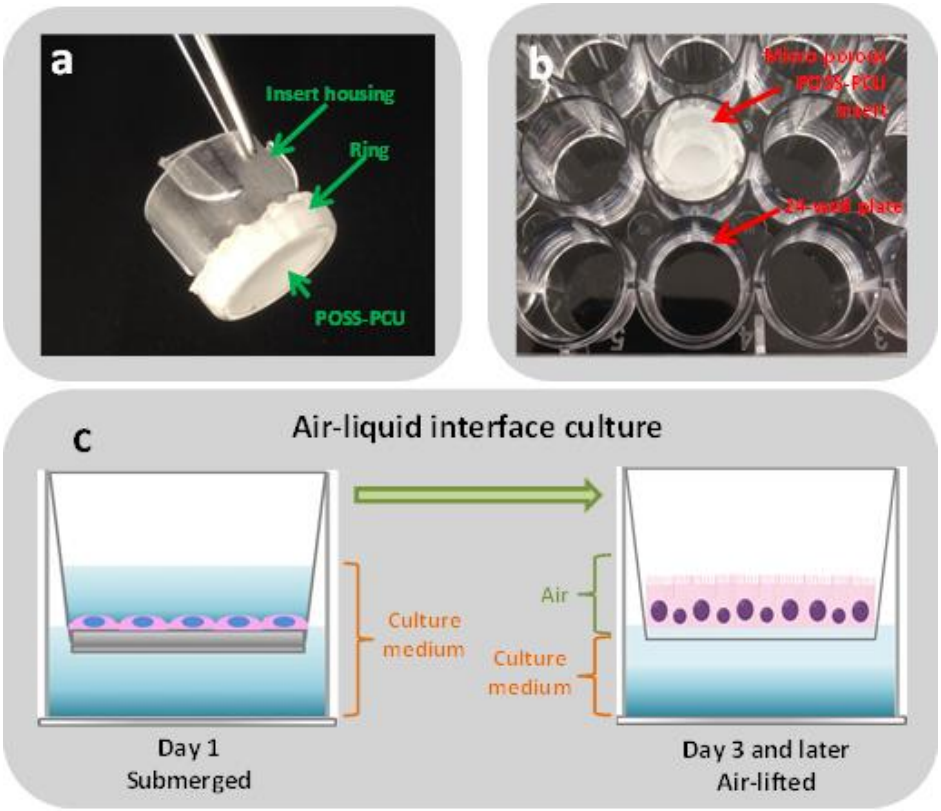

Figure 6.1 Illustration of a) POSS-PCU material clipped in housing inserts, b) the insert was put in transwell, and c) schematics of changing submerged culture (air-lifting) to air-liquid interface cultures (PneumacultTM –ALI) after 3 days.

6.2.2.4 Assessment of cell proliferation

Due to the limitation of cell viability assay that cells need to be submerged in culture media, only the total DNA quantification assay was employed as a measure cell proliferation. The procedure was performed as described in section 3.10.

6.2.3 Characterisation of HBECs and differentiated HBECs

HBECs were characterised via immunofluorescent staining using fluorescence dye and antibodies listed in Table 6.1 to demonstrate specific proteins, features, and structures of the cells. List of antibodies and fluorescent dyes were provided in Table 6.1.

Table 6.1 List of fluorescent dyes and conjugated antibodies.

Catalogue No.	Dilution	Chemicals	Company	Target
14530	0.01 µg/mL	Hoechst 33258	Sigma-Aldrich, Gillingham, UK	Nucleus
A12379	1 unit/200 µL	Alexa Fluor® 488 phalloidin	Life-technologies, Paisley, UK	F-actin
ab16667		Rabbit anti- Ki-67 (primary antibody)	Abcam, Cambridge, UK	Nuclear localised proliferative cell marker
ab195877	0.5 µg/mL	Mouse anti-vimentin Alexa Fluor® 488	Abcam, Cambridge, UK	Class III intermediate filament, Messenchymal marker
ab24610	1 µg/mL	Mouse anti-acetylated α-tubulin	Abcam, Cambridge, UK	Microtubule, cilia structure
ab24071	0.1 µg/mL	Mouse anti- Mucin 5AC	Abcam, Cambridge, UK	Mucin 5AC, airway secretory mucous
560061	1 µL/50 µL	Mouse anti-E-cadherin Alexa Fluor® 488	BD Biosciences, Oxford, UK	E-cadherin, adherens junction
ab53121	1 µg/mL	Rabbit anti - keratin 5 (Primary antibody)	Abcam, Cambridge, UK	Intracellular keratin 5, basal epithelial marker
MAB3234	1 µg/mL	Mouse anti-keratin 18 (Primary antibody)	Millipore, California, USA	Intracellular keratin 18, differentiated epithelial marker
ab150116	1 µg/mL	Goat anti-mouse Alexa Fluor® 594	Abcam, Cambridge, UK	Primary antibody
ab150077	1 µg/mL	Goat anti-rabbit Alexa Fluor® 488	Abcam, Cambridge, UK	Primary antibody
ab150080	1 µg/mL	Goat anti-rabbit Alexa Fluor® 594	Abcam, Cambridge, UK	Primary antibody
ab150117	1 µg/mL	Goat anti-mouse Alexa Fluor® 488	Abcam, Cambridge, UK	Primary antibody

6.2.3.1 Cell fixing and staining for histological analysis

All cellular samples were fixed in -20^{o} C with molecular grade absolute ethanol (Sigma-Aldrich, Gillingham, UK) for 30 minutes or up to overnight before being subjected to the staining process. For histological sectioning, the scaffolds were fixed in cold 4% paraformaldehyde (Sigma-Aldrich, Gillingham, UK) for 30 minutes or up to overnight (18h).

6.2.3.2 Histology

Fixed samples (n = 2 per condition) were sent to UCL IQPath (UCL, London, UK) for processing, scaffold sectioning and staining. Briefly, the scaffolds with cells were embedded in paraffin blocks and cut to 4 µm thick sections using a rotary microtome, Leica RM2235 (Leica Microsystem (UK) Ltd., Milton Keynes, UK). The slides mounted with sections were deparaffinised and treated with hematoxylin and eosin (H&E) staining to indicate the gross morphology of the cells and periodic acid-schiff staining to identify cells with mucosal substances according to IQPath's in-house protocol.

For antibody staining, the slides obtained from IQPath must first be deparaffinised. Briefly, the slides were immersed in a series of xylene and ethanol (Sigma-Aldrich, Gillingham, UK) to remove the paraffin in the following step-by-step manner:

1. 1st Xylene 3 minutes
2. 2nd Xylene 3 minutes
3. 1:1 Xylene-Ethanol 3 minutes
4. 100% Ethanol 3 minutes
5. 70% Ethanol 3 minutes
6. 50% Ethanol 3 minutes
7. 30% Ethanol 3 minutes
8. PBS 1 minutes

Next, the slides were gently tapped to remove excess PBS from the surrounding area of the section using Kimwipes (Kimberly-Clark Professional, Georgia, USA). A circle was

then drawn surrounding the sections on each slide using an ImmEdge hydrophobic barrier pen (Vector Laboratories, Peterborough, UK) to create a small staining area and prevent spillage of the stain.

The slides were stained with primary and secondary antibodies according to standard procedures outlined previously and were incubated in a humidified chamber to prevent evaporation.

6.2.3.3 Blocking of non-specific protein binding

After fixing, the samples were washed 2 times with 1 mL of PBS and a blocking step comprising of adding 1mL the blocking solution containing 1% (w/v) BSA and 0.25% (v/v) triton X100 in PBS was performed to reduce non-specific binding. The samples were then incubated at room temperature for 1 h. Next, the samples were rinsed twice in PBS washes. For antibody staining, the blocking solution was supplemented with an extra 10% of goat serum, then the same incubation and washing steps were repeated.

6.2.3.4 F-actin cytoskeleton staining

Following the blocking, incubating and rinsing steps, 1:200 phalloidin conjugated to

Alexa Fluor® 488 phallotoxin (Life-technologies, Paisley, UK) was diluted in PBS and added to the samples, then incubated for 1h before a washing step was performed using PBS as previously described above.

6.2.3.5 Antibody staining

After each blocking step, scaffolds were washed twice with PBS. Diluted primary antibody (in PBS) was added to cover each scaffold (200 µL). The samples were incubated at 4^{o} C overnight. The next day, the scaffolds were washed twice with 1ml PBS, the secondary antibody added and incubated for another 1h before carry out nuclear staining.

6.2.3.6 Nuclear staining

Nuclear staining was achieved by using 0.01 µg/mL Hoechst 33258 which is a DNA intercalating agent (Sigma-Aldrich, Gillingham, UK) in PBS for 10 minutes as a final step in the staining procedure.

6.2.3.7 Fluorescence Imaging

The image was visualised and captured using EVOS® Imaging System (Life-technologies, Paisley, UK) at the exposure around 20-30% of 120 ms for blue channel (Ex 357 nm, Em 447 nm), 50-70% of 500 ms for green channel (Ex 470 nm, Em 510 nm), and red channel (Ex 585 nm, Em 624 nm). The images were further processed such as the cell count or mean area measurement using ImageJ version 1.47 (National Institutes of Health, Maryland, USA).

6.2.4 Statistical Analysis

Means and standard deviations were determined for each sampled followed by a two-way ANOVA analysis to evaluate the difference in protein adsorption, cell viability, proliferation, and cell number on each of the nanocomposite material samples. Correlation analysis was performed on metabolic activity and total DNA measurements. P-value < 0.05 was considered to be statistically significant. All statistical analysis was conducted using GraphPad Prism version 5.01 (2007).

6.3 Results

6.3.1 Culture media adsorption and HBECs growth on microporous POSS-PCU

6.3.1.1 Optimisation of pre-adsorption time of cell culture media

There was no significant difference of protein adsorption amount in TCP control, 30% $NaHCO_3$, and 50% $NaHCO_3$ scaffolds after pre-adsorption in BEpiCM culture medium for 6h – 48h ($P > 0.05$) (Figure 6.2). However, M70% $NaHCO_3$ showed a significant increase in adsorption over a period of 6h – 24h ($P < 0.001$) while there was no further adsorption from 24h – 48h ($P > 0.05$).

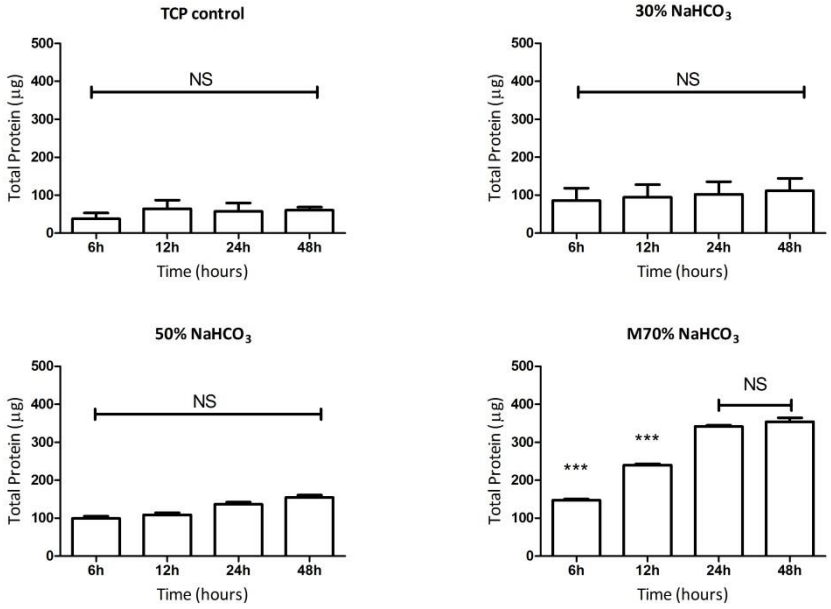

Figure 6.2 Protein adsorption of TCP and microporous POSS-PCUs over a 48h period. (n=4)

6.3.1.2 HBEC's growth on microporous POSS-PCUs

The metabolic activity of HBEC were examined and presented in Figure 6.3. Overall, the metabolic activity of cells on TCP increased faster than those of microporous POSS-PCU samples ($P < 0.001$ from day 1-14). Then the metabolic activity of the TCP samples levelled off around day 7-11, and significantly dropped on day 11-14, probably because of reaching

the confluent state. For 30% $NaHCO_3$ samples, the metabolic activity increased from day 1-7 and levelled off on day 7-14. However, the 50% $NaHCO_3$ samples showed a significant increase over the time course with the higher rate comparing to the 30% $NaHCO_3$ samples. Finally, the M70% $NaHCO_3$ presented the highest increasing rate of metabolic activity comparing to other POSS-PCU samples over the time course. The metabolic activity of the M70% $NaHCO_3$ constantly increased and day 14 measurement was comparable to the TCP's on day 4, leading to the prediction that it possibly reach the same point as TCP if the time course was extended.

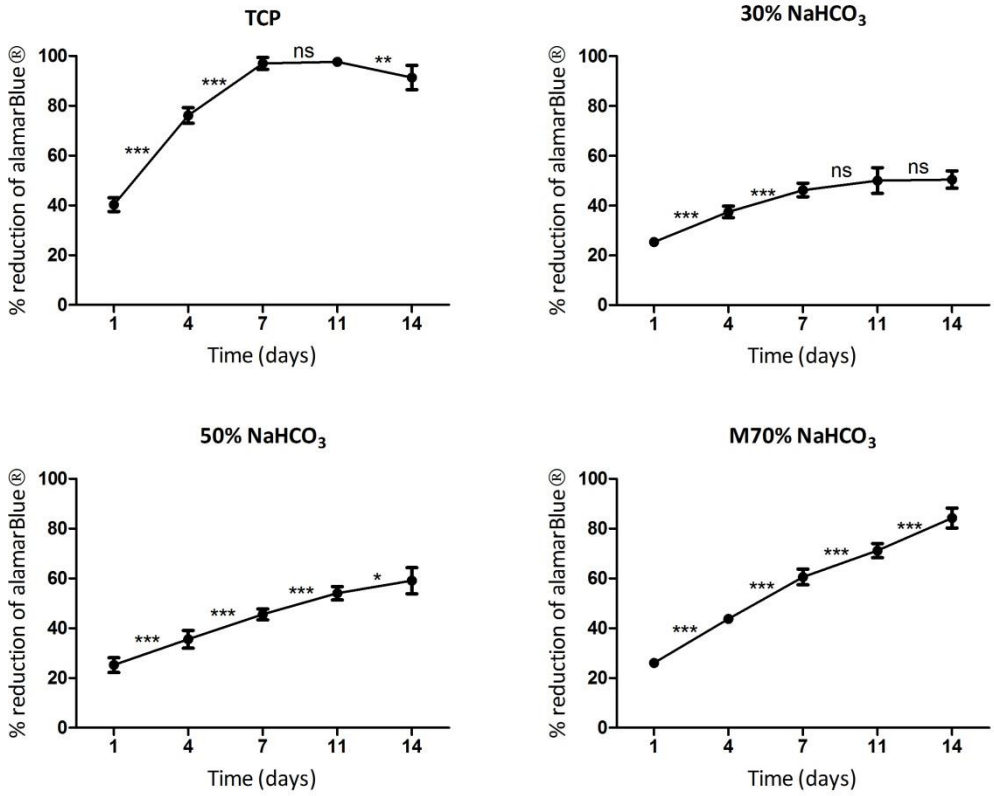

Figure 6.3 Metabolic activity of HBEC on TCP and microporous POSS-PCUs, **P* < 0.5, ***P* < 0.01, ****P* < 0.001, and ns = non-significant (*P* > 0.05). (n=6)

Total DNA quantification of d1, d7, and d14 of each material was presented in Figure 6.4. There were increases of DNA amount over time course in all samples (*P* < 0.001), indicating HBEC population proliferated and increased the cell number.

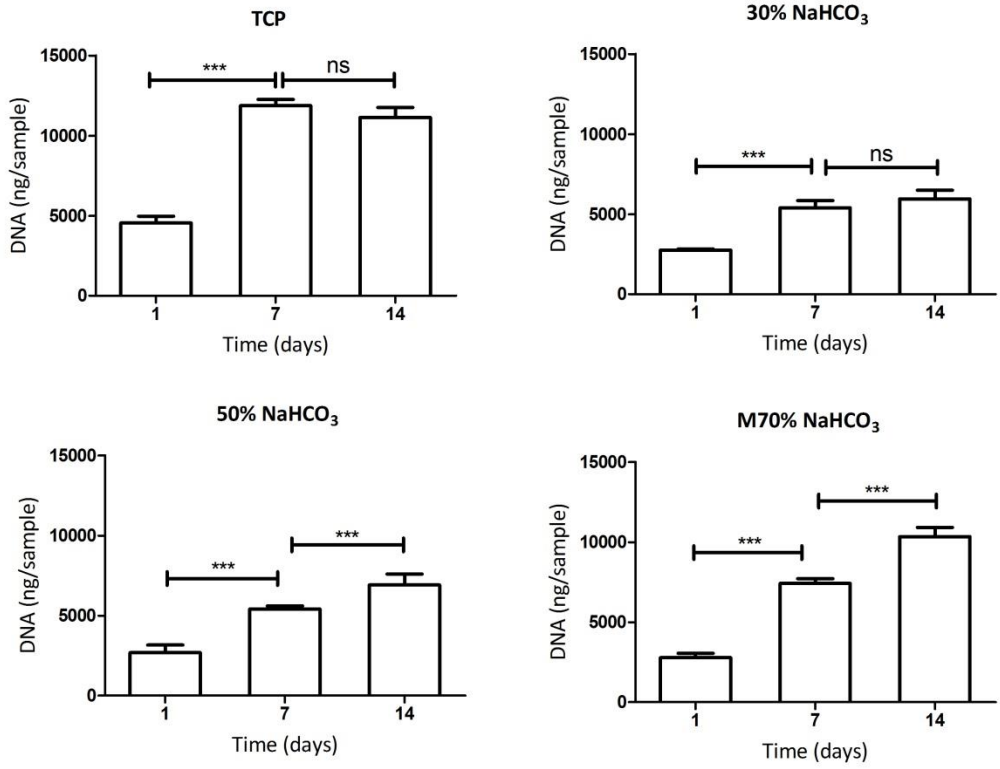

Figure 6.4 Total DNA quantity of HBEC on TCP and microporous POSS-PCUs, ****P* < 0.001, and ns = non-significant (*P* > 0.05). (n=3 per time point)

Correlation of DNA amount against metabolic activity at day 1, day 7, and day 14 (Table 6.3) was analysed to see whether the cells just increased their metabolic activity without proliferation or if an increase in cell proliferation caused the higher rate metabolic activity measured. As an R^2 value close to 1.00 was obtained (Table 6.2), there is a direct correlation between the metabolic activity and rate of proliferation, meaning the metabolic activity increased due to a proportional increase in amount of DNA.

Table 6.2 Correlation between metabolic activity and amount of DNA on TCP and microporous POSS-PCU.

Material	**Correlation of metabolic activity and DNA**	**R^2**
TCP	$P = 0.0016 < 0.001$	1.0000
30% $NaHCO_3$	$P = 0.0023$, <0.001	1.0000
50% $NaHCO_3$	$P = 0.0325$, <0.05	0.9974
M70% $NaHCO_3$	$P = 0.0142$, <0.05	0.9995

To demonstrate HBECs' cell-surface interactions with microporous POSS-PCU samples, F-actin staining was carried out 1 day after cell seeding. The staining showed cells flattened and spread on the material surfaces of both TCP and microporous POSS-PCU. Lamellipodia (example in greyscale window) was also seen in images where the actin micro-filaments protruded to the edge of cell membrane to help attachment (Figure 6.5).

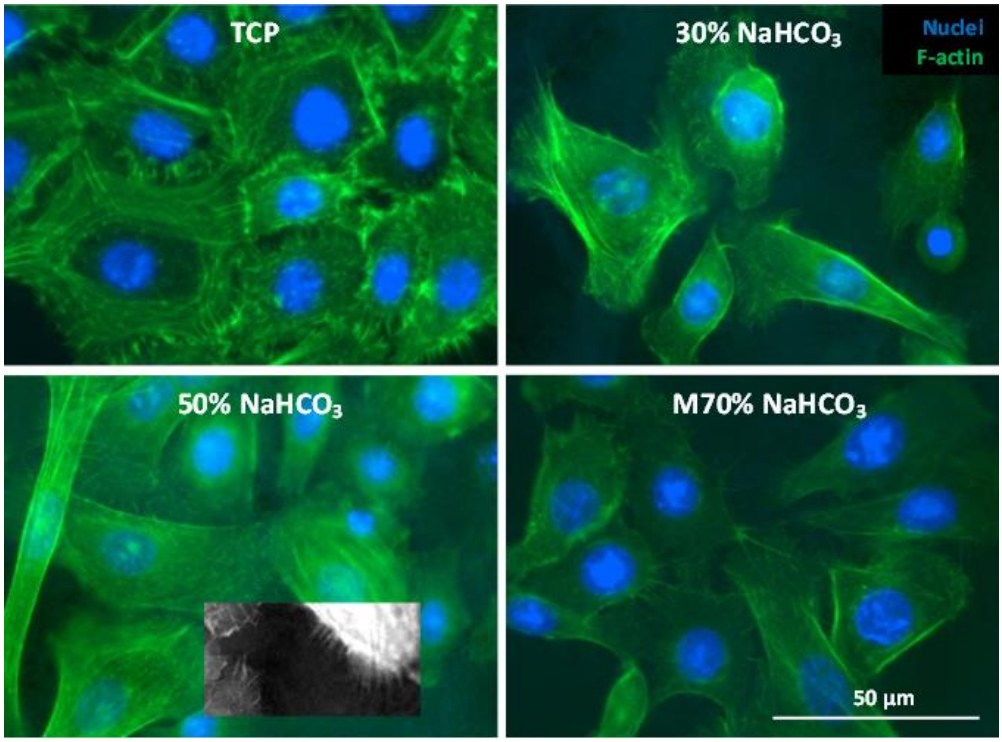

Figure 6.5 Primary HBECs on material surfaces (d1 post seeding) showed all cells extended their lamellipodia around the edge of the cells to adhere to the materials (the microfilament as example in greyscale window). Magnification = 400X. Scale bar = 50 µm.

Qualitative images of basal cell marker (keratin 5, red) were assessed in HBECs in all samples. Every cell expressed keratin 5 (Figure 6.6). Also, there was no difference between HBECs on POSS-PCU samples compared with TCP controls.

However, the quality of HBEC on each material was examined further using mesenchymal or proliferative markers such as vimentin and Ki-67, respectively. Total counts per frame and staining images at day 7 (middle stage of culture) were illustrated in Figure

6.7. TCP showed higher number of cells per frame comparing to the cells on microporous POSS-PCU materials ($P < 0.05$). However, every sample showed that HBECs expressed vimentin (green) and Ki-67 (red), indicating proliferative populations which is relevant to cell viability and total DNA results with growing number of cells.

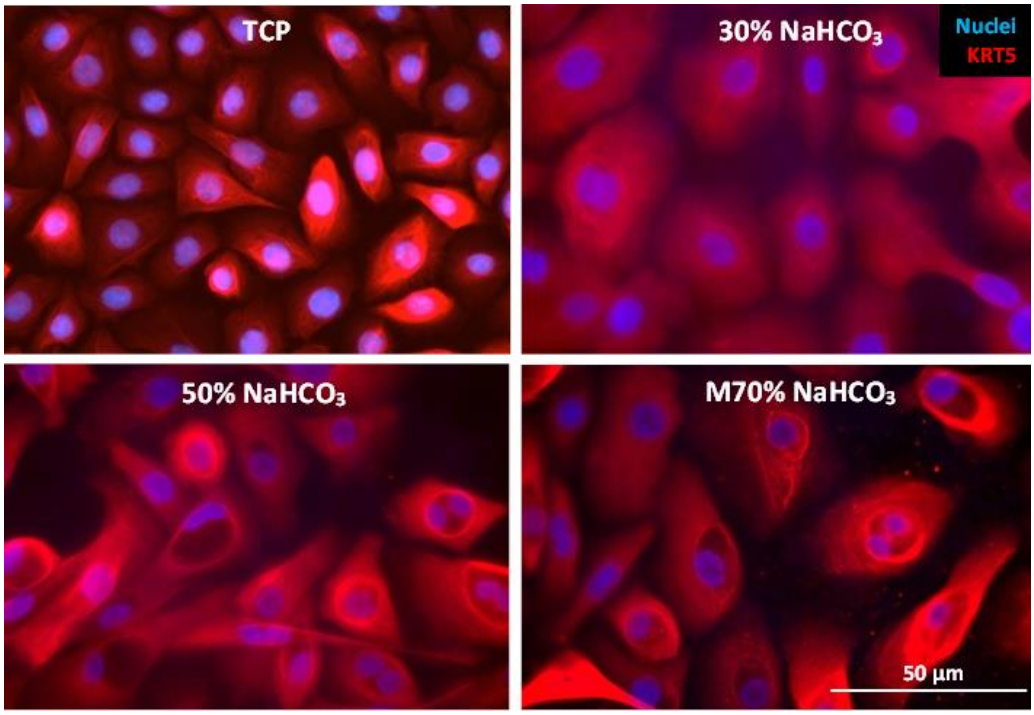

Figure 6.6 Expression of keratin 5 of HBECs on d7 culture on TCP and POSS-PCUs. Magnification = 400X. Scale bar = 50 µm.

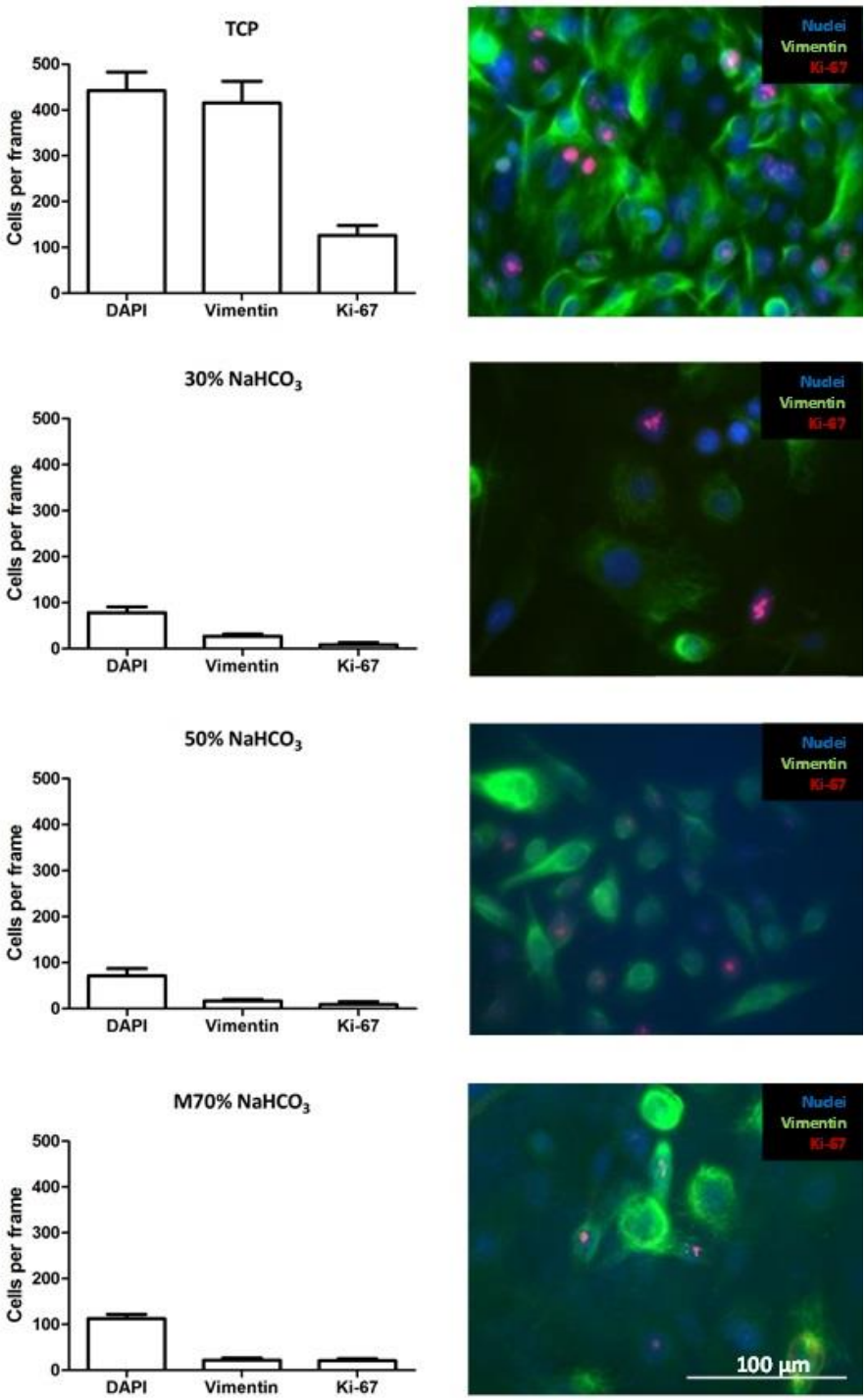

Figure 6.7 Expression of vimentin and Ki-67 of HBECs on TCP and POSS-PCUs. Magnification = 400X. Scale bar = 100 µm. (n=6)

6.3.2 Differentiation of HBECs via air-liquid interface cultures

Normalised total DNA on material from day 1 – day 35 was illustrated in Figure 6.8. In all conditions, the amount of DNA increased and peaked at around d14 – d21, indicating cells were in a growing stage. After that, the amount of DNA gradually reduced until day 35. Characterisation of differentiated HBECs was investigated at specific time-point presented in the following results.

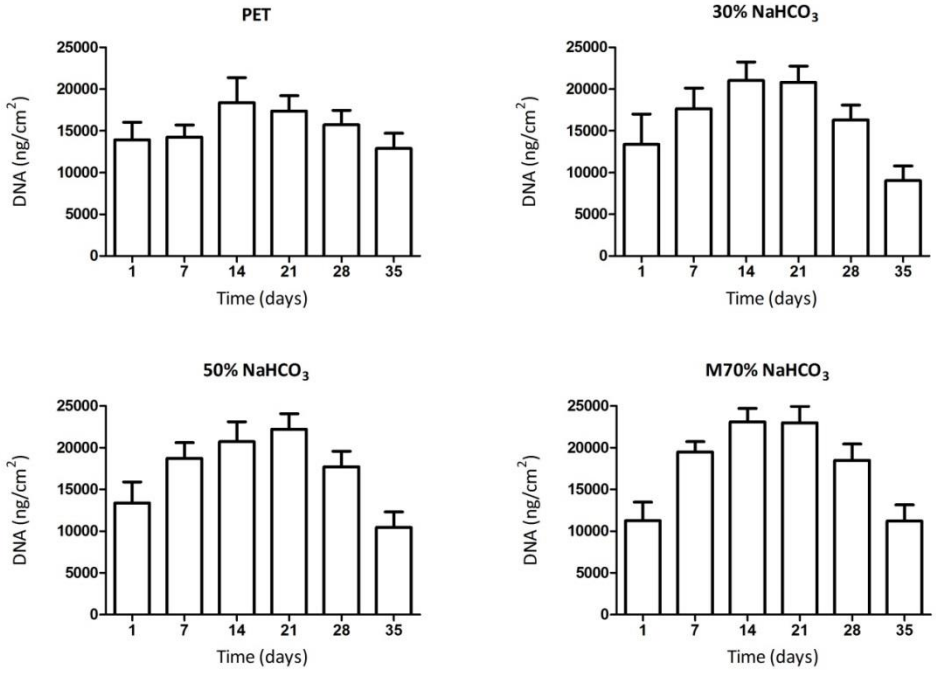

Figure 6.8 Total DNA of HBEC cells cultured on control and POSS-PCU nanocomposite films over a period of 35 days. (n=4 per time point)

6.3.3 Characterisation of differentiated HBECs

6.3.3.1 Gross cell morphological analysis

Pneumacult™ differentiation medium for air-liquid interface cultures was employed to induce primary HBECs to form mature HBECs with functional cilia. Time-lapse images from day 1 – day 14 are shown in Figure 6.9. On day 1 when the cells were still cultured in BEpiCM, they were dispersed across the surface, as separated cells in a mono layer. After day 1, the medium was changed to Pnemacult™ and cells were having interactions by packing together with obvious reorganisation of F-actin filaments on day 7. On day 14, the cells had formed into a complete layer with a mature phenotype, with joining in a polygonal shape. At this point, the optimal point was defined to study mature morphology of HBECs. According to our results on total DNA, overlaid images, and company's instruction, the optimal point should be around day 21 when cells developed maximum growth with differentiated morphology.

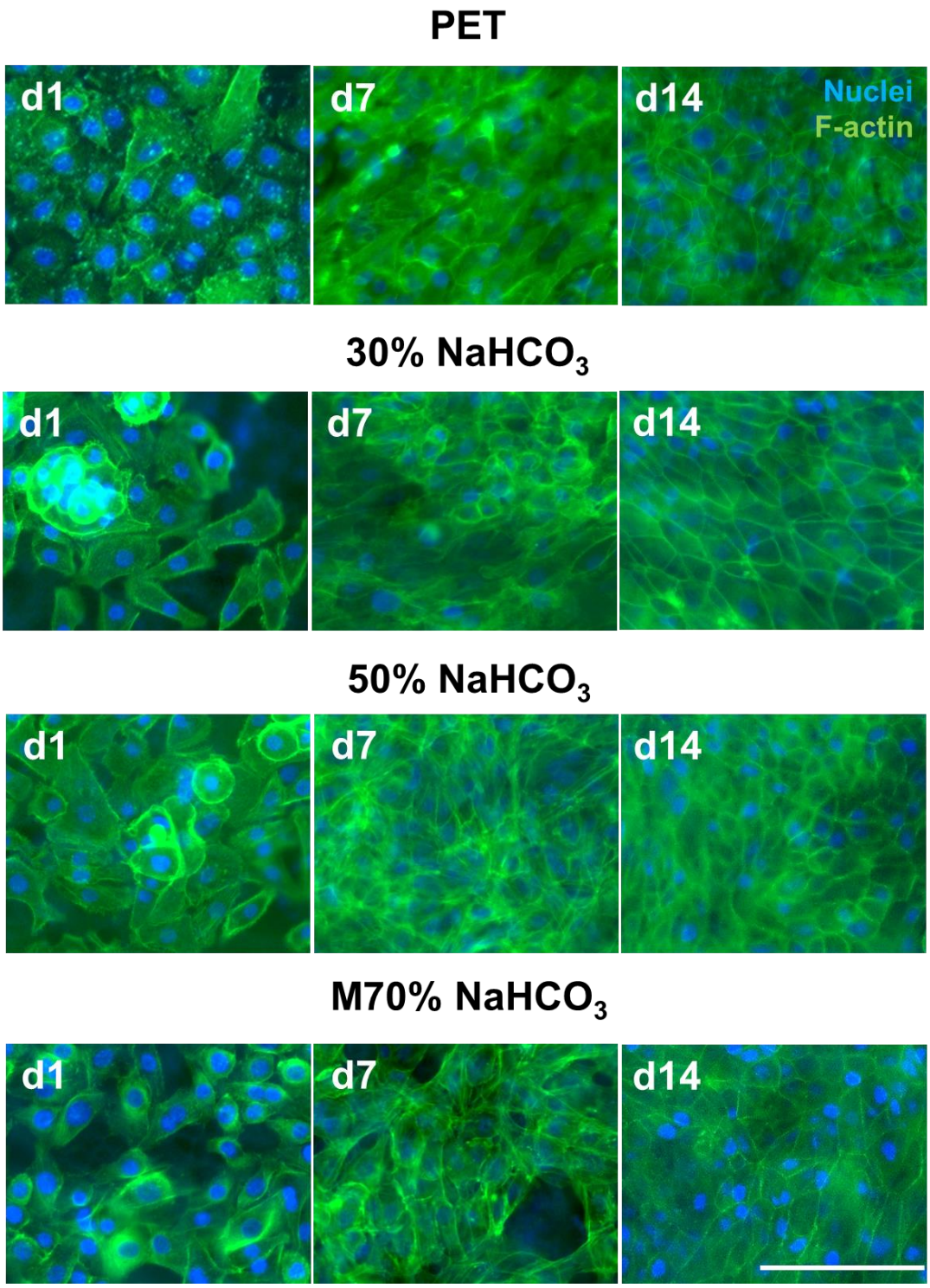

Figure 6.9 Time-lapse images of HBEC proliferation and morphology on PET and POSS-PCU nanocomposite films Magnification = 200X. Scale bar = 100 µm.

6.3.3.2 Ciliated epithelia, cadherin tight junctions, and epithelial stratification.

Scaffolds on day 21 was fixed and stained with acetylated α-tubulin which was presented mainly in the cilia of airway epithelium. Our results demonstrated the ciliated cells (Figure 6.10, red) were presented in all samples and distributed across the surface. Moreover, they were stained with E-Cadherin (Figure 6.10, green), and confirmed that differentiated HBEC formed not only the shape but also the function of surface barrier cells via expression of cadherin junction proteins. The results were confirmed by SEM images presented in Figure 6.11 that cells had these specific morphologies.

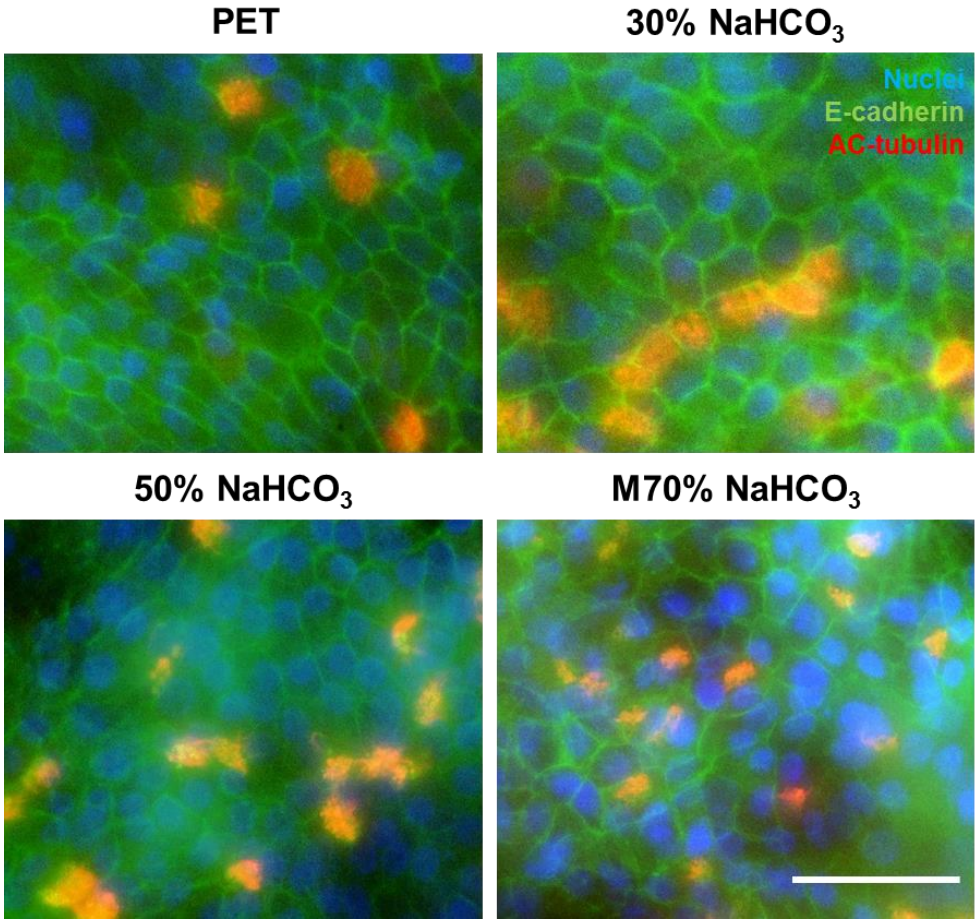

Figure 6.10 E-cadherin staining of HBECs on PET and microporous POSS-PCU materials at day 21. Magnification = 400X. Scale bar = 50 µm.

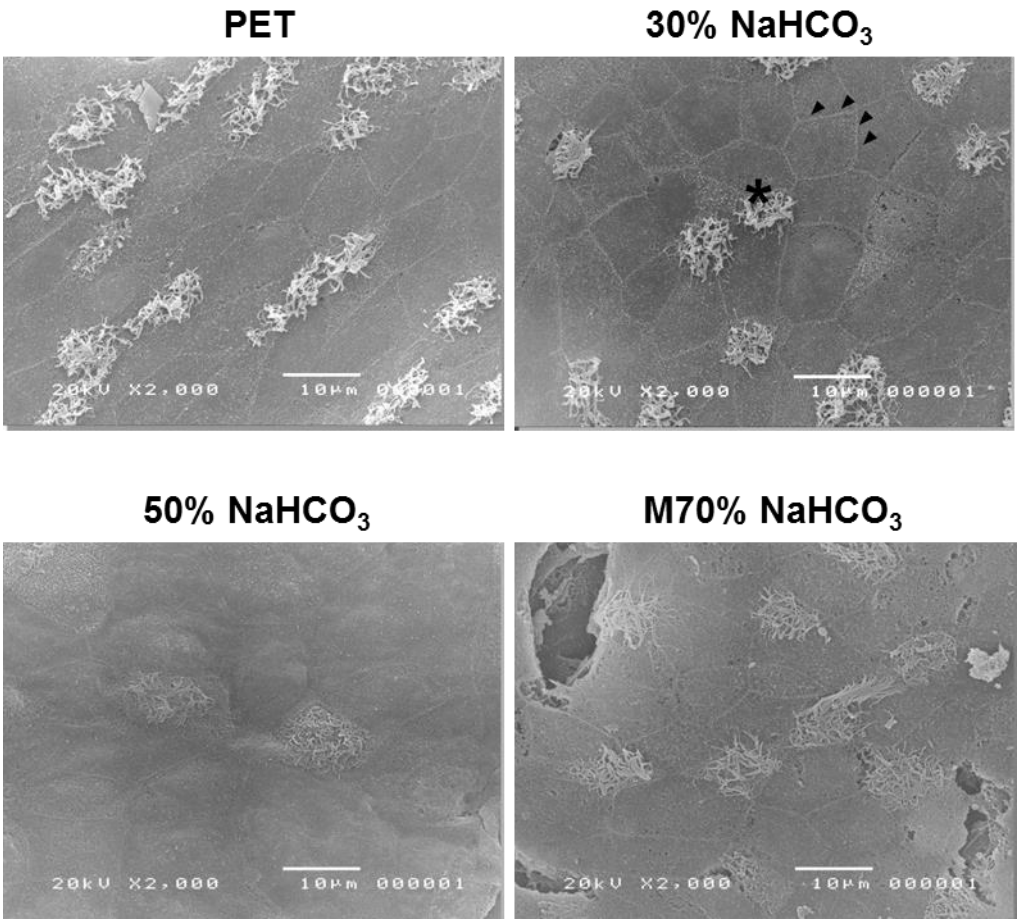

Figure 6.11 SEM images presenting morphologic structure of cilia (*) and polygon shape of intercellular junction (arrow head) of differentiated HBEC (d21). Magnification = 2,000X. Scale bar = 10 µm.

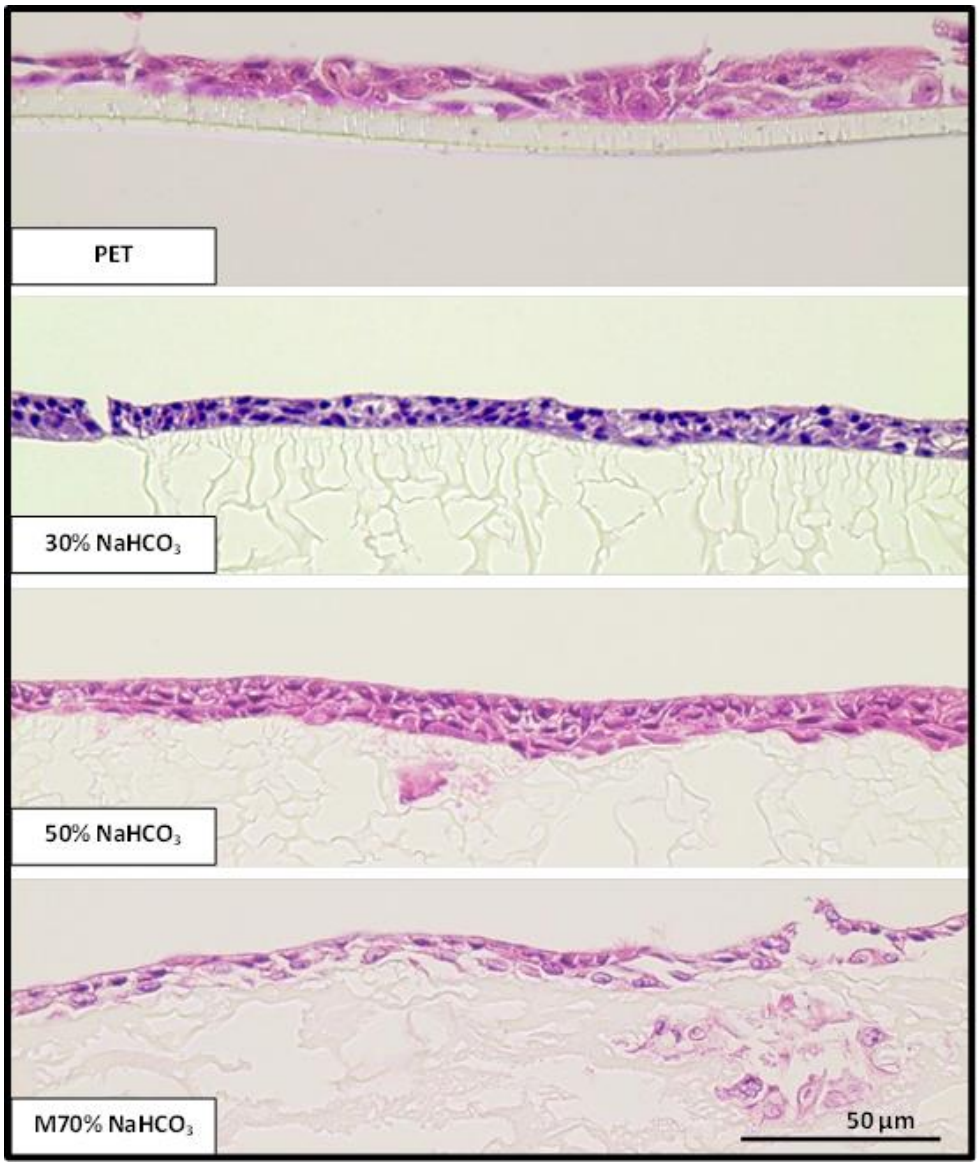

Figure 6.12 Cross-sectional image of d21 epithelium on scaffolds, presenting a pseudostratified layer on scaffold surface and some cells migrated inside the scaffolds. Magnification = 400X. Scale bar = 50 µm.

Epithelial stratification was presented in Figure 6.12. HBECs on day 21 formed a complete multilayer of cells with epithelial polarity, which is the fundamental feature of cells orientated in a vertical direction and resulting in the round or vertically oval nuclei, especially the apical zone.

Also, the basal-like cells were demonstrated in the region connected to the material where the cells were aligned horizontally, resulting in the flat or horizontally oval nuclei.

6.3.3.3 Cell mucus production

Cells on scaffold were stained with different techniques to confirm that they could become differentiated into goblet cells, which produce mucus- an important feature of pulmonary tracts. Here it demonstrated in Figure 6.14 that cells were expressing Mucin-5AC (red, counter stained with DAPI and E-Cadherin). Samples sectioned and treated with a Periodic acid-Schiff stain to demonstrate the vertical position of the goblet cells. Figure 6.13 illustrated the presence of mucosal substances on the superficial layer, which was the correct position to secrete the mucus to cover epithelium.

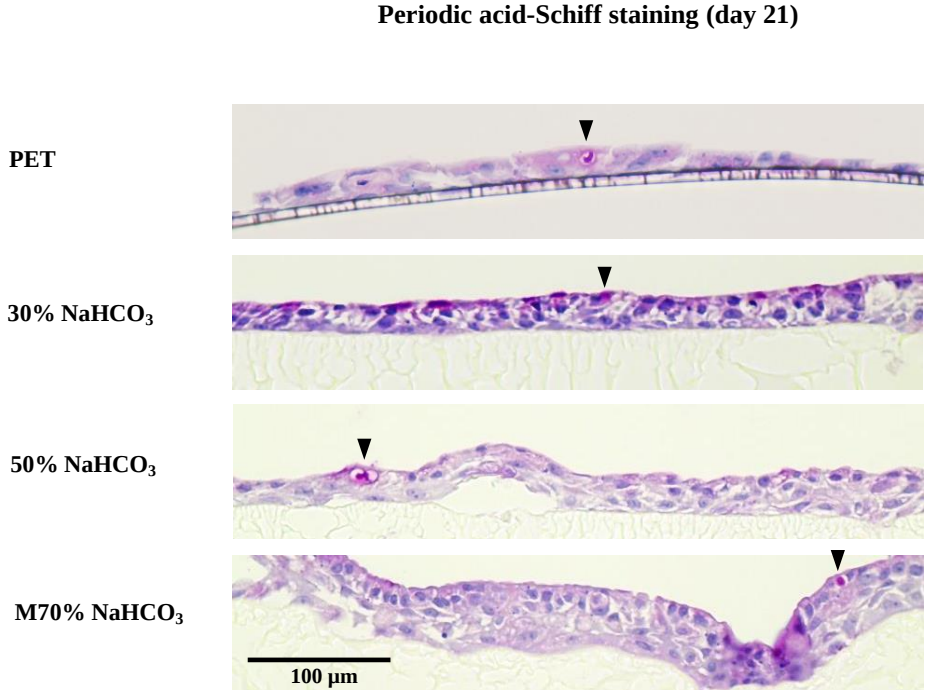

Figure 6.13 PAS staining of cross-sectional slices showed some cells on scaffolds developed muco-substance (magenta at arrow head) as in respiratory mucosa. Magnification = 400X. Scale bar = 100 µm.

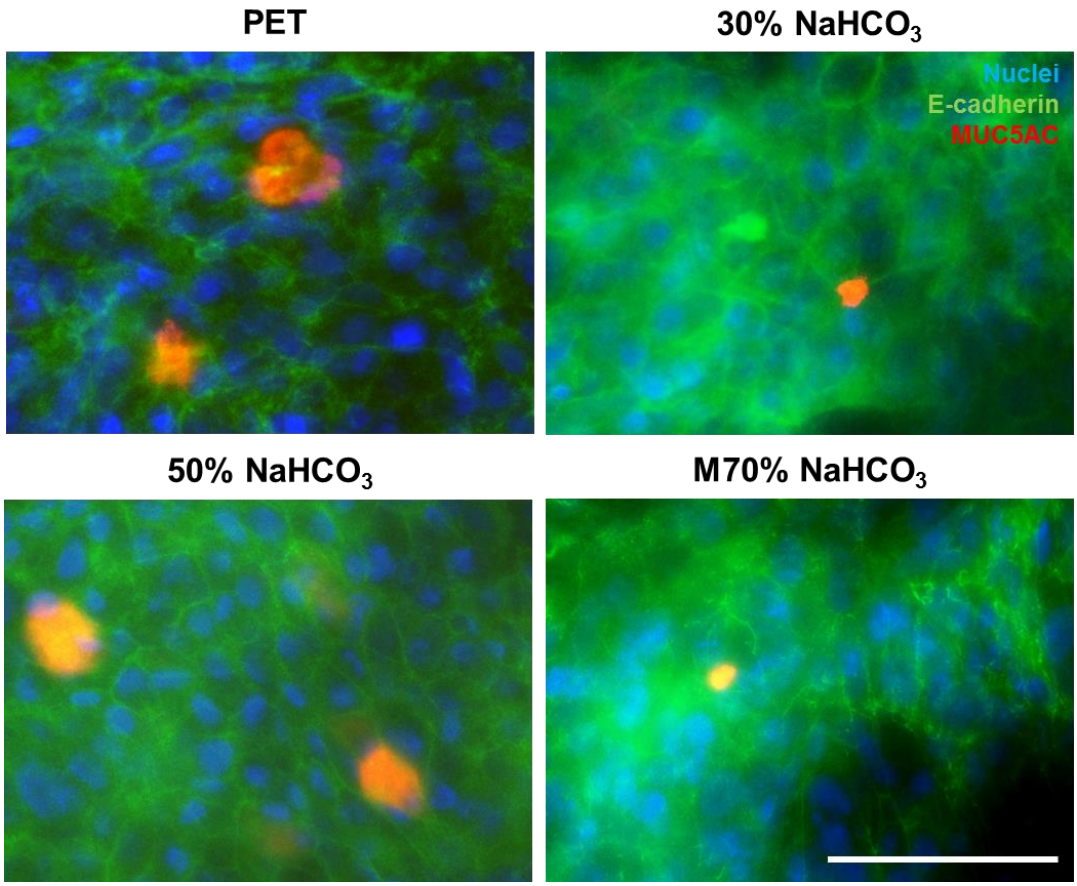

Figure 6.14 Specific antibody staining of scaffold on d21 confirmed that it was the glycoprotein Mucin 5AC that presents in respiratory tract epithelium. Magnification = 400X. Scale bar = 50 µm.

6.3.3.4 HBEC migration and integration into the nanocomposite materials

Microporous POSS-PCU scaffolds on day 35 were performed histology section and stained with haematoxylin and eosin to demonstrate the cell migration in to the 3D construct. In 30% $NaHCO_3$, cells were limited on upper superficial surface with migration just a few microns below. For 50% $NaHCO_3$, cells migrated further to attach to the pore cavity below and also reached the lower surface (200 – 300 µm). Finally, the M70% $NaHCO_3$ illustrated the cells were also able to migrate to the lower surface with a large group of cells integrated inside the scaffold (Figure 6.15).

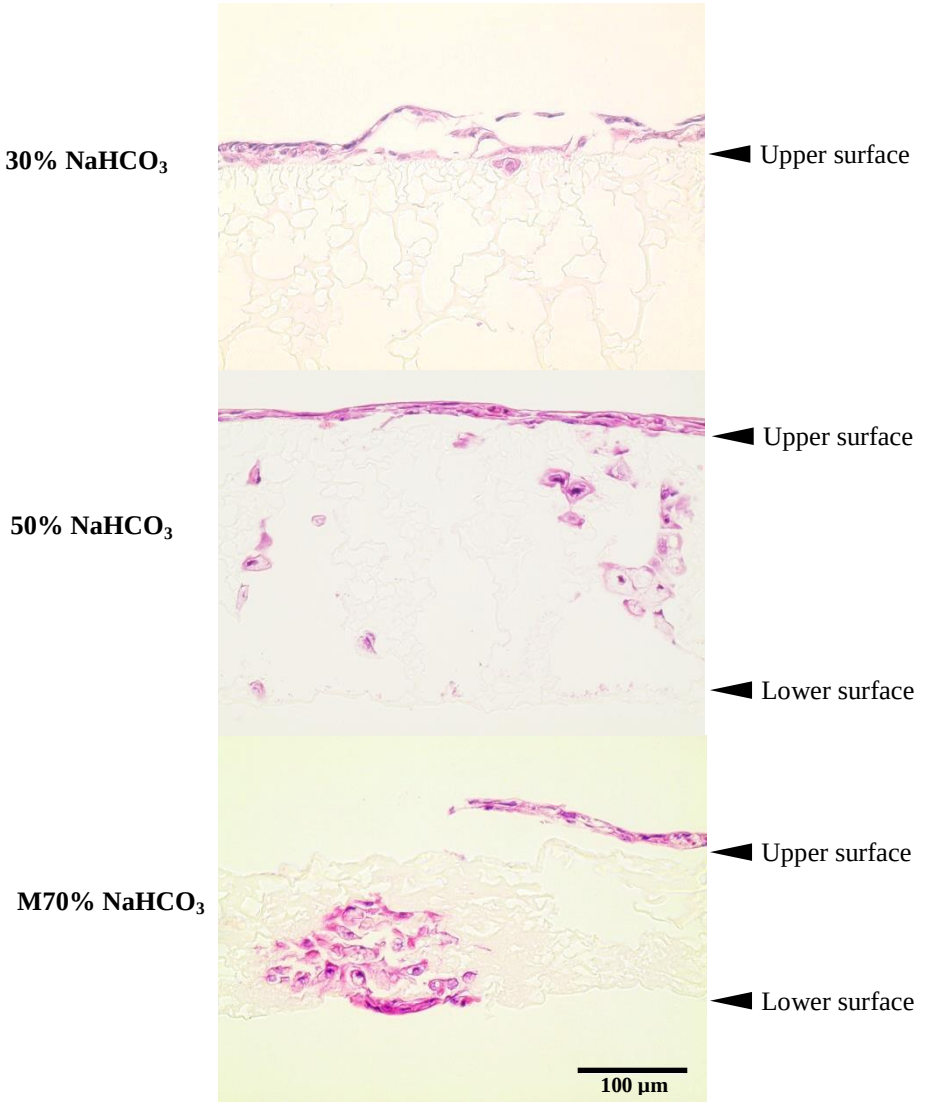

Figure 6.15 H&E stained sections of the scaffolds showing the degrees of migration of the HBECs in to the scaffolds at day 35. Magnification = 200X. Scale bar = 100 µm.

6.3.3.5 Expression of basal cell and differentiated cell markers

HBECs on scaffolds on day 21 and day 35 were stained with keratin 5 for basal cells and keratin 18 for differentiated cells to distinguish the basal layer and differentiated layer. At day 21, the keratin 5 (red) was mostly visible on the basal layer (cell-material interface) while keratin 18 was visible on the upper layer of the epithelium. However, on the M70% $NaHCO_3$ some areas of the epithelium still did not have distinctive layer and cells presented

both markers. On d35, cells became more differentiated-like by presenting more keratin 18 while keratin 5 in the basal layer was diminished comparing to d21 (Figure 6.16).

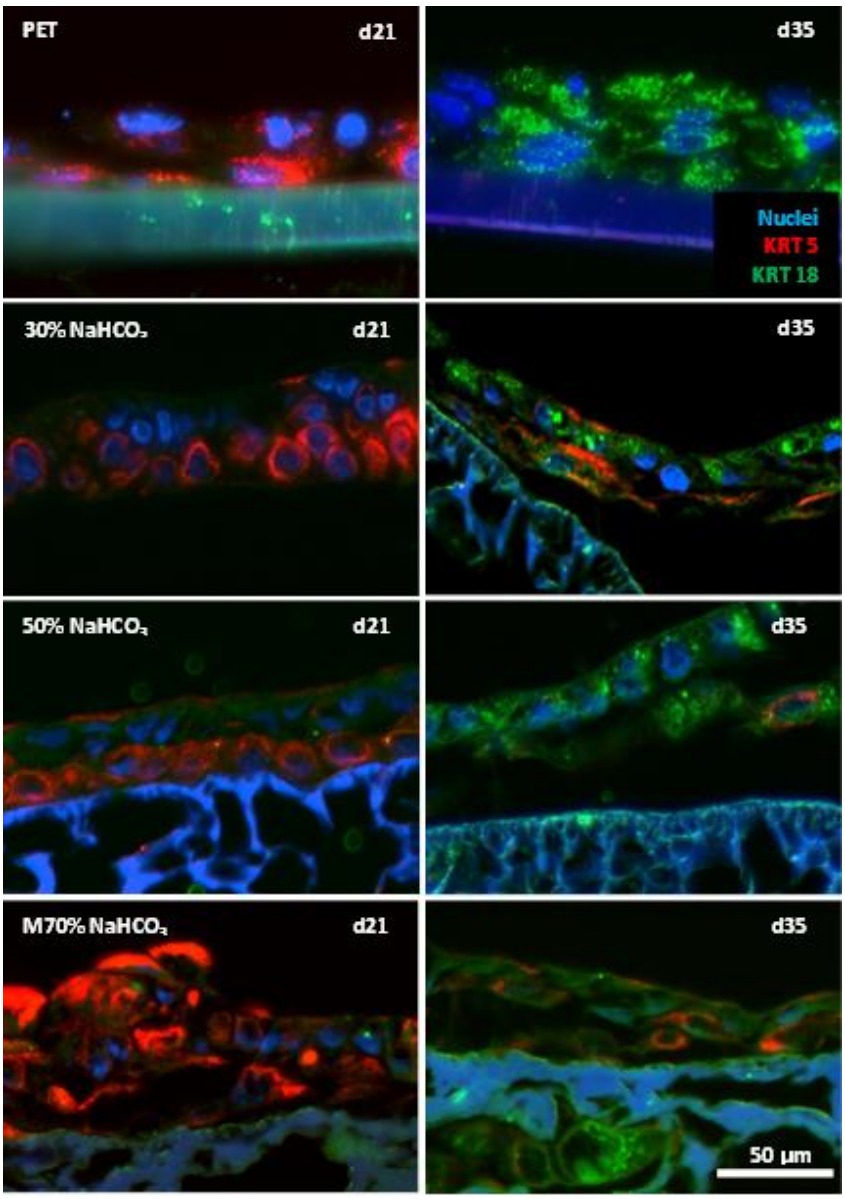

Figure 6.16 Immunofluorescent staining (keratin 5 and keratin 18) indicating the organisation of cells and the differences in the epithelium at day 21 and day 35 on PET and POSS-PCU nanocomposite films.

6.4 Discussion

6.4.1 Optimisation of pre-adsorption time.

The effects of protein adsorption examined further on cell behaviour in vitro. The level of protein adsorption on material affects how cell adhere and grow, so the pre-adsorption times were optimised. Protein adsorption on material can occur within a few seconds on 2D surface[138]; however, that might be different for 3D structure such as our microporous POSS-PCU scaffolds due to the extra luminal surface presented inside the pores. The amount of adsorbed protein was presented in Figure 6.2, where no significant different was found in TCP, 30% $NaHCO_3$, and 50% $NaHCO_3$. This suggested the adsorption of those 3 conditions had reached the saturated point after 6h; however, the M70% $NaHCO_3$ presented continuous adsorption until 24h. Related back to the highest porosity and the ability to adsorb BSA in the previous chapters, it may be one of the reasons why the saturated point of M70% $NaHCO_3$ was delayed. However, the 24h duration was chosen as the best pre-adsorption time to provide protein saturation on every material before starting of cell seeding.

The protein adsorption is dynamic when including the Vroman effect and changing of pH. Vroman effect occurs when the random types of proteins will adsorb on the surface and later, followed by the replacement of higher affinity proteins[142]. Therefore, the lower affinity ones will be released back in to bulk solution. The other effect might be the pH changing of the cell culture medium because Sharpe et al. demonstrated different pH altered different amount of protein adsorption on the material[157]. Therefore, the deeper studies on protein-material interaction need to be investigated in the future to explain the process, especially when the materials come into contact with human serum or blood.

6.4.2 HBECs attached and grew on microporous POSS-PCU over 14 days with expression of CK5, vimentin, and Ki-67.

The cell viability measurement via metabolic activity revealed cells significantly grew in all POSS-PCU samples but slower than TCP control. The M70% $NaHCO_3$ had higher cell

metabolic activity than 30% and 50% $NaHCO_3$ ($P < 0.001$) and constantly increased over 14 days of measurement. In addition, it was comparable to the TCP's on day 4, leading to the prediction that it possibly reach the same point as TCP if the time course was extended. To confirm that cells also proliferated and not just increase in metabolic activity, total DNA contents were evaluated on day 1, day 7, and day 14, and compared the correlation with metabolic activity. The correlation analysis showed that total DNA amount relatively increased when metabolic activity increase ($P < 0.05$). This suggested the DNA amount was also increasing due to the cell proliferation, resulted in metabolic activity was getting higher. The cell markers were additionally explored, which are filamentous actin, keratin 5, vimentin and Ki-67, respectively, to explain cell behaviour on the material.

The ability of cells to respond to external environment relies on the coordinated disassembly and assembly of cytoskeleton filamentous actin (F-actin). This ability is critical for various cell functions including adhesion, wound healing, division, and locomotion[158]. Furthermore, cells can mechanically sense their local environment, as they spread more, and migrate to the stiffer substrates[158]. In particular, networks of F-actin and its protein cross-linkers have been implicated as major contributors to the mechanical properties of the cell[159]. Our results showed HBECs spread on microporous POSS-PCU surface in the similar way to the TCP control. In addition, lamellipodia structures were presented in all cells by protruding out around the edge of cytoplasm which indicated HBECs had interactions with the material leading to cell attachment.

Keratin 5 was employed to characterise basal-cell phenotype of HBECs which has the ability to differentiate in to mature phenotype later on[160]. Cells on material on d7 were further assessed to prove that the cells still express basal cell marker. It was demonstrated that all cells expressed keratin 5 and did not have significant difference between POSS-PCU conditions and TCP control. Also, other markers were used to explain the growth of cell population which are Ki-67 and vimentin.

Ki-67 is a human nuclear protein which is expressed strictly in association with cell proliferation and which is routinely used in pathology as a "proliferation marker"[161]. The Ki-67 protein presents during all active phases of the cell cycle such as G1, S, G2, and mitosis, but is absent from resting cells at G0, makes it a good marker to define the growing cells of a given population[162]. Vimentin is a type III intermediate filament protein that is expressed in mesenchymal cells and plays significant role in supporting organelle location in the cytosol by attaching to the nucleus, endoplasmic reticulum, and mitochondria, either laterally or terminally[163]. However, there was evidence that vimentin was co-expressed with keratin in the basal part of human nasal epithelium[164]. Vimentin also helped maintenance cell mechanical properties and integrity of the cytoplasm, as well as the resilience of the other cytoskeletal systems[165]. Therefore, HBEC characterisation using vimentin was carried out in addition to Ki-67.

HBECs on materials in each condition on day 7 were immuno-stained with anti-vimentin and anti-Ki-67 (Figure 6.7). It demonstrated that microporous POSS-PCU expressed vimentin and Ki-67 but was relatively low compared to the TCP positive control ($P < 0.05$). This might explain by the lower cell viability and total DNA on day 7 of microporous POSS-PCU samples that exhibited lower new population of HBECs. Overall, 3D POSS-PCU, which has great potential for regenerative medicine, needs to be tested in further detail using appropriate system to show us the differences between it 2D material.

6.4.3 HBECs grew and differentiated on microporous POSS-PCUs under air-liquid interface culture

The air-liquid interface technique (ALI) was employed to study the differentiation of primary HBEC to a pseudostratified columnar epithelial layer. Cell seeding at confluent state was performed to make sure the cells cover all the entire surface of scaffold material. A Transwell® insert was employed as positive control as it has been the gold standard material for epithelial culture and differentiation in vitro[166–169]. Because the culture area of PET

insert and POSS-PCU insert were different, the total DNA data were normalised to per cm^2 to make them comparable. Normalised total DNA showed the cells had grown from day 1 to day 14 and peaked around day 14 to day 21. After that, the total DNA amount had declined until termination of the experiment at day 35, which suggests that the maximum growth takes place between day 14 and day 21. Figure 6.9 showed the remarkable changing of F-actin organisation of HBEC when BEpiCM was replaced with differentiation medium (Pneumacult™). HBECs had more cell interaction, packed together, and formed a complete layer with a net-like mesh work which is the morphology of epithelial cells[170,171].

Cells on all materials were positive when stained with anti-acetylated α-tubulin and anti-E-cadherin. Acetylated α-tubulin is presented mostly in cilia in ciliated cell[172,173] and E-cadherin is junction adherent proteins that connect epithelial cells together to form a barrier[174–176]. Cells on both PET and POSS-PCU scaffolds expressed these proteins and it was also confirmed by SEM images that cells had intercellular junctions. Moreover, the cross-sectional H&E images demonstrated the organisation of pseudostratified layer with epithelial polarisation which is the important characteristic of tissue-engineered epithelium[177,178]. Another characteristic of airway epithelial cells is mucin production. Mucin is the gel-like substance that is produced from goblet cell to keep the moisture, and protect the infection or chemicals[80,179–181]. It was confirmed that the differentiated HBECs on both PET and POSS-PCU material produced mucin at the apical layer via PAS and anti-Muc 5AC staining.

The further examination of the vertical migration on microporous POSS-PCU scaffolds also revealed the cells migrated through the thickness of 50% and M70% $NaHCO_3$ scaffolds. However, the 30% $NaHCO_3$ showed the cells were accumulated on the surface with only a few microns of migration. This incident suggested the permeability of the scaffold also had an influence on the cell migration on different porosities of microporous POSS-PCU scaffolds. The best porosity for the scaffold remains unanswered because another aspect such

as the neovascularisation after implantation is needed for mucosal regeneration[155]. Also, the control of epithelial to just the superficial layer is important to get the right mucosal structure and avoid unwanted integration to the material[152]. The future studies such as co-culture, material coating and *in vivo* implantation, might give more information to help decide the right porosity for controlling mucosal structures.

Keratin 5 and keratin 18 were employed to differentiate basal cell and differentiated cell, respectively[79,160,172]. HBECs on PET and POSS-PCU material on d21 presented keratin 5 expressed mostly in the basal layer while slightly expression of keratin 18 was found on the apical layer. However, on later d35, the cells expressed more keratin 18 throughout epithelial layer with diminishing trend of keratin 5 expression in the basal region. This relevant to the reduction of total DNA amount on d35 that might affect by the reduction of proliferative basal cells population and becoming more differentiated type as indicated in keratin staining.

In conclusion, the experiment illustrated the success of regenerating artificial airway epithelium on microporous POSS-PCU material for the first time, with the growth and characteristic of artificial epithelium comparable to in vitro gold standard Transwell® insert. This model could represent the real interactions between HBECs and POSS-PCU material under in vitro condition and could be used as a base-line for further development and functionalisation to enhance the material properties.

6.5 Conclusion

This chapter demonstrated the success of regenerating in vitro artificial airway epithelium on microporous POSS-PCU scaffolds. The differentiated epithelial cells had epithelial characteristics such as cilia, junction adherens, pseudostratification, and mucin production. The material showed comparable cell growth and differentiation ability to the commercial Transwell® insert but with additional migration and integration of cells due to its 3D porous structure. Microporous POSS-PCU could be useful for further in vivo study for tissue

integration and angiogenesis in the future and presented the great potential to be developed for laryngotracheal application as well as other epithelial-derived organs.

Chapter 7 Human bone-marrow mesenchymal stem cell culture and *in vitro* chondrogenic differentiation on microporous POSS-PCU scaffold

7.1 Introduction

The fields of regenerative medicine and tissue engineering address the replacement of organs and tissues due to clinical trauma, disease or congenital defect. Biomaterial scaffolds are intended to facilitate the construction of a biomimetic environment to enhance cell growth and differentiation[182]. While somatic cells, such as osteoblasts and chondrocytes, were the first to be used in bone and cartilage tissue-engineering, the more recent addition of stem cells to tissue engineering has extended its therapeutic potential[183]. Among adult tissue-derived stem cells, mesenchymal stem cells (MSCs) have been extensively studied, due to their ease of expansion and multipotency for differentiation into cells of myogenic, osteogenic, and the chondrogenic cell lineage[184].

MSCs became an attractive cell source for clinical therapies because the cells could be isolated with relative ease from multiple sources, including bone marrow, fat and skeletal tissue[183]. Bone-marrow mesenchymal stem cells (BM-MSCs) are attractive candidates for laryngotracheal regeneration[185] due to its capability in tissue remodelling, and reduction of fibrosis and scars[73,76,77]. In addition, they share cell surface antigen expression with vocal fold fibroblasts, which are the main population involved laryngeal epithelial response to injury[186]. BM-MSCs seeded on 3D scaffolds helped generate extracellular matrix by

remodelling the surrounding tissue better than the non-seeded scaffolds in recent in vivo laryngeal tissue engineering studies[187,188].

POSS-PCU materials have shown great promise in cartilage tissue engineering studies. Oseni et al. demonstrated that when chondrocytes were cultured on POSS-PCU scaffolds, extracellular matrix components such as sGAG and collagen were generated[189]. POSS-PCU scaffolds also facilitated the growth of human adipose tissue-derived stem cell (hADSC) and chondrogenic differentiation into cartilage[190]. In this chapter, the potential of microporous POSS-PCU was explored to support BM-MSCs in terms of cytocompatibility, growth, and chondrogenic differentiation. This is to test its feasibility for future repair of laryngotracheal defects.

7.2 Materials and methods

7.2.1 BM-MSC culture and seeding

BM-MSCs were subcultured and expanded with Mesenchymal Stemm Cell Medium, MSCM (Sciencell, California, USA), in T75 cm^2 flask according to section 3.7.2 and 3.8. Before seeding, T75 cm^2 flask with a confluent layer of BM-MSCs was washed with 10 mL sterile PBS (20 mM). After washing, PBS was aspirated using a serological pipette and 3 mL of 0.25% trypsin-EDTA (Life-technologies, Paisley, UK) was added to the flask and allowed to incubate at 37^o C for 3 min until the cells can be detached with gentle tapping at the side of the flask. Then, 3 mL of trypsin was neutralised by adding 7 mL of fresh MSCM. The cell suspension was transferred in to a 15 mL centrifuge tube, and spun at 1,200 rpm for 5 min to concentrate the cell population. After centrifugation, the supernatant was discarded, and the cell pellet was resuspended in 2 mL of fresh MSCM. A viable cell count was performed using Trypan Blue staining, and haemocytometer to determine the amount of live cells using the Trypan Blue exclusion assay. Approximately 5 X 10^4 cells/mL were seeded on to each

well of a 24 TCP plate containing microporous POSS-PCU, which had been preadsorbed with 1 mL of MSCM after 24h prior to cell seeding.

7.2.2 Cell viability and proliferation of BM-MSCs on microporous POSS-PCU scaffold

The viability of BM-MSCs on POSS-PCU materials and TCP controls was tested using Alamar Blue™ assay for cell metabolic activity at time point of day 1, 4, 7, 11 and 14, as described previously in section 3.9. Cell proliferation was measured by freeze-and-thaw of the scaffold to extract their total DNA and using Hoechst 33258 fluorescent dye at time points of day 1, 7 and 14 via the methods described in detail in section 3.10.

7.2.3 Immunofluorescence staining

After fixing the cells in cold absolute ethanol, the samples were washed twice with 1 mL of sterile PBS. In blocking step, 1mL of blocking solution (1% (w/v) BSA and 0.25% (v/v) triton X100) in PBS was added to reduce non-specific protein binding. The samples were incubated at room temperature for 1 h.

After blocking, the samples were rinsed twice with PBS, and 1:200 phalloidin Alexa Fluor® 488 (Life-technologies, Paisley, UK) diluted in PBS and was added into each sample. The incubation was performed at room temperature for 1 h, followed by rinsing twice with PBS as described previously. Finally, nuclear staining was achieved by using 0.01 µg/mL Hoechst 33258 (Sigma-Aldrich, Gillingham, UK) in PBS for 10 min as a final step in the staining procedure.

The image was visualised and captured using EVOS® Imaging System (Life-technologies, Paisley, UK) at the exposure around 20-30% of 120 ms for blue fluorescence (Ex 357 nm, Em 447 nm), 50-70% of 500 ms for green fluorescence (Ex 470 nm, Em 510 nm).

7.2.4 Chondrogenic differentiation of BM-MSCs on microporous POSS-PCUs

7.2.4.1 Chondrogenic differentiation

Human BM-MSCs were subcultured in T75 cm^2 flask supplemented with MSCM medium (Sciencell™ Research Laboratories, California, USA) according to section 3.7.2 and 3.8. BM-MSCs were typsinised and seeded on to each material as previously described in 7.2.1 with 1mL of MSCM medium as detailed in Table 7.1.

Table 7.1 BM-MSC culture conditions and assessment

Sample	Seeded cell/sample	Material	sGAG quantification	DNA quantification	Histology assessment
Chondrogenic spheroids	1 X 10^6	15 mL polypropylene centrifuge tube			✓
Tissue Culture Polystyrene (TCP)	5 X 10^4	24-well plate	✓	✓	
Microporous POSS-PCUs	5 X 10^4	1.6 mm Microporous POSS-PCU discs of 30%, 50% and M70% $NaHCO_3$	✓	✓	✓

Chondrogenic differentiation was carried out on day 1 post seeding. Briefly, MSCM medium was discarded and replaced with 1 mL of Mesenchymal Stem Cell Chondrogenic Differentiation Medium (MCDM) supplemented with chondrogenic differentiation supplement, 5% penicillin/streptomycin (Sciencell™ Research Laboratories, California, USA), and 10 ng/mL Transforming growth factor beta-3(TGF-β3) (Miltenyi Biotec Ltd., Surrey, UK). Fresh MCDM was replaced in every third day of culture according to the company's instruction throughout the 5-week culture. TCP and microporous POSS-PCU samples were collected at day 1, 7, 14, 21, 28, and 35 to study sGAG synthesis and DNA

content. Chondrogenic spheroids and POSS-PCU samples on day 28 were used in histology assessment to study ECM forming with H&E, Alcian Blue, and van Gieson staining.

7.2.4.2 Assessment of sulfated glycosaminoglycan (sGAG) synthesis

Sulfated glycosaminoglycan is one of the main components for structural integrity of cartilage[191]. Current well-established protocol for BM-MSCs differentiation allows us to investigate the differentiation process of BM-MSCs to chondrogenic lineage with cartilage-like ECM production *in vitro*[192]. TCP and microporous POSS-PCUs were seeded with 5 X 10^4 cells per sample and a change of MSCM medium to MDCM chondrogenic differentiation medium was carried out day 1 post seeding as previously described in section 7.2.4.1. The equal sets of samples were still maintained in MSCM medium to use as negative controls for non-differentiation state of BM-MSCs on each material. The arrangement of sample number was illustrated in Table 7.2.

Table 7.2 Number of samples in each condition per time point for sGAG and DNA quantification studies.

Material	Non-differentiated BM-MSCs (per time point)		Differentiated BM-MSCs (per time point)	
	sGAG quantification	DNA quantification	sGAG quantification	DNA quantification
TCP	N = 4	N = 4	N = 4	N = 4
30% $NaHCO_3$	N = 4	N = 4	N = 4	N = 4
50% $NaHCO_3$	N = 4	N = 4	N = 4	N = 4
M70% $NaHCO_3$	N = 4	N = 4	N = 4	N = 4

7.2.4.2.1 Papain pre-extraction

TCP and microporous POSS-PCU samples (N = 4 per condition) were pre-extracted on day 1, 7, 14, 21, 28, and 35 using papain extraction reagent according to the company's instruction (Biocolor Ltd., Antrim, UK). Briefly, 50 mL of 0.2M sodium phosphate buffer,

pH 6.4 was prepared by dissolving 400mg sodium acetate, 200 mg EDTA disodium salt, and 40 mg cysteine HCl together in deionised water. Papain enzyme at 0.1 mg was introduced to every 1 mL of 0.2M sodium phosphate buffer to make a complete extraction reagent. All chemicals in this step were purchased from Sigma-Aldrich (Gillingham, UK). Each sample was added with 500 µL of extraction reagent and incubated at 65^{o} C for 3 h with occasional mixing. After 3 h, the extracted solutions were transferred to 1.5 mL micro-centrifuge tubes and spun at 10,000g for 10 min to remove the debris from the solution. Retain supernatants were used in sulphated glycosaminoglycan quantification and DNA quantification[193].

7.2.4.2.2 Sulfated glycosaminoglycan (sGAG) quantification

Sulfated glycosaminoglycan was quantified using Blyscan™ sulphated glycosaminoglycan assay (Biocolor Ltd., Antrim, UK). Extracted suspensions from 7.2.4.2.1 of 250 µL were transferred to new micro-centrifuge tubes and 1 mL of Blyscan dye reagent was added into each tube (n=4 per condition). The tubes were placed on a gentle mechanical shaker for 30 minutes. During this period, sGAG-dye complex formed and precipitated out from the soluble unbound dye. Then, the tube was spun at 12,000 rpm for 10 min and the supernatant was carefully removed. 0.5 mL of dissociation reagent was added to the pellet with interval mixing in vortex to help resuspend the sGAG-dye complex. Finally, 200 µL of each suspension was transferred to a clear 96-well plate and read the absorbance at 630 nm using a microplate reader (Biotek, Swindon, UK). The absorbance was calculated using a standard curve generated from glycosaminoglycan standards provided with the kit and was corrected with a dilution factor of 2.

7.2.4.2.3 DNA quantification

DNA quantification (n = 4 per condition) was also carried out to demonstrate the cell proliferation and the ratio of sGAG per DNA. Extracted suspension from 7.2.4.2.1 of 100 µL was mixed with 100 µL of 1 µg/mL Hoechst 33258 (Sigma-Aldrich, Gillingham, UK) in

black 96-well plate. The plate was read the fluorescence at 380 nm excitation and 420 nm emission using the Fluoroscan Ascent FL (Thermo Fischer Scientific, Massachusetts, USA). The data were compared to standard curve generated from standard calf thymus DNA provided with the kit and were corrected with dilution factor of 5.

7.2.4.3 Histology

Chondrogenic spheroids (day 28), non-differentiated BM-MSC on POSS-PCUs (day 14 and 28), and differentiated BM-MSC on POSS-PCUs (day 28) were fixed in 4% PFA in saline buffer (n = 2 per condition). Samples were sent to UCL Institute of Neurology (London, UK) to process the sample sections prior to staining. Briefly, the samples with cells were embedded in a paraffin block and cut in to 4 µm-thick sections using rotary microtome, Leica RM2235 (Leica Microsystem (UK) Ltd., Milton Keynes, UK). The slide gross sections were deparaffinised and stained with haematoxylin and eosin (H&E) stain, to indicate the gross cell morphology. The cartilage-like ECM production was investigated using Alcian Blue staining for polysaccharide (e.g. glycosaminoglycans) and van Gieson staining for collagen indication.

7.2.5 Statistical analysis

The mean and standard deviation data were compared using a two-way ANOVA to evaluate the difference of cell viability, cell proliferation, and sGAG quantification between materials with post hoc tests using Bonferroni's multiple comparisons test on each time point. P-value ≤ 0.05 was considered statistically significant between control and test samples. All statistical analysis was performed on the data sets using GraphPad Prism version 5.01 (2007) (GraphPad Software, Inc., California, USA).

7.3 Results

7.3.1 Cell viability of BM-MSCs on microporous POSS-PCU scaffold

Metabolic activity of BM-MSCs on both TCP and microporous POSS-PCUs (Figure 7.1) showed a linear increase over 14 days of experiment ($P \leq 0.001$). BM-MSC on TCP control had a significant higher metabolic activity than the microporous group from day 4 to 14 comparing based on each time point ($P \leq 0.001$). However, there was no significant difference in the trend when comparing 30%, 50% and M70% microporous POSS-PCUs ($P > 0.05$ for each time point, day 1-14).

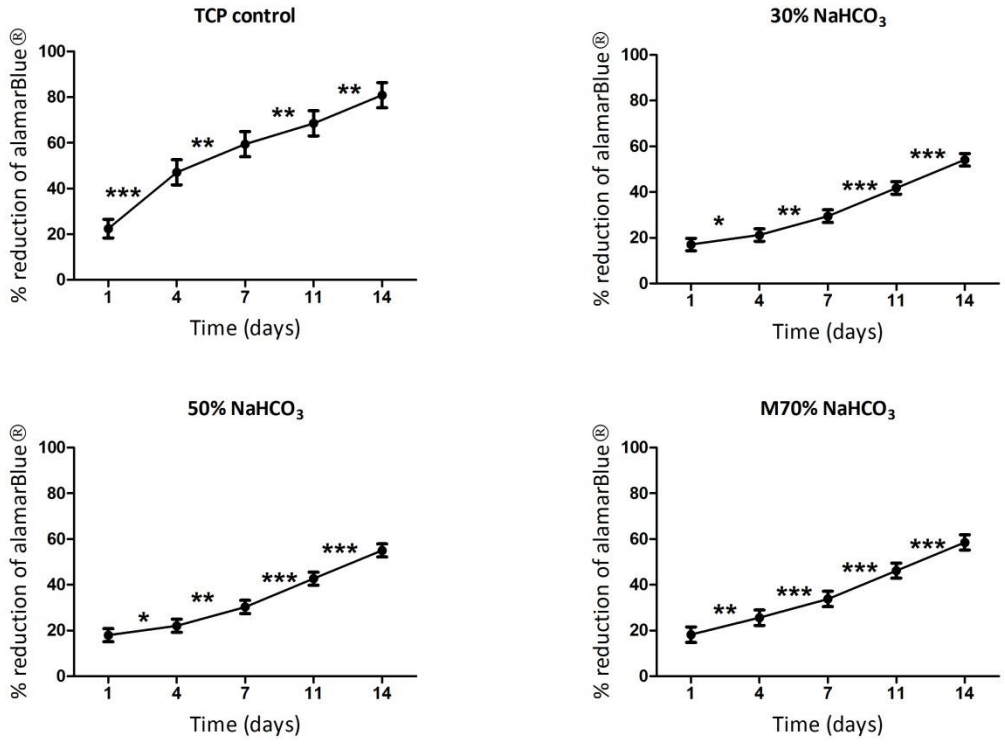

Figure 7.1 Metabolic activity of BM-MSCs on TCP and microporous POSS-PCU materials on day 1 to day 14. (n=6)

Total DNA quantification of BM-MSCs on TCP and microporous POSS-PCUs (Figure 7.2) also demonstrated an increase from day 1 to day 14 with linearity ($P \leq 0.001$). Similar to metabolic activity, the total DNA of TCP was significantly different from the microporous

POSS-PCUs when comparing each time point ($P \leq 0.001$). However, there was no significant difference in the microporous group comparing each time point ($P > 0.05$). The increasing of DNA content from each time point in all materials also correlated with the increase of metabolic activity ($P \leq 0.001$), suggesting the cell population was proliferating on the material.

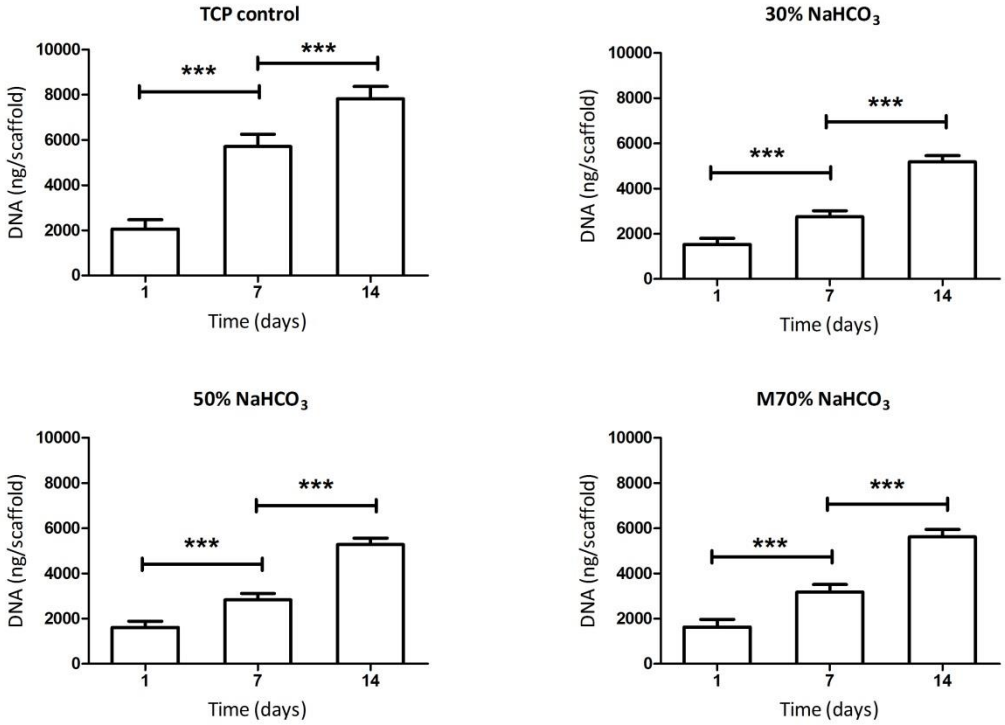

Figure 7.2 Metabolic activity of BM-MSCs on TCP and microporous POSS-PCU materials on day 1 to day 14. (n=3 per time point)

F-actin staining (Figure 7.3) and H&E staining (Figure 7.4) of BM-MSCs on TCP and microporous POSS-PCU presented a nearly confluent state on the surface. The cells were packed and elongated across the surface in almost a mono layer.

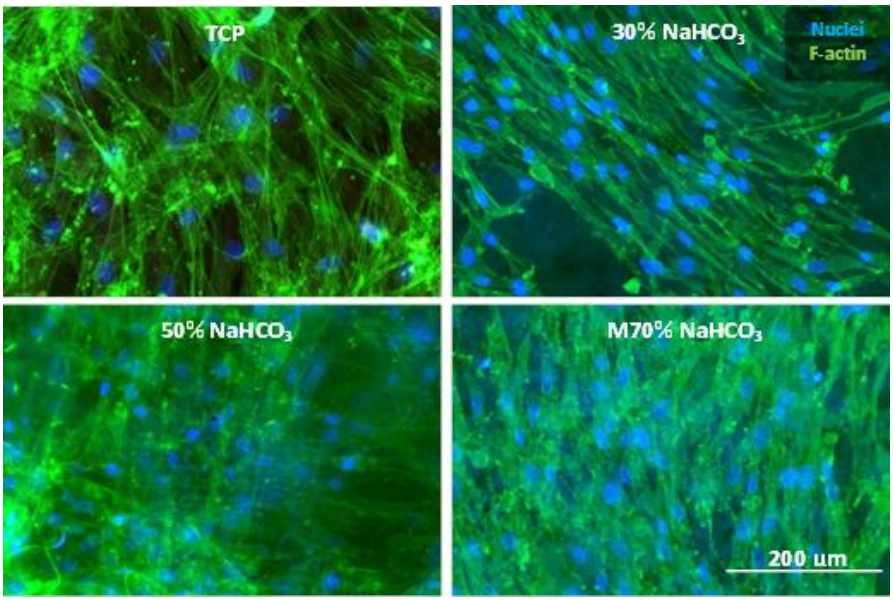

Figure 7.3 F-actin staining of BM-MSCs on TCP and microporous POSS-PCU surface on day 14 of culture.

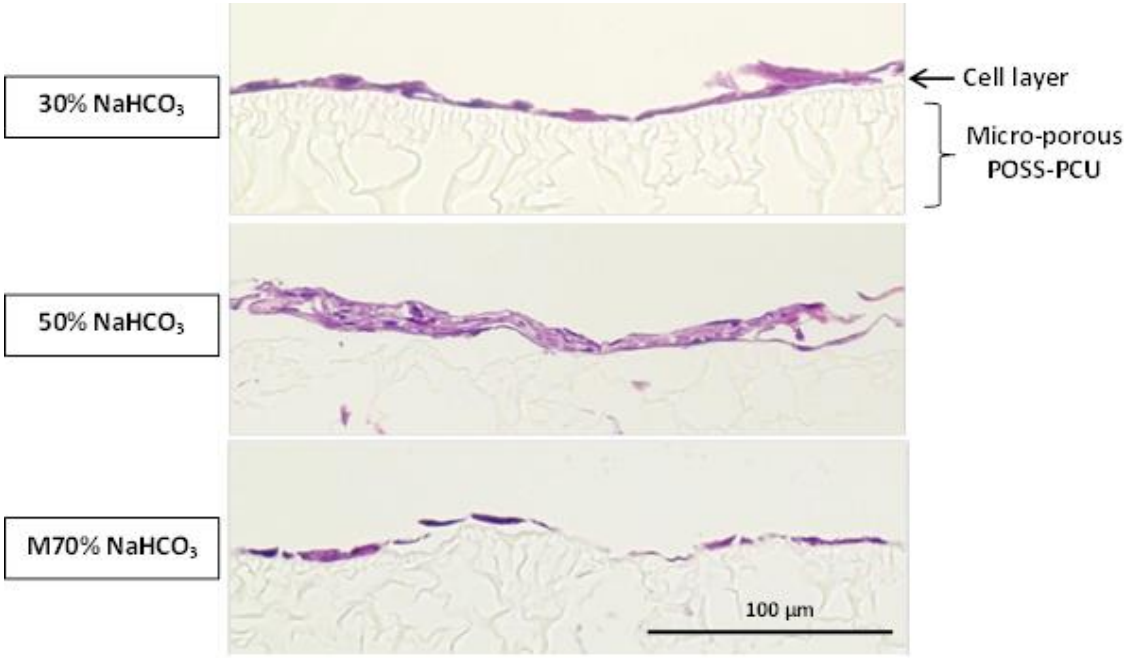

Figure 7.4 H&E staining of BM-MSCs on cross-sectioned microporous POSS-PCU surface on day 14 of culture.

7.3.2 Chondrogenic differentiation of BM-MSCs on microporous POSS-PCUs

7.3.2.1 Sulfated-glycosaminoglycans (sGAG) synthesis

Validation of Blyscan™ on sGAG quantification using standard glycosaminoglycan is illustrated in Figure 7.5. The absorbance at 630 nm and amount of sGAG from 0 – 6 µg showed a linear relationship ($P \leq 0.01$) with $R^2 = 0.997$. This standard curve was also used to calculate the amount of sGAG on each material in subsequent experiments.

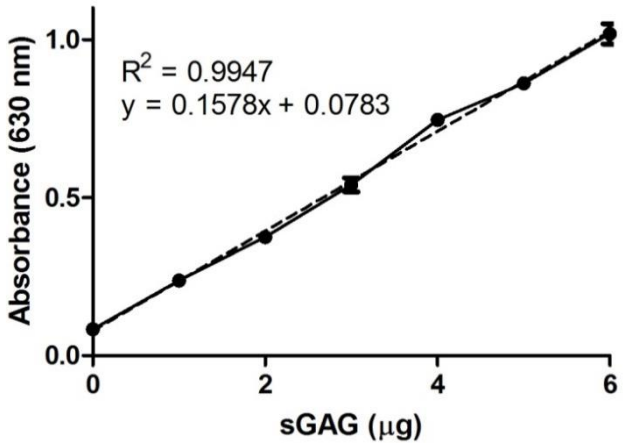

Figure 7.5 Linearity of sGAG quantification

Total sGAG syntheses of non-differentiated and differentiated BM-MSCs on all materials are presented in Figure 7.6. The patterns of sGAG synthesis were similar in all materials. Non-differentiated BM-MSCs on all materials exhibited an increase on day 1-14 and plateau out on day 14 -35. Differentiated BM-MSCs on all materials demonstrated different trends with an exponential increase on day 1-14, reaching the plateau around day 14-28, and the decrease from day 28-35. The mean sGAG syntheses of non-differentiated BM-MSCs were significantly different from differentiated BM-MSCs in all materials from day 7-35 ($P \leq 0.01$).

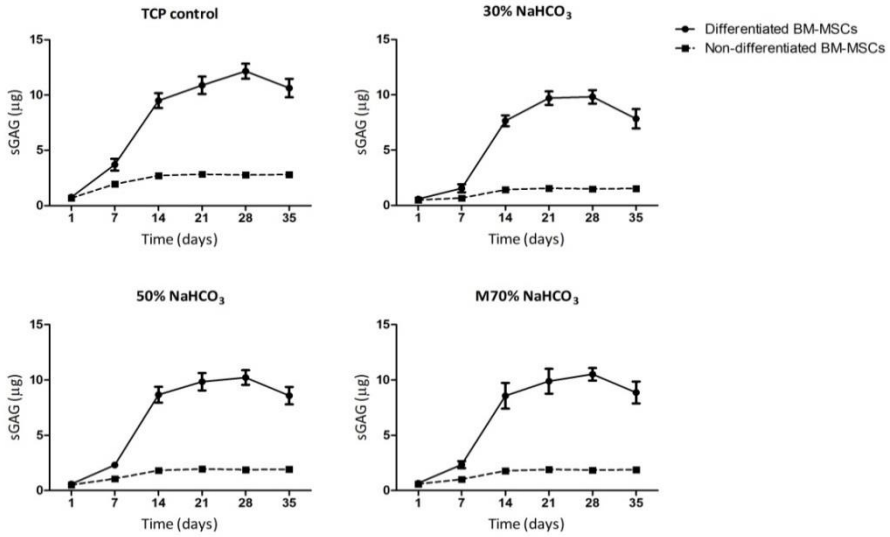

Figure 7.6 Total sGAG quantification of non-differentiated and differentiated BM-MSCs on TCP and microporous POSS-PCU materials. (n=4 per time point)

Total DNA quantification demonstrated in figure showing an increase on day 1-14 and plateau out on day 14-35 of culture in both non-differentiated and non-differentiated conditions (Figure 7.7). The Bonferroni's comparisons at each time point indicated that there was no significant difference between non-differentiated and differentiated BM-MSCs on all materials ($P > 0.05$).

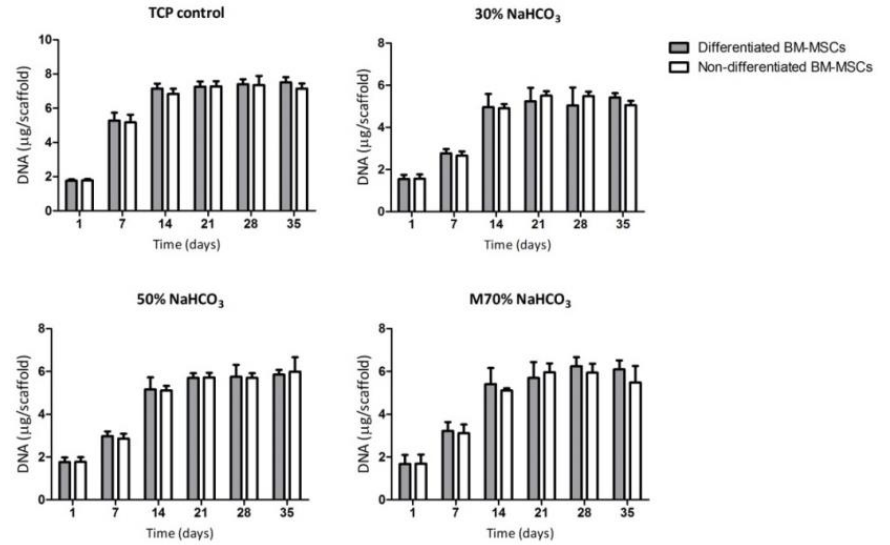

Figure 7.7 Total DNA quantification of non-differentiated and differentiated BM-MSCs on TCP and microporous POSS-PCU materials. (n=4 per time point)

The ratio of sGAG/DNA is illustrated in Figure 7.8. The sGAG/DNA ratios of non-differentiated BM-MSCs in all materials demonstrated an almost constantly straight line over 5 weeks of culture with no significant difference ($P > 0.05$), despite the increase of proliferation indicated by total DNA. However, differentiated BM-MSCs in all materials showed a significant difference of sGAG/DNA ratio comparing to the non-differentiated samples (day 7-35, $P < 0.01$), suggesting the extra amount of sGAG was produced in differentiated samples over the 5-week culture.

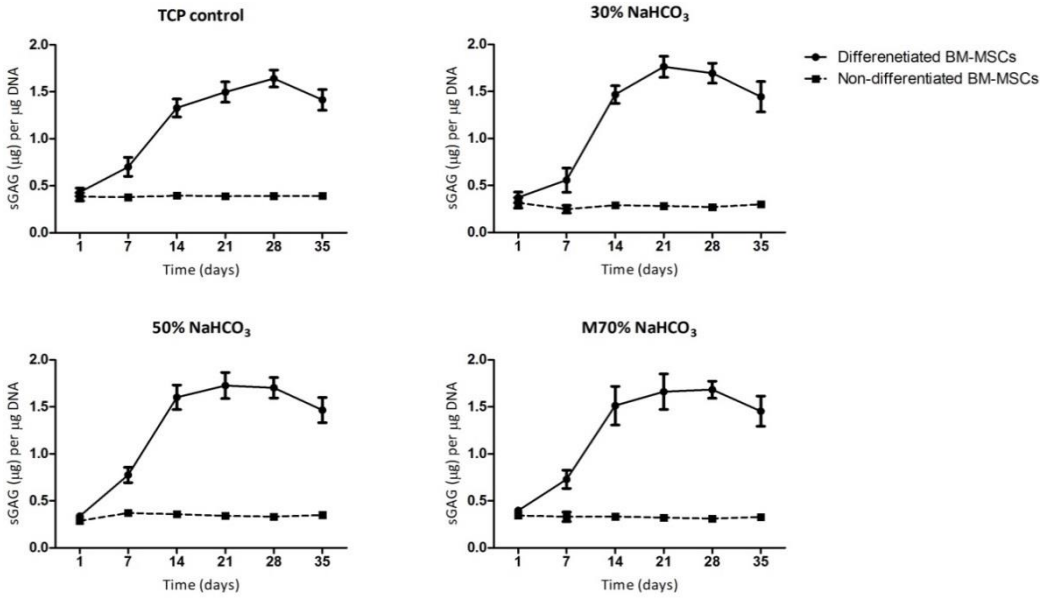

Figure 7.8 Ratio of sGAG/DNA of non-differentiated and differentiated BM-MSCs on TCP and microporous POSS-PCU materials. (n=4 per time point)

7.3.2.2 Morphological characterisation via histology

7.3.2.2.1 Cell Spheroids

Chondrogenic differentiation assay on day 28 demonstrated cells aggregated and formed a spherical structure with production of fibrous-like features around the spheroid (Figure 7.9). Three techniques of staining were employed to differentiate the characteristics of spheroids and they presented the expected outcome of positive chondrogenesis. H&E staining revealed a bi-layer of spheroid construct, which the aggregations of cells were inside and the outside covered with denser fibrous-like structure with the cells embedded within the spheroids. GAG production throughout the spheroid was confirmed by Alcian Blue staining whereas Van Gieson staining revealed the collagen was produced only at the covered fibrous-like layer. These results were used as a positive control to demonstrate the success of differentiation protocol, and were compared with the differentiation of BM-MSCs on microporous POSS-PCU materials.

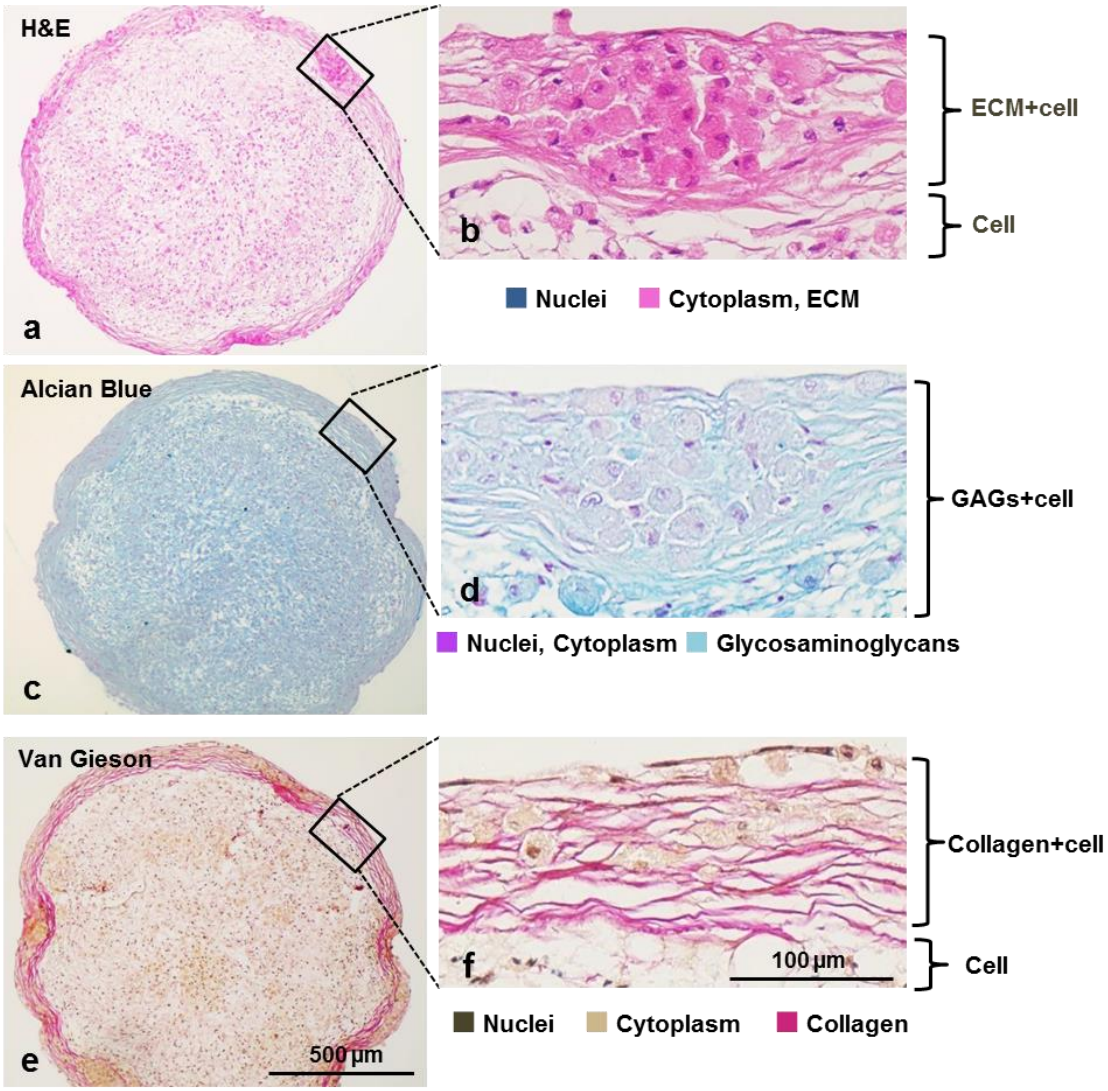

Figure 7.9 Chondrogenic spheroid differentiated from BM-MSCs after 28 days stained by H&E (a and b), Alcain Blue (c and d), and Van Gieson's staining (e and f). Magnification = 100X and scale bar = 500 µm (a, c, and e). Magnification = 400X and scale bar = 100 µm (b, d, and f).

7.3.2.2.2 Cells on POSS-PCU materials

H&E staining of undifferentiated and differentiated BM-MSCs on microporous POSS-PCU (day 28) is shown in Figure 7.10. Negative controls show BM-MSCs maintained almost a mono-layer of cells on each material while differentiated cells present a thicker multi-layer of cells with ECM to about 70 – 120 µm.

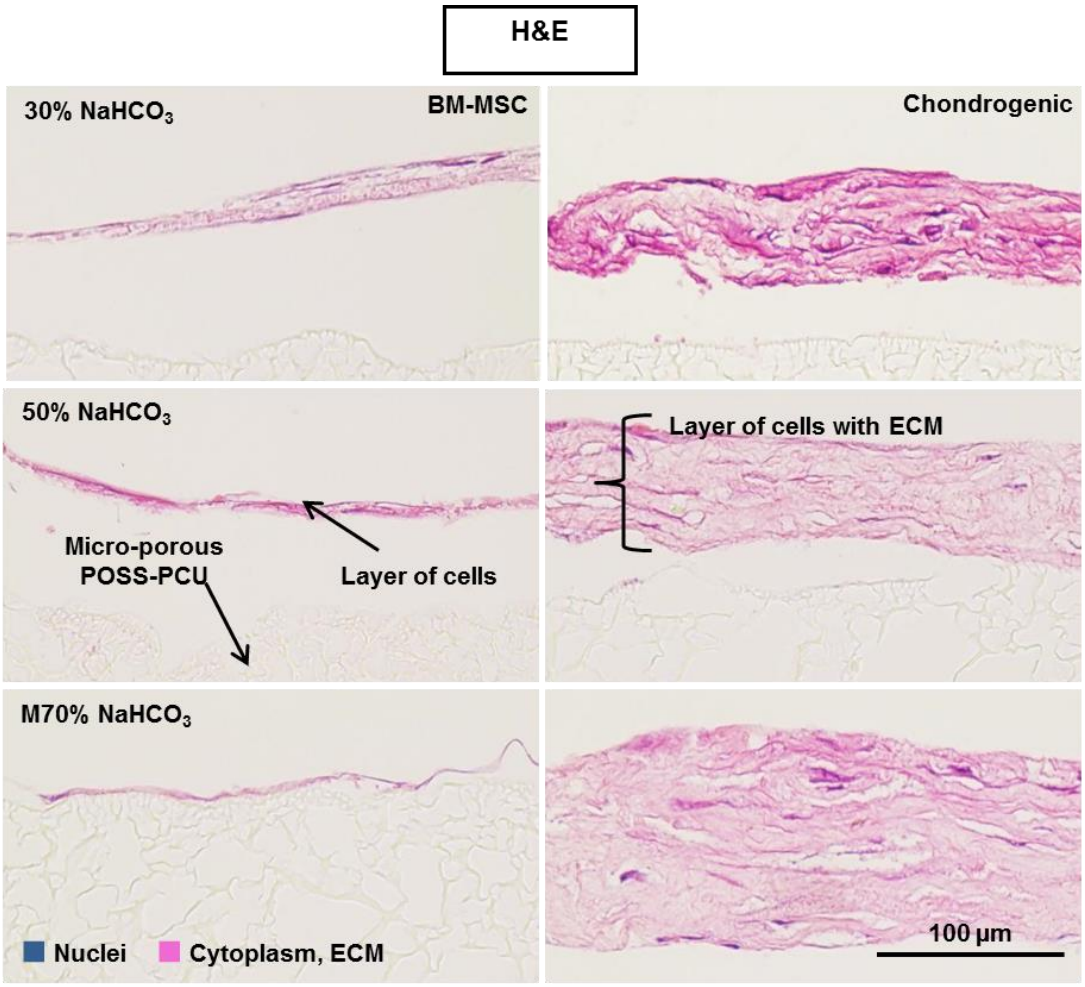

Figure 7.10 H&E staining of non-differentiated BM-MSCs (left panel) and differentiated chondrogenic-like cells (right panel) after 28 days on microporous POSS-PCU materials. Magnification = 400X and scale bar = 100 µm.

Alcian Blue staining (Figure 7.11) revealed more details of GAG deposition pattern between undifferentiated and differentiated BM-MSCs. Undifferentiated BM-MSCs

(negative control) on all microporous POSS-PCU materials organised into a thin layer of cells (red/pink colours) on top of the materials with no or very little GAG deposition (blue colour) in extracellular space, whereas the differentiated chondrogenic-like cells exhibited a multi-layer of cells with a significant deposition of GAGs in the extracellular space. The constructs were fibrous-like and similar to that of the outer layer of spheroid positive control, where the fibrous-like structure was integrated with cells. However, the differentiated cells on POSS-PCU materials did not form spheroid structures similar to those of the positive control. Instead, they spread and aligned along the surface of the microporous POSS-PCU.

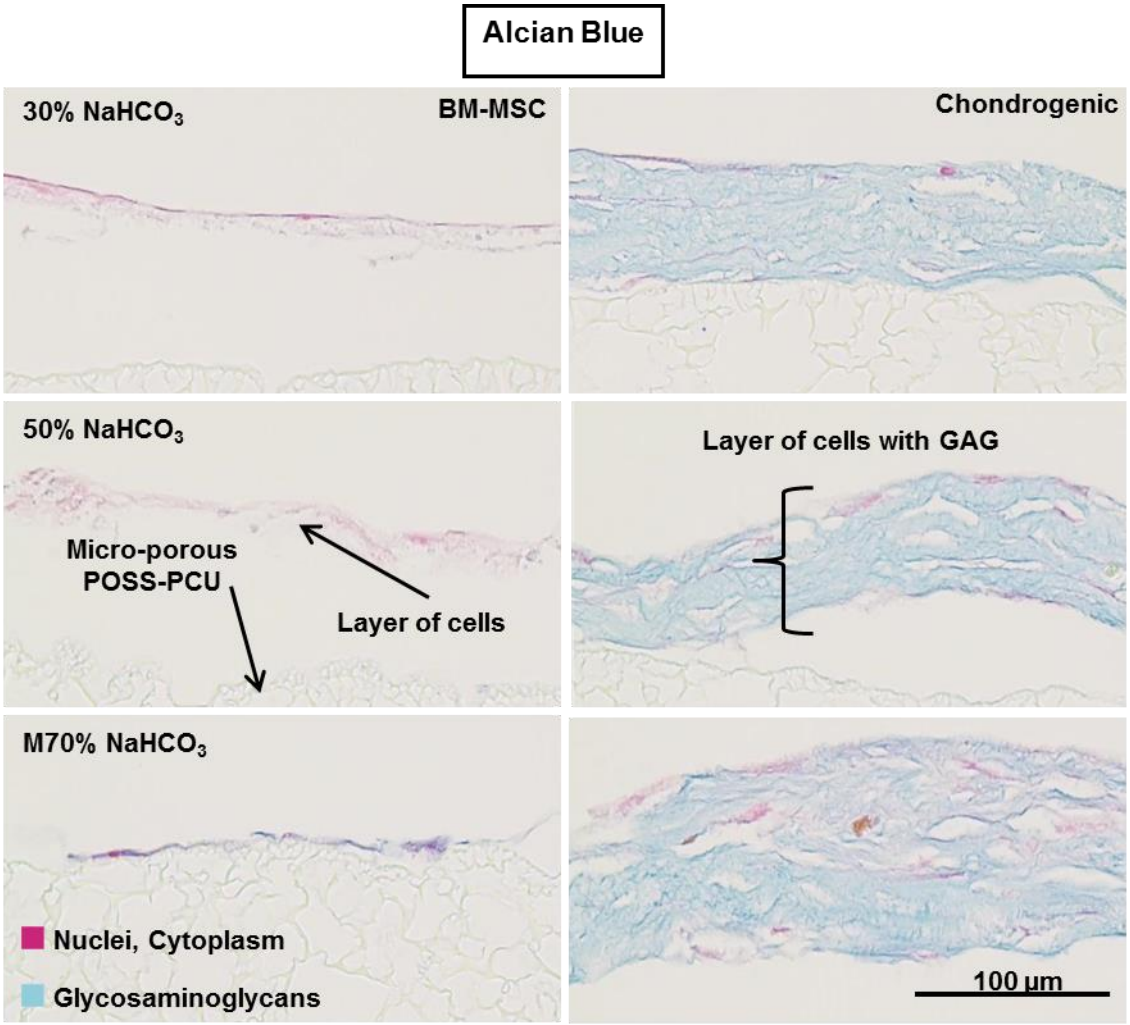

Figure 7.11 Alcian Blue staining of non-differentiated BM-MSCs (left panel) and differentiated chondrogenic-like cells (right panel) after 28 days on microporous POSS-PCU materials. Magnification = 400X and scale bar = 100 µm.

Van Gieson's staining (Figure 7.12) demonstrated the similar pattern to the Alcian Blue staining. Undifferentiated BM-MSCs in all microporous POSS-PCU studies organised in a thin layer of cells (dark brown/brown colours) on top of the materials without collagen deposition (pink colour) in the extracellular space while the differentiated chondrogenic-like cells exhibited a multi-layer of cells with a significant deposition of collagen in extracellular space.

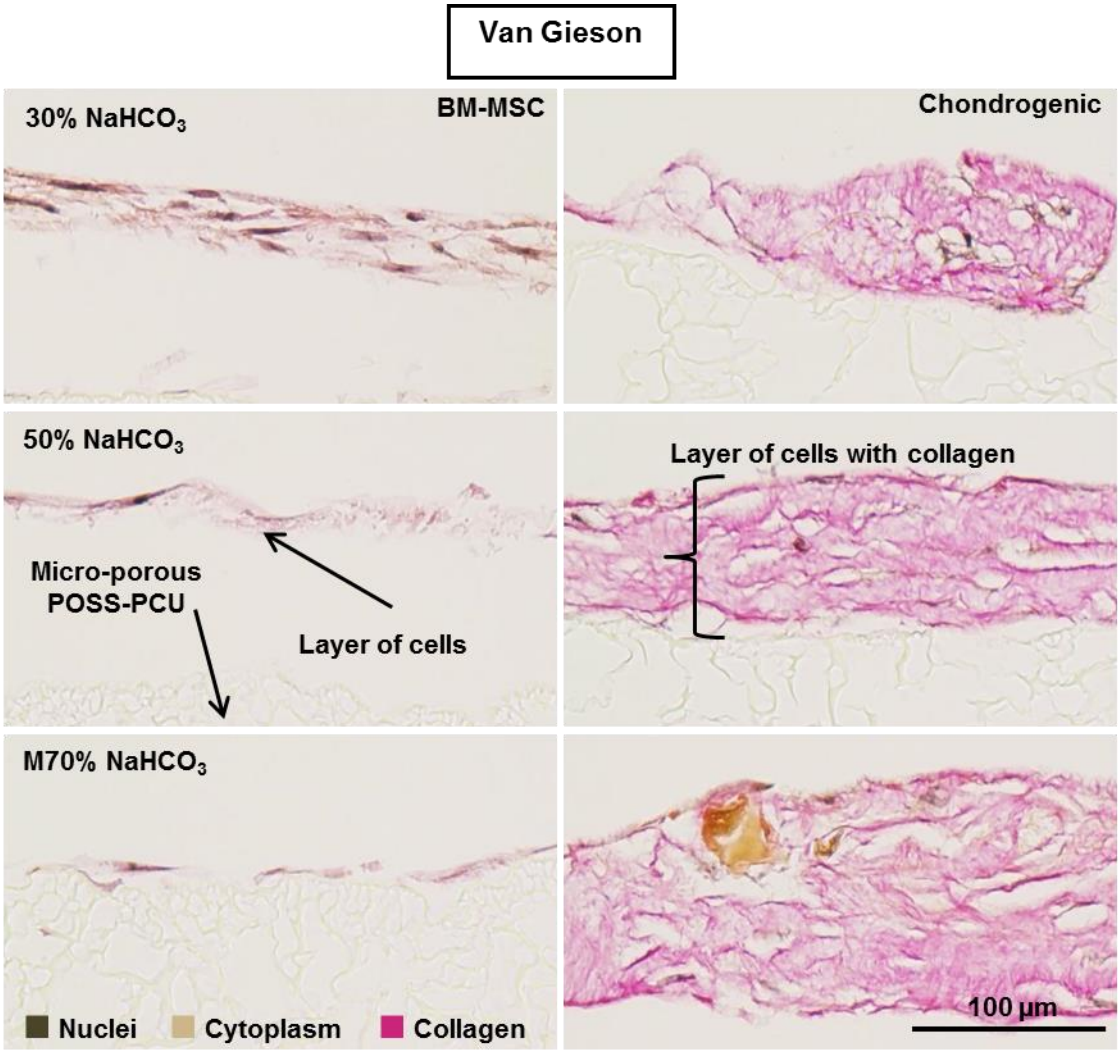

Figure 7.12 Van Gieson staining of non-differentiated BM-MSCs (left panel) and differentiated chondrogenic-like cells (right panel) after 28 days on microporous POSS-PCU materials. Magnification = 400X and scale bar = 100 µm.

7.4 Discussion

Cytocompatibility studies of microporous POSS-PCU were presented with human bronchial epithelial cell in chapter 6. In this chapter, the response was investigated in the same material using human bone-marrow mesenchymal stem cells (BM-MSCs), both differentiated and undifferentiated, with a view to assessing potential use of this combination in tissue engineering applications.

Fourteen days culture of BM-MSCs on TCP, 30%, 50% and M70% $NaHCO_3$ microporous POSS-PCUs demonstrated a linear growth over 14 days of culture indicated by the increase of both metabolic activity and DNA content. Nuclear, f-actin and H&E staining on day 14 demonstrated the BM-MSCs formed a confluent layer on TCP and microporous POSS-PCU.

Differentiation of BM-MSCs to chondrogenic lineage using a well-established protocol was performed and the behaviour of these cells examined on microporous POSS-PCU to 35 days of culture. Phenotype was measured indirectly via cartilaginous extracellular matrix production over the culture period. The behaviour of differentiated BM-MSCs was quantitatively measured by sGAG production and qualitatively by histochemical evidence of deposition of ECM, GAG, and collagen.

The production of sGAG in differentiated BM-MSCs on all materials was significantly different between days 7 and 35 ($P \leq 0.01$) from that of undifferentiated BM-MSCs. The ratio of sGAG/DNA exhibited the same trend ($P \leq 0.01$) while that of undifferentiated samples was constant throughout 35 days, despite progressive cell proliferation in both conditions. This suggested the differentiated samples produced more sGAG. Histology of day 28 samples (time point of maximum production) demonstrated location of sGAG deposition.

Chondrogenic spheroids (day 28) were used as positive control for histochemistry because of the facility with which they can be micro-sectioned. An aggregation of cells and a

visible spheroid construct was formed over 28 days and gave a circular shape when it was micro-sectioned. A distinctive 2 layer-structure was revealed by H&E: dense outer layer of cellularised fibrous-like structure; less dense inner layer composed of cells only. Alcian Blue staining showed blue colour throughout, more so in the outer layer, indicating GAG production. Van Gieson staining showed an outer layer composed of red-coloured collagen fibres, suggestive of ECM deposition, with cells throughout both layers.

Chondrogenic differentiation of BM-MSCs on microporous POSS-PCU materials revealed a combination ECM and cell layer spread across the material surface whereas the undifferentiated samples showed a thin layer of cells without significant ECM production. H&E staining of differentiated samples showed a thick layer of fibrous-like ECM with cells embedded inside, whilst undifferentiated samples were composed of thin confluent cell layers on the material surface. Alcian Blue and van Gieson staining showed similar structure of GAG layers with cells and collagen layers with cells, respectively, whereas the undifferentiated samples did not have a significant "ECM" component.

This experiment suggests that BM-MSCs can be grown and differentiated on microporous POSS-PCU materials. The difference in morphology between differentiated and undifferentiated samples may relate to the sGAG/DNA ratio results. The significant difference in sGAG/DNA ratio between undifferentiated and differentiated samples might be due to the extra deposition of sGAG in the extracellular space in differentiated samples and was confirmed by staining pictures. However, more studies could be further carried out in the future to gather more evidences by detection of cell surface antigen or gene expression such as CD44, CD54, collagen type II, and aggrecan[194–196].

Microporous POSS-PCU appears to support BM-MSC growth and chondrogenic differentiation *in vitro*. In this study, the same material was employed as in previous studies of human bronchial epithelial cells. The results showed the chondrogenic-like mass aggregates mainly on the top of microporous surface with low permeation into the pores. The

pore size used was 25 – 53 μm, a size previously shown to support epithelial growth. However, a different pore size may be required to optimise and promote MSC-chondrocyte integration. A pore range of 100 – 300 μm in 3D porous poly(epsilon-caprolactone) and silk-fibroin scaffolds has been described to better facilitate cell infiltration, chondrogenic or osteogenic differentiation of human BM-MSCs, resulted in uniform matrix formation across the depth of the scaffolds, possibly for its micro-architechture reasons[197–199]. There are also limitations to using ECM-production alone as a marker of chondrocytic differentiation. More detailed characterisation of these cells might include measurement of gene expression, detailed immunophenotyping or cytokine production[194–196].

7.5 Conclusion

Microporous POSS-PCU supported BM-MSC growth and probable chondrogenic differentiation *in vitro* with sGAG and collagen production mimicking ECM. Further *in vivo* studies of POSS-PCU are warranted to confirm safety and potential efficacy as a scaffold material for laryngotracheal tissue engineering.

Chapter 8 Summary and Future Outlook

Functional laryngeal replacement would be life-changing for patients who undergo total laryngectomy or suffer from severe structural airway disorders. The treatment for laryngectomised patients has not changed for decades[2]. Commercially available implants for total laryngectomies such as Montgomery T tube[200], and Provox[201], allow patients to breathe through open tracheostoma. However, current laryngeal implants are unable to meet all functional needs due to their suboptimal voice function and tissue integration in particular[202,203]. Therefore, researchers are currently investigating using tissue-engineering and regenerative medicine approaches to improve the quality and function of laryngeal implants to match these clinical needs.

A novel nanocomposite with enhanced physiochemical properties and superior biological stability has been developed by our group. Formed by incorporating polyhedral oligomeric silesquioxane (POSS) into poly(carbonate-urea) urethane, POSS-PCU may offer new potential for the development of a new generation of laryngeal implants, due to its superior mechanical properties and biocompatibility than current industry standard materials such as ePTFE[204]. POSS-PCU is currently in use for a range of tissue engineering applications and has been successfully implanted in human in the form of a small calibre cardiac bypass graft[83], lacrimal duct conduit[71], and more recently as the basis of a synthetic trachea[30].

Chapter 4 demonstrated that the solvent evaporation technique (casted POSS-PCU) and phase inversion/particulate leaching technique (microporous POSS-PCU) allow the manufacture of customised POSS-PCU laryngeal implants that replicate the shape of a porcine larynx. The materials produced have similar structural and mechanical properties

compared to a porcine larynx (cartilage and epithelium). The key findings were that non-porous casted POSS-PCU had closer elastic moduli to porcine cartilage while that of microporous POSS-PCU was closer to that of epithelium. This evidence suggested that POSS-PCU may be tailored to suit diverse tissue-replacement needs. Casted POSS-PCU can be used to provide the integrity of the whole implant to keep the hollow tube open and prevent stenosis while the microporous POSS-PCU fully coated outside, might be used for cell growth and tissue integration with re-epithelialisation, as well as reduced graft extrusion. A previous *in vivo* study of an implant composed of casted POSS-PCU coated with microporous POSS-PCU (one-side coated) in pigs showed that the grafts extruded after implantation (Lange, personal communication). Histology revealed that contacted casted non-porous POSS-PCU did not demonstrate good tissue integration at the anastomosis site. Thus, the study on fully coated microporous POSS-PCU was chosen.

Microporous POSS-PCU was tested as a candidate material to replace the vocal cords, and in this setting produced comparable 'voice' in a controlled air-flow system. The generated sound quality was similar to that of the human voice regarding fundamental frequency and sound energy. Pitch (fundamental frequency) was varied by a change in material thickness and strain, whereas sound energy could be increased or decreased by controlling airflow. In this model, it illustrated the superior quality of sound generated compared to that of a recent clinical titanium implant[2]. However, this model has some limitations that can be improved in the future. The additional apparatus such as temperature-humidifier[101–103] can be integrated into the testing system to control the condition instead of the ambient temperature and moisturised air employed in our experiment. How such cords may be made to move to fulfil the needs of speech, breathing, coughing and airway protection remain to be determined. The potential roles of pneumatic artificial muscles (PAMs)[205] and electro-conductive actuators are currently explored, to address this substantial challenge[206]. The materials of these actuators are usually silicone or

polyurethane based. Coating these devices with POSS-PCU may increase their biocompatibility and thus their ability to mimic normal human motion.

In Chapter 5, the porogen size of 25-53 µm was chosen to do further characterisation because our previous study showed HBEC fell through the microporous POSS-PCU with the bigger porogen size (105-150 µm). Regarding sterilisation techniques, there was a significant reduction in hydrophobicity by using ethanol rinsing, with changes in surface characteristics of the material, and subsequently increased protein adsorption and HBEC growth while the autoclave samples did not (as summarised in Figure 8.1). However, autoclaved POSS-PCU showed no significant change in mechanical properties compared to control. Therefore, the combination of the ethanol rinsing technique to activate the POSS-PCU surface followed by steam sterilisation (autoclave) might be an ideal sterilisation sequence because the steam sterilisation is an acceptable standard for medical devices.

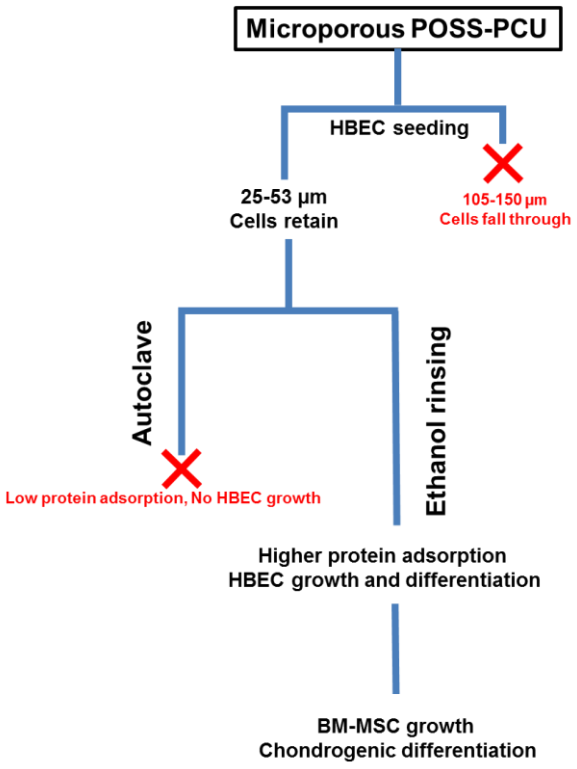

Figure 8.1 Summary of optimisations on material for cell cultures

Controlling porosity is vital for balancing the need for vascularisation with biomechanical strength[207,208]. The results demonstrated greater control in reproducible porosity in microporous POSS-PCU manufacturing by incorporating the different amount of porogen ($NaHCO_3$) to vary porosity. Higher %$NaHCO_3$ generated a more porous structure at the outermost surface, and increased interconnected pores, as shown by water permeability testing. This supports the idea of using a microporous structure to coat the outside of the laryngeal framework and merits study of tissue integration or vascularisation *in vivo*.

POSS-PCU previously has been tested and validated for cytocompatibility of different cell types such as dermal fibroblasts[135], chondrocytes[189], and endothelial cells[209]. In chapter 6, human bronchial epithelial cells (HBECs) were grown successfully on microporous POSS-PCU materials while maintaining epithelial cell markers. Additionally, the differentiated HBECs had all the expected characteristics such as layer stratification, intercellular tight-junction, mucin production and ciliation. This evidence suggested the growth and the differentiation of HBECs on POSS-PCU *in vitro*. The continuing work might be the measurement of cilia beating and investigation on other epithelial cell markers comparing with native airway tissue. This finding could also pave the way to use this material for other epithelial-derived conduits such as oesophagus and bile duct. Further work on improving epithelialisation of POSS-PCU conduits is required. The result showed that higher %$NaHCO_3$ provides better cell migration and integration into microporous POSS-PCU. The further investigation of using these materials *in vivo* (either polymer alone or in combination with an epithelial-sheet / decellularised tissue) is recommended.

In chapter 7, microporous POSS-PCU showed cytocompatibility for human bone-marrow derived mesenchymal stem cells (BM-MSCs). BM-MSCs were grown and maintained on the material under *in vitro* condition over 35 days. BM-MSCs could also be differentiated to the chondrogenic lineage with a production of an ECM with some features of cartilage, composed of sGAG and collagen. The future challenge remains to studying this material

together with stem-cells to support cartilage replacement for laryngotracheal applications. The obtained pore size was around 25 – 53 μm and supported a good epithelial layer with in-growth of cells (Chapter 6). A pore size range of 100 – 300 μm of other biomaterials, such as 3D porous poly(epsilon-caprolactone) has been shown to support better chondrogenic or osteogenic differentiation of human BM-MSCs regarding integrated scaffold-matrix formation [197–199]. The future study of microporous POSS-PCU of similarly bigger pore size might be necessary to optimise the scaffold-cartilage formation.

The results demonstrated the use of POSS-PCU materials in non-porous form and microporous foam-form, suitable for the design the 3D laryngeal frameworks with air-flow responsive voice function. Moreover, the prototype larynx proved to exhibit biomechanical characteristics similar to porcine laryngeal tissues, and surface enhancements accommodated HBECs growth and differentiation. This supports the possibility of developing POSS-PCU as a biomaterial for laryngotracheal tissue engineering, as well as other related applications.

Having identified a promising biomaterial for airway tissue engineering, there are many steps before this can be applied in early phase clinical trials. More work is required to confirm biocompatibility *in vivo*, including the rate of tissue integration, neo-vascular formation, tissue fibrosis/stenosis, extrusion rate of the implants. If this work confirms the promise, standard operating procedures will be developed for clinical grade production, so that validated and reliable data that proves the new approach is ready for clinical trials in human patients. Good Laboratory Practice (GLP) studies in an appropriate large animal model will be used to generate safety, toxicity and potential efficacy data for a Medicines and Healthcare products Regulatory Agency (MHRA) and Clinical Trials Authorisation (CTA). In this way, the work herein will lead to the new generation of total-replacement laryngeal implants for patients in desperate need.

Bibliography

[1] Rossi VC, Fernandes FL, Ferreira MAA, Bento LR, Pereira PSG, Chone CT. Larynx cancer: quality of life and voice after treatment. Braz J Otorhinolaryngol 2014;80:403–8.

[2] Debry C, Dupret-Bories A, Vrana NE, Hemar P, Lavalle P, Schultz P. Laryngeal replacement with an artificial larynx after total laryngectomy: The possibility of restoring larynx functionality in the future. Head Neck 2014.

[3] Cox SR, Theurer JA, Spaulding SJ, Doyle PC. The multidimensional impact of total laryngectomy on women. J Commun Disord 2015;56:59–75.

[4] Offerman MPJ, Pruyn JFA, de Boer MF, Busschbach JJ V, Baatenburg de Jong RJ. Psychosocial consequences for partners of patients after total laryngectomy and for the relationship between patients and partners. Oral Oncol 2015;51:389–98.

[5] Hirani I, Siddiqui AH, Muhammad Khyani IA. Apprehensions and problems after laryngectomy: Patients' perspective. J Pak Med Assoc 2015;65:1214–8.

[6] Boscolo-Rizzo P, Maronato F, Marchiori C, Gava A, Da Mosto MC. Long-term quality of life after total laryngectomy and postoperative radiotherapy versus concurrent chemoradiotherapy for laryngeal preservation. Laryngoscope 2008;118:300–6.

[7] Baiguera S, Gonfiotti A, Jaus M, Comin CE, Paglierani M, Del Gaudio C, et al. Development of bioengineered human larynx. Biomaterials 2011;32:4433–42.

[8] Strome M, Stein J, Esclamado R, Hicks D, Lorenz RR, Braun W, et al. Laryngeal transplantation and 40-month follow-up. N Engl J Med 2001;344:1676–9.

[9] Lorenz RR, Strome M. Total laryngeal transplant explanted: 14 years of lessons learned. Otolaryngol Head Neck Surg 2014;150:509–11.

[10] De Bartolo L, Bader A. Biomaterials for Stem Cell Therapy: State of Art and Vision for the Future. CRC Press, Italy; 2013.

[11] Mor N, Blitzer A. Functional Anatomy and Oncologic Barriers of the Larynx. Otolaryngol Clin North Am 2015;48:533–45.

[12] Berke GS, Long JL. Handbook of Mammalian Vocalization - An Integrative Neuroscience Approach. vol. 19. Elsevier; 2010.

[13] Shiba K. Handbook of Mammalian Vocalization - An Integrative Neuroscience Approach. vol. 19. Elsevier; 2010.

[14] Plant RL, Younger RM. The interrelationship of subglottic air pressure, fundamental frequency, and vocal intensity during speech. J Voice 2000;14:170–7.

[15] Holmberg EB, Hillman RE, Perkell JS. Glottal airflow and transglottal air pressure measurements for male and female speakers in soft, normal, and loud voice. J Acoust Soc Am 1988;84:511–29.

[16] Titze I. Phonation threshold pressure: a missing link in glottal aerodynamics. J Acoust Soc Am 1992;91:2926–35.

[17] Gray SD. Cellular physiology of the vocal folds. Otolaryngol Clin North Am 2000;33:679–98.

[18] Gray SD, Titze IR, Chan R, Hammond TH. Vocal fold proteoglycans and their influence on biomechanics. Laryngoscope 1999;109:845–54.

[19] Farran AJE, Teller SS, Jha AK, Jiao T, Hule RA, Clifton RJ, et al. Effects of matrix composition, microstructure, and viscoelasticity on the behaviors of vocal fold fibroblasts cultured in three-dimensional hydrogel networks. Tissue Eng Part A

2010;16:1247–61.

[20] Parkin DM, Bray F, Ferlay J, Pisani P. Global cancer statistics, 2002. CA Cancer J Clin 55:74–108.

[21] Larizadeh MH, Damghani MA, Shabani M. Epidemiological characteristics of head and neck cancers in southeast of iran. Iran J Cancer Prev 2014;7:80–6.

[22] Jégu J, Binder-Foucard F, Borel C, Velten M. Trends over three decades of the risk of second primary cancer among patients with head and neck cancer. Oral Oncol 2013;49:9–14.

[23] Agrawal N, Goldenberg D. Primary and salvage total laryngectomy. Otolaryngol Clin North Am 2008;41:771–80, vii.

[24] Flint PW, Haughey BH, Robbins KT, Thomas JR, Niparko JK, Lund VJ, et al. Cummings Otolaryngology - Head and Neck Surgery. 6th ed. Saunders; 2015.

[25] Brook I. Neck cancer: a physician's personal experience. Arch Otolaryngol Head Neck Surg 2009;135:118.

[26] Kandakure VT, Mishra S, Lahane VJ. Management of Post-traumatic Laryngotracheal Stenosis: Our Experience. Indian J Otolaryngol Head Neck Surg 2014;67:255–60.

[27] Shapshay SM, Beamis JF, Hybels RL, Bohigian RK. Endoscopic treatment of subglottic and tracheal stenosis by radial laser incision and dilation. Ann Otol Rhinol Laryngol 96:661–4.

[28] Ciccone AM, De Giacomo T, Venuta F, Ibrahim M, Diso D, Coloni GF, et al. Operative and non-operative treatment of benign subglottic laryngotracheal stenosis. Eur J Cardiothorac Surg 2004;26:818–22.

[29] Elliott MJ, De Coppi P, Speggiorin S, Roebuck D, Butler CR, Samuel E, et al. Stem-

cell-based, tissue engineered tracheal replacement in a child: a 2-year follow-up study. Lancet (London, England) 2012;380:994–1000.

[30] Jungebluth P, Alici E, Baiguera S, Le Blanc K, Blomberg P, Bozóky B, et al. Tracheobronchial transplantation with a stem-cell-seeded bioartificial nanocomposite: a proof-of-concept study. Lancet (London, England) 2011;378:1997–2004.

[31] Omori K, Tada Y, Suzuki T, Nomoto Y, Matsuzuka T, Kobayashi K, et al. Clinical application of in situ tissue engineering using a scaffolding technique for reconstruction of the larynx and trachea. Ann Otol Rhinol Laryngol 2008;117:673–8.

[32] Fishman JM, Lowdell M, Birchall M a. Stem cell-based organ replacements-Airway and lung tissue engineering. Semin Pediatr Surg 2014;23:119–26.

[33] Fishman JM, Lowdell MW, Urbani L, Ansari T, Burns AJ, Turmaine M, et al. Immunomodulatory effect of a decellularized skeletal muscle scaffold in a discordant xenotransplantation model. Proc Natl Acad Sci U S A 2013;110:14360–5.

[34] Crapo PM, Gilbert TW, Badylak SF. An overview of tissue and whole organ decellularization processes. Biomaterials 2011;32:3233–43.

[35] Elliott MJ, De Coppi P, Speggiorin S, Roebuck D, Butler CR, Samuel E, et al. Stem-cell-based, tissue engineered tracheal replacement in a child: A 2-year follow-up study. Lancet 2012;380:994–1000.

[36] Olausson M, Patil PB, Kuna VK, Chougule P, Hernandez N, Methe K, et al. Transplantation of an allogeneic vein bioengineered with autologous stem cells: A proof-of-concept study. Lancet 2012;380:230–7.

[37] Gonfiotti A, Jaus MO, Barale D, Baiguera S, Comin C, Lavorini F, et al. The first tissue-engineered airway transplantation: 5-year follow-up results. Lancet (London, England) 2014;383:238–44.

[38] Badylak SF. The extracellular matrix as a scaffold for tissue reconstruction. Semin Cell Dev Biol 2002;13:377–83.

[39] Huber JE, Spievack A, Simmons-Byrd A, Ringel RL, Badylak S. Extracellular matrix as a scaffold for laryngeal reconstruction. Ann Otol Rhinol Laryngol 2003;112:428–33.

[40] Xu CC, Chan RW, Tirunagari N. A biodegradable, acellular xenogeneic scaffold for regeneration of the vocal fold lamina propria. Tissue Eng 2007;13:551–66.

[41] Xu CC, Chan RW, Weinberger DG, Efune G, Pawlowski KS. A bovine acellular scaffold for vocal fold reconstruction in a rat model. J Biomed Mater Res A 2010;92:18–32.

[42] Hou N, Cui P, Luo J, Ma R, Zhu L. Tissue-engineered larynx using perfusion-decellularized technique and mesenchymal stem cells in a rabbit model. Acta Otolaryngol 2011;131:645–52.

[43] Elliott MJ, De Coppi P, Speggiorin S, Roebuck D, Butler CR, Samuel E, et al. Stem-cell-based, tissue engineered tracheal replacement in a child: a 2-year follow-up study. Lancet (London, England) 2012;380:994–1000.

[44] Long JL, Zuk P, Berke GS, Chhetri DK. Epithelial differentiation of adipose-derived stem cells for laryngeal tissue engineering. Laryngoscope 2010;120:125–31.

[45] Gray SD, Pignatari SS, Harding P. Morphologic ultrastructure of anchoring fibers in normal vocal fold basement membrane zone. J Voice 1994;8:48–52.

[46] Chen X, Thibeault SL. Biocompatibility of a synthetic extracellular matrix on immortalized vocal fold fibroblasts in 3-D culture. Acta Biomater 2010;6:2940–8.

[47] Chen WYJ, Abatangelo G. Functions of hyaluronan in wound repair. Wound Repair Regen 1999;7:79–89.

[48] Park H, Karajanagi S, Wolak K, Aanestad J, Daheron L, Kobler JB, et al. Three-dimensional hydrogel model using adipose-derived stem cells for vocal fold augmentation. Tissue Eng Part A 2010;16:535–43.

[49] Thibeault SL, Klemuk SA, Chen X, Quinchia Johnson BH. In Vivo engineering of the vocal fold ECM with injectable HA hydrogels-late effects on tissue repair and biomechanics in a rabbit model. J Voice 2011;25:249–53.

[50] Omori K, Nakamura T, Kanemaru S, Kojima H, Magrufov A, Hiratsuka Y, et al. Cricoid regeneration using in situ tissue engineering in canine larynx for the treatment of subglottic stenosis. Ann Otol Rhinol Laryngol 2004;113:623–7.

[51] Omori K, Tada Y, Suzuki T, Nomoto Y, Matsuzuka T, Kobayashi K, et al. Clinical application of in situ tissue engineering using a scaffolding technique for reconstruction of the larynx and trachea. Ann Otol Rhinol Laryngol 2008;117:673–8.

[52] Ohno S, Hirano S, Tateya I, Kanemaru S, Umeda H, Suehiro A, et al. Atelocollagen sponge as a stem cell implantation scaffold for the treatment of scarred vocal folds. Ann Otol Rhinol Laryngol 2009;118:805–10.

[53] Yamshita M, Kanemaru S, Hirano S, Umeda H, Kitani Y, Omori K, Nakamura T IJ. Glottal reconstruction with a tissue engineering technique using polypropylene mesh: a canine experiment. Ann Otol Rhinol Laryngol 2010;119:110–7.

[54] Nomoto Y, Okano W, Imaizumi M, Tani A, Nomoto M, Omori K. Bioengineered prosthesis with allogenic heterotopic fibroblasts for cricoid regeneration. Laryngoscope 2012;122:805–9.

[55] Petroianu A, Barbosa AJ. Experimental reconstruction of anterior and circumferential defects of the cervical trachea. Laryngoscope 1993;103:1259–63.

[56] Behrend M, Klempnauer J. Tracheal reconstruction under tension: an experimental

study in sheep. Eur J Surg Oncol 2001;27:581–8.

[57] Krupa D, Baszkiewicz J, Kozubowski JA, Barcz A, Sobczak JW, Bilińiski A, et al. Effect of calcium-ion implantation on the corrosion resistance and biocompatibility of titanium. Biomaterials 2001;22:2139–51.

[58] Nakajima H, Okabe T. Titanium in dentistry: development and research in the U.S.A. Dent Mater J 1996;15:77–90.

[59] Schultz P, Vautier D, Chluba J, Marcellin L, Debry C. Survival analysis of rats implanted with porous titanium tracheal prosthesis. Ann Thorac Surg 2002;73:1747–51.

[60] Janssen LM, van Osch GJVM, Li JP, Kops N, de Groot K, Von den Hoff JW, et al. Tracheal reconstruction: mucosal survival on porous titanium. Arch Otolaryngol Head Neck Surg 2009;135:472–8.

[61] Seifalian A, Salacinski H, Hancock S. Polymer for use in conduits and medical devices. WO Pat WO/2005/070,998 2005.

[62] Ghanbari H, de Mel A, Seifalian AM. Cardiovascular application of polyhedral oligomeric silsesquioxane nanomaterials: a glimpse into prospective horizons. Int J Nanomedicine 2011;6:775–86.

[63] Kannan RY, Salacinski HJ, Butler PE, Seifalian AM. Polyhedral oligomeric silsesquioxane nanocomposites: the next generation material for biomedical applications. Acc Chem Res 2005;38:879–84.

[64] Ghanbari H, Cousins BG, Seifalian AM. A nanocage for nanomedicine: Polyhedral oligomeric silsesquioxane (POSS). Macromol Rapid Commun 2011;32:1032–46.

[65] Kannan RY, Salacinski HJ, Odlyha M, Butler PE, Seifalian AM. The degradative resistance of polyhedral oligomeric silsesquioxane nanocore integrated

polyurethanes: An in vitro study. Biomaterials 2006;27:1971–9.

[66] Salacinski HJ, Odlyha M, Hamilton G, Seifalian AM. Thermo-mechanical analysis of a compliant poly(carbonate-urea)urethane after exposure to hydrolytic, oxidative, peroxidative and biological solutions. Biomaterials 2002;23:2231–40.

[67] Salacinski HJ, Tai NR, Carson RJ, Edwards A, Hamilton G, Seifalian AM. In vitro stability of a novel compliant poly(carbonate-urea)urethane to oxidative and hydrolytic stress. J Biomed Mater Res 2002;59:207–18.

[68] Kidane AG, Burriesci G, Edirisinghe M, Ghanbari H, Bonhoeffer P, Seifalian AM. A novel nanocomposite polymer for development of synthetic heart valve leaflets. Acta Biomater 2009;5:2409–17.

[69] Kannan RY, Salacinski HJ, Ghanavi J, Narula A, Odlyha M, Peirovi H, et al. Silsesquioxane nanocomposites as tissue implants. Plast Reconstr Surg 2007;119:1653–62.

[70] De Mel A, Punshon G, Ramesh B, Sarkar S, Darbyshire A, Hamilton G, et al. In situ endothelialisation potential of a biofunctionalised nanocomposite biomaterial-based small diameter bypass graft. Biomed Mater Eng 2009;19:317–31.

[71] Chaloupka K, Motwani M, Seifalian AM. Development of a new lacrimal drainage conduit using POSS nanocomposite. Biotechnol Appl Biochem 2011;58:363–70.

[72] Baiguera S, Jungebluth P, Burns A, Mavilia C, Haag J, De Coppi P, et al. Tissue engineered human tracheas for in vivo implantation. Biomaterials 2010;31:8931–8.

[73] Quinchia Johnson B, Fox R, Chen X, Thibeault S. Tissue regeneration of the vocal fold using bone marrow mesenchymal stem cells and synthetic extracellular matrix injections in rats. Laryngoscope 2010;120:537–45.

[74] Thibeault SL, Klemuk SA, Chen X, Quinchia Johnson BH. In Vivo engineering of

the vocal fold ECM with injectable HA hydrogels-late effects on tissue repair and biomechanics in a rabbit model. J Voice 2011;25:249–53.

[75] Hahn MS, Teply BA, Stevens MM, Zeitels SM, Langer R. Collagen composite hydrogels for vocal fold lamina propria restoration. Biomaterials 2006;27:1104–9.

[76] Hiwatashi N, Hirano S, Mizuta M, Tateya I, Kanemaru S, Nakamura T, et al. Adipose-derived stem cells versus bone marrow-derived stem cells for vocal fold regeneration. Laryngoscope 2014;124:E461–9.

[77] Bartlett RS, Gaston JD, Yen TY, Ye S, Kendziorski C, Thibeault SL. Biomechanical Screening of Cell Therapies for Vocal Fold Scar. Tissue Eng Part A 2015;21:2437–47.

[78] Quinchia Johnson B, Fox R, Chen X, Thibeault S. Tissue regeneration of the vocal fold using bone marrow mesenchymal stem cells and synthetic extracellular matrix injections in rats. Laryngoscope 2010;120:537–45.

[79] Rock JR, Randell SH, Hogan BLM. Airway basal stem cells: a perspective on their roles in epithelial homeostasis and remodeling. Dis Model Mech 2010;3:545–56.

[80] Cho H-Y, Miller-DeGraff L, Park S, Lao H-C, Langenbach R, Kleeberger S. Role of Mucin 5ac in Murine Airways. FASEB J 2015;29:1014.1.

[81] Imaizumi M, Sato Y, Yang DT, Thibeault SL. In vitro epithelial differentiation of human induced pluripotent stem cells for vocal fold tissue engineering. Ann Otol Rhinol Laryngol 2013;122:737–47.

[82] Firth AL, Dargitz CT, Qualls SJ, Menon T, Wright R, Singer O, et al. Generation of multiciliated cells in functional airway epithelia from human induced pluripotent stem cells. Proc Natl Acad Sci U S A 2014;111:E1723–30.

[83] Ahmed M, Ghanbari H, Cousins BG, Hamilton G, Seifalian AM. Small calibre

polyhedral oligomeric silsesquioxane nanocomposite cardiovascular grafts: influence of porosity on the structure, haemocompatibility and mechanical properties. Acta Biomater 2011;7:3857–67.

[84] Mardini S, Salgado CJ, Kim Evans KF, Chen H-C. Reconstruction of the esophagus and voice. Plast Reconstr Surg 2010;126:471–85.

[85] Hansen JK, Thibeault SL. Current understanding and review of the literature: Vocal fold scarring. J Voice 2006;20:110–20.

[86] Rosen CA. Vocal fold scar: evaluation and treatment. Otolaryngol Clin North Am 2000;33:1081–6.

[87] Ahmad I, Kumar BN, Radford K, O'Connell J, Batch AJ. Surgical voice restoration following ablative surgery for laryngeal and hypopharyngeal carcinoma. J Laryngol Otol 2000;114:522–5.

[88] de Carpentier JP, Ryder WD, Saeed SR, Woolford TJ. Survival times of Provox valves. J Laryngol Otol 1996;110:37–42.

[89] Ringel RL, Kahane JC, Hillsamer PJ, Lee AS, Badylak SF. The application of tissue engineering procedures to repair the larynx. J Speech Lang Hear Res 2006;49:194–208.

[90] Sittel C. Larynx: implants and stents. GMS Curr Top Otorhinolaryngol Head Neck Surg 2009;8:1–6.

[91] Taylor SR, Gibbons DF. Effect of surface texture on the soft tissue response to polymer implants. J Biomed Mater Res 1983;17:205–27.

[92] Friedrich G. Titanium vocal fold medializing implant: Introducing a novel implant system for external vocal fold medialization. Ann Otol Rhinol Laryngol 1999;108:79–86.

[93] Benninger MS, Chota RL, Bryson PC, Drake RL. Custom implants for medialization laryngoplasty: a model that considers tissue compression. J Voice 2015;29:363–9.

[94] Preciado D, Zalzal G. Laryngeal and tracheal stents in children. Curr Opin Otolaryngol Head Neck Surg 2008;16:83–5.

[95] Ghanbari H, de Mel A, Seifalian AM. Cardiovascular application of polyhedral oligomeric silsesquioxane nanomaterials: a glimpse into prospective horizons. Int J Nanomedicine 2011;6:775–86.

[96] Ahmed M, Punshon G, Darbyshire A, Seifalian AM. Effects of sterilization treatments on bulk and surface properties of nanocomposite biomaterials. J Biomed Mater Res B Appl Biomater 2013;101:1182–90.

[97] Rice MA, Dodson BT, Arthur JA, Anseth KS. Cell-based therapies and tissue engineering. Otolaryngol Clin North Am 2005;38:199–214.

[98] Liu C, Xia Z, Czernuszka JT. Design and Development of Three-Dimensional Scaffolds for Tissue Engineering. Chem Eng Res Des 2007;85:1051–64.

[99] O'Brien FJ. Biomaterials & scaffolds for tissue engineering. Mater Today 2011;14:88–95.

[100] Conroy ER, Hennick TM, Awan SN, Hoffman MR, Smith BL, Jiang JJ. Effect of Variations to a Simulated System of Straw Phonation Therapy on Aerodynamic Parameters Using Excised Canine Larynges. J Voice 2014;28:1–6.

[101] Hoffman MR, Rieves AL, Budde AJ, Surender K, Zhang Y, Jiang JJ. Phonation Instability Flow in Excised Canine Larynges. J Voice 2012;26:280–4.

[102] Li L, Zhang Y, Calawerts W, Jiang JJ. Vibratory Dynamics of Four Types of Excised Larynx Phonations. J Voice 2015;8:1–7.

[103] Zhang Y, Huang N, Calawerts W, Li L, Maytag AL, Jiang JJ. Quantifying the

Subharmonic Mucosal Wave in Excised Larynges via Digital Kymography. J Voice 2016:Epub ahead of print.

[104] Titze IR. The physics of small-amplitude oscillation of the vocal folds. J Acoust Soc Am 1988;83:1536–52.

[105] Hunter EJ, Titze IR. Variations in intensity, fundamental frequency, and voicing for teachers in occupational versus nonoccupational settings. J Speech Lang Hear Res 2010;53:862–75.

[106] Zdrahala RJ, Zdrahala IJ. Biomedical applications of polyurethanes: a review of past promises, present realities, and a vibrant future. J Biomater Appl 1999;14:67–90.

[107] Agnihotri A, Garrett JT, Runt J, Siedlecki CA. Atomic force microscopy visualization of poly(urethane urea) microphase rearrangements under aqueous environment. J Biomater Sci Polym Ed 2006;17:227–38.

[108] Garrett JT, Siedlecki CA, Runt J. Microdomain morphology of poly(urethane urea) multiblock copolymers. Macromolecules 2001;34:7066–70.

[109] Xu L-C, Soman P, Runt J, Siedlecki CA. Characterization of surface microphase structures of poly(urethane urea) biomaterials by nanoscale indentation with AFM. J Biomater Sci Polym Ed 2007;18:353–68.

[110] Coury AJ, Slaikeu PC, Cahalan PT, Stokes KB, Hobot CM. Factors and Interactions Affecting the Performance of Polyurethane Elastomers in Medical Devices. J Biomater Appl 1988;3:130–79.

[111] Edwards A, Carson RJ, Szycher M, Bowald S. In vitro and in vivo biodurability of a compliant microporous vascular graft. J Biomater Appl 1998;13:23–45.

[112] Tang YW, Labow RS, Santerre JP. Enzyme-induced biodegradation of polycarbonate polyurethanes: dependence on hard-segment concentration. J Biomed

Mater Res 2001;56:516–28.

[113] Xu L-C, Siedlecki CA. Microphase separation structure influences protein interactions with poly(urethane urea) surfaces. J Biomed Mater Res A 2010;92:126–36.

[114] Ratner BD, Hoffman AS, Schoen FJ, Lemons JE. Biomaterials Science:: An Introduction to Materials in Medicine. Academic Press; 2001.

[115] Wang K, Zhou C, Hong Y, Zhang X. A review of protein adsorption on bioceramics. Interface Focus 2012;2:259–77.

[116] Rouahi M, Gallet O, Champion E, Dentzer J, Hardouin P, Anselme K. Influence of hydroxyapatite microstructure on human bone cell response. J Biomed Mater Res A 2006;78:222–35.

[117] Bracco G, Holst B. Surface science techniques. Springer Ser Surf Sci 2013;51.

[118] Von Fraunhofer JA. Adhesion and cohesion. Int J Dent 2012:8.

[119] Anderson L, Anderson NG. High resolution two-dimensional electrophoresis of human plasma proteins. Proc Natl Acad Sci U S A 1977;74:5421–5.

[120] Ge S, Kojio K, Takahara A, Kajiyama T. Bovine serum albumin adsorption onto immobilized organotrichlorosilane surface: influence of the phase separation on protein adsorption patterns. J Biomater Sci Polym Ed 1998;9:131–50.

[121] Yan Y, Yang H, Su Y, Qiao L. Albumin adsorption on CoCrMo alloy surfaces. Sci Rep 2015;5:18403.

[122] Boulos SP, Davis TA, Yang JA, Lohse SE, Alkilany AM, Holland LA, et al. Nanoparticle-protein interactions: a thermodynamic and kinetic study of the adsorption of bovine serum albumin to gold nanoparticle surfaces. Langmuir 2013;29:14984–96.

[123] Akkas T, Citak C, Sirkecioglu A, Güner FS. Which is more effective for protein adsorption: surface roughness, surface wettability or swelling? Case study of polyurethane films prepared from castor oil and poly(ethylene glycol). Polym Int 2013;62:1002–209.

[124] van Wachem PB, Beugeling T, Feijen J, Bantjes A, Detmers JP, van Aken WG. Interaction of cultured human endothelial cells with polymeric surfaces of different wettabilities. Biomaterials 1985;6:403–8.

[125] van Wachem PB, Hogt AH, Beugeling T, Feijen J, Bantjes A, Detmers JP, et al. Adhesion of cultured human endothelial cells onto methacrylate polymers with varying surface wettability and charge. Biomaterials 1987;8:323–8.

[126] Dewez JL, Lhoest JB, Detrait E, Berger V, Dupont-Gillain CC, Vincent LM, et al. Adhesion of mammalian cells to polymer surfaces: From physical chemistry of surfaces to selective adhesion on defined patterns. Biomaterials, vol. 19, 1998, p. 1441–5.

[127] Lee JH, Lee HB. A wettability gradient as a tool to study protein adsorption and cell adhesion on polymer surfaces. J Biomater Sci Polym Ed 1993;4:467–81.

[128] Zdrahala RJ, Zdrahala IJ. Biomedical applications of polyurethanes: a review of past promises, present realities, and a vibrant future. J Biomater Appl 1999;14:67–90.

[129] Xue L, Greisler HP. Biomaterials in the development and future of vascular grafts. J Vasc Surg 2003;37:472–80.

[130] Dehghani F, Annabi N. Engineering porous scaffolds using gas-based techniques. Curr Opin Biotechnol 2011;22:661–6.

[131] Lips PAM, Velthoen IW, Dijkstra PJ, Wessling M, Feijen J. Gas foaming of segmented poly(ester amide) films. Polymer (Guildf) 2005;46:9396–403.

[132] Zeng S, Liu L, Shi Y, Qiu J, Fang W, Rong M, et al. Characterization of Silk Fibroin/Chitosan 3D Porous Scaffold and In Vitro Cytology. PLoS One 2015;10:e0128658.

[133] Park HJ, Lee OJ, Lee MC, Moon BM, Ju HW, Lee J min, et al. Fabrication of 3D porous silk scaffolds by particulate (salt/sucrose) leaching for bone tissue reconstruction. Int J Biol Macromol 2015;78:215–23.

[134] Zargar R, Nourmohammadi J, Amoabediny G. Preparation, characterization, and silanization of 3D microporous PDMS structure with properly sized pores for endothelial cell culture. Biotechnol Appl Biochem 2015;63:190–9.

[135] Nayyer L, Birchall M, Seifalian AM, Jell G. Design and development of nanocomposite scaffolds for auricular reconstruction. Nanomedicine 2014;10:235–46.

[136] Devalia JL, Sapsford RJ, Wells CW, Richman P, Davies RJ. Culture and comparison of human bronchial and nasal epithelial cells in vitro. Respir Med 1990;84:303–12.

[137] Aydin HM, El Haj AJ, Pişkin E, Yang Y. Improving pore interconnectivity in polymeric scaffolds for tissue engineering. J Tissue Eng Regen Med 2009;3:470–6.

[138] Wilson CJ, Clegg RE, Leavesley DI, Pearcy MJ. Mediation of biomaterial-cell interactions by adsorbed proteins: a review. Tissue Eng 2005;11:1–18.

[139] Tamada Y, Ikada Y. Effect of Preadsorbed Proteins on Cell Adhesion to Polymer Surfaces. J Colloid Interface Sci 1993;155:334–9.

[140] Sánchez-Pérez JA, Gallardo-Moreno AM, González-Martín ML, Vadillo-Rodríguez V. BSA adsorption onto nanospheres: Influence of surface curvature as probed by electrophoretic light scattering and UV/vis spectroscopy. Appl Surf Sci 2015;353:1095–102.

[141] Khorasani MT, Moemenbellah S, Mirzadeh H, Sadatnia B. Effect of surface charge and hydrophobicity of polyurethanes and silicone rubbers on L929 cells response. Colloids Surf B Biointerfaces 2006;51:112–9.

[142] Latour RA. Biomaterials: protein surface interactions. Encycl Biomater Biomed Eng 2005:1–15.

[143] Soleas JP, Paz A, Marcus P, McGuigan A, Waddell TK. Engineering airway epithelium. J Biomed Biotechnol 2012;2012:982971–81.

[144] Daniel RA. Experimental Studies on the Repair of Wounds and Defects of the Trachea and Bronchi. CHEST J 1950;17:426–41.

[145] Wykoff TW. A preliminary report on segmental tracheal prosthetic replacement in dogs. Laryngoscope 1973;83:1072–7.

[146] Borrie J. Prosthetic tracheal replacement. Thorax 1970;60:829–35.

[147] Borrie J, Redshaw NR, Dobbinson TL. Silastic tracheal bifurcation prosthesis with subterminal dacron suture cuffs. J Thorac Cardiovasc Surg 1973;65:956–62.

[148] Demos NJ, Mitnick H, McCally D, Feinberg E, McKeon J, Timmes JJ. Tracheal regeneration in long-term survivors with silicone prosthesis. N Y State J Med 1973;73:2694–5.

[149] Cheng WF, Takagi H, Akutsu T. Prosthetic reconstruction of the trachea. Surgery 1969;65:462–9.

[150] Doss AE, Dunn SS, Kucera KA, Clamson LA, Zwischenberger JB. Tracheal Replacements: Part 2. Am Soc Artif Intern Organs 2007:631–9.

[151] Kocatürk S, Beriat GK, Doğan C. Spontaneous displacement of silastic prosthesis 10 years after type 1 thyroplasty: a case report. Kulak Burun Bogaz Ihtis Derg 19:268–71.

[152] Vrana NE, Dupret-Bories A, Schultz P, Debry C, Vautier D, Lavalle P. Titanium microbead-based porous implants: bead size controls cell response and host integration. Adv Healthc Mater 2014;3:79–87.

[153] Schultz P, Vautier D, Charpiot A, Lavalle P, Debry C. Development of tracheal prostheses made of porous titanium: a study on sheep. Eur Arch Otorhinolaryngol 2007;264:433–8.

[154] Dupret-Bories A, Schultz P, Vrana NE, Lavalle P, Vautier D, Debry C. Development of surgical protocol for implantation of tracheal prostheses in sheep. J Rehabil Res Dev 2011;48:851–64.

[155] Janssen LM, Van Osch GJVM, Li JP, Kops N, De Groot K, Feenstra L, et al. Laryngotracheal reconstruction with porous titanium in rabbits: Are vascular carriers and mucosal grafts really necessary? J Tissue Eng Regen Med 2010;4:395–403.

[156] Crowley C, Birchall M, Seifalian AM. Trachea transplantation: from laboratory to patient. J Tissue Eng Regen Med 2015;9:357–67.

[157] Sharpe JR, Sammons RL, Marquis PM. Effect of pH on protein adsorption to hydroxyapatite and tricalcium phosphate ceramics. Biomaterials 1997;18:471–6.

[158] Van Citters KM, Hoffman BD, Massiera G, Crocker JC. The role of F-actin and myosin in epithelial cell rheology. Biophys J 2006;91:3946–56.

[159] Laurent VM, Fodil R, Cañadas P, Féréol S, Louis B, Planus E, et al. Partitioning of cortical and deep cytoskeleton responses from transient magnetic bead twisting. Ann Biomed Eng 2003;31:1263–78.

[160] Rock JR, Onaitis MW, Rawlins EL, Lu Y, Clark CP, Xue Y, et al. Basal cells as stem cells of the mouse trachea and human airway epithelium. Proc Natl Acad Sci U S A 2009;106:12771–5.

[161] Schlüter C, Duchrow M, Wohlenberg C, Becker MH, Key G, Flad HD, et al. The cell proliferation-associated antigen of antibody Ki-67: a very large, ubiquitous nuclear protein with numerous repeated elements, representing a new kind of cell cycle-maintaining proteins. J Cell Biol 1993;123:513–22.

[162] Scholzen T, Gerdes J. The Ki-67 protein: from the known and the unknown. J Cell Physiol 2000;182:311–22.

[163] Katsumoto T, Mitsushima A, Kurimura T. The role of the vimentin intermediate filaments in rat 3Y1 cells elucidated by immunoelectron microscopy and computer-graphic reconstruction. Biol Cell 1990;68:139–46.

[164] Kasper M, Stosiek P. The expression of vimentin in epithelial cells from human nasal mucosa. Eur Arch Oto-Rhino-Laryngology 1990;248:53–6.

[165] Goldman RD, Khuon S, Chou YH, Opal P, Steinert PM. The function of intermediate filaments in cell shape and cytoskeletal integrity. J Cell Biol 1996;134:971–83.

[166] Lin H, Li H, Cho H-J, Bian S, Roh H-J, Lee M-K, et al. Air-liquid interface (ALI) culture of human bronchial epithelial cell monolayers as anin vitro model for airway drug transport studies. J Pharm Sci 2007;96:341–50.

[167] Ghio AJ, Dailey LA, Soukup JM, Stonehuerner J, Richards JH, Devlin RB. Growth of human bronchial epithelial cells at an air-liquid interface alters the response to particle exposure. Part Fibre Toxicol 2013;10:25.

[168] Bals R, Beisswenger C, Blouquit S, Chinet T. Isolation and air-liquid interface culture of human large airway and bronchiolar epithelial cells. J Cyst Fibros 2004;3 Suppl 2:49–51.

[169] Müller L, Brighton LE, Carson JL, Fischer W a, Jaspers I. Culturing of human nasal

epithelial cells at the air liquid interface. J Vis Exp 2013:1–7.

[170] Hartsock A, Nelson WJ. Adherens and tight junctions: structure, function and connections to the actin cytoskeleton. Biochim Biophys Acta 2008;1778:660–9.

[171] Balda MS, Matter K. Tight junctions at a glance. J Cell Sci 2008;121:3677–82.

[172] Firth a. L, Dargitz CT, Qualls SJ, Menon T, Wright R, Singer O, et al. Generation of multiciliated cells in functional airway epithelia from human induced pluripotent stem cells. Proc Natl Acad Sci 2014;111:E1723–30.

[173] Piperno G, LeDizet M, Chang XJ. Microtubules containing acetylated alpha-tubulin in mammalian cells in culture. J Cell Biol 1987;104:289–302.

[174] van Roy F, Berx G. The cell-cell adhesion molecule E-cadherin. Cell Mol Life Sci 2008;65:3756–88.

[175] Baum B, Georgiou M. Dynamics of adherens junctions in epithelial establishment, maintenance, and remodeling. J Cell Biol 2011;192:907–17.

[176] Fristrom D. The cellular basis of epithelial morphogenesis. A review. Tissue Cell 1988;20:645–90.

[177] Soleas JP, Waddell TK, McGuigan AP. Topographically grooved gel inserts for aligning epithelial cells during air–liquid-interface culture. Biomater Sci 2015;3:121–33.

[178] Paz AC, Soleas J, Poon JCH, Trieu D, Waddell TK, McGuigan AP. Challenges and opportunities for tissue-engineering polarized epithelium. Tissue Eng Part B Rev 2014;20:56–72.

[179] Buisine M-P, Devisme L, Copin M-C, Durand-Réville M, Gosselin B, Aubert J-P, et al. Developmental Mucin Gene Expression in the Human Respiratory Tract. Am J Respir Cell Mol Biol 1999;20:209–18.

[180] Rose MC, Voynow JA. Respiratory tract mucin genes and mucin glycoproteins in health and disease. Physiol Rev 2006;86:245–78.

[181] Seregni E, Botti C, Massaron S, Lombardo C, Capobianco A, Bogni A, et al. Structure, function and gene expression of epithelial mucins. Tumori 1997;83:625–32.

[182] Vacanti CA. The history of tissue engineering. J Cell Mol Med 2006;10:569–76.

[183] Brown PT, Handorf AM, Jeon WB, Li W-J. Stem cell-based tissue engineering approaches for musculoskeletal regeneration. Curr Pharm Des 2013;19:3429–45.

[184] Vishnubalaji R, Al-Nbaheen M, Kadalmani B, Aldahmash A, Ramesh T. Comparative investigation of the differentiation capability of bone-marrow- and adipose-derived mesenchymal stem cells by qualitative and quantitative analysis. Cell Tissue Res 2012;347:419–27.

[185] Caplan AI. Adult Mesenchymal Stem Cells for Tissue Engineering Versus Regenerative Medicine. J Cell Physiol 2007;213:341–7.

[186] Hanson SE, Kim J, Johnson BHQ, Bradley B, Breunig MJ, Hematti P, et al. Characterization of mesenchymal stem cells from human vocal fold fibroblasts. Laryngoscope 2010;120:546–51.

[187] Johnson BQ, Fox R, Chen X, Thibeault S. Tissue regeneration of the vocal fold using bone marrow mesenchymal stem cells and synthetic extracellular matrix injections in rats. Laryngoscope 2010;120:537–45.

[188] Kim Y-M, Yi T, Choi J-S, Lee S, Jang YH, Kim C-H, et al. Bone marrow-derived clonal mesenchymal stem cells as a source of cell therapy for promoting vocal fold wound healing. Ann Otol Rhinol Laryngol 2013;122:121–30.

[189] Oseni AO, Butler PE, Seifalian AM. The application of POSS nanostructures in

cartilage tissue engineering: the chondrocyte response to nanoscale geometry. J Tissue Eng Regen Med 2013:3–4.

[190] Guasti L, Vagaska B, Bulstrode NW, Seifalian AM, Ferretti P. Chondrogenic differentiation of adipose tissue-derived stem cells within nanocaged POSS-PCU scaffolds: a new tool for nanomedicine. Nanomedicine 2014;10:279–89.

[191] Stubendorff JJ, Lammentausta E, Struglics A, Lindberg L, Heinegård D, Dahlberg LE. Is cartilage sGAG content related to early changes in cartilage disease? Implications for interpretation of dGEMRIC. Osteoarthritis Cartilage 2012;20:396–404.

[192] Bean AC, Tuan RS. Fiber diameter and seeding density influence chondrogenic differentiation of mesenchymal stem cells seeded on electrospun poly(ε-caprolactone) scaffolds. Biomed Mater 2015;10:015018.

[193] Chase LCG, Rao MSG, Vemuri MS. Mesenchymal Stem Cell Assays and Applications Methods in Molecular Biology. vol. 698. Humana Press; 2011.

[194] Campbell DD, Pei M. Surface markers for chondrogenic determination: a highlight of synovium-derived stem cells. Cells 2012;1:1107–20.

[195] Hamada T, Sakai T, Hiraiwa H, Nakashima M, Ono Y, Mitsuyama H, et al. Surface markers and gene expression to characterize the differentiation of monolayer expanded human articular chondrocytes. Nagoya J Med Sci 2013;75:101–11.

[196] Xu J, Wang W, Ludeman M, Cheng K, Hayami T, Lotz JC, et al. Chondrogenic differentiation of human mesenchymal stem cells in three-dimensional alginate gels. Tissue Eng Part A 2008;14:667–80.

[197] Mehr NG, Li X, Chen G, Favis BD, Hoemann CD. Pore size and LbL chitosan coating influence mesenchymal stem cell in vitro fibrosis and biomineralization in 3D

porous poly(epsilon-caprolactone) scaffolds. J Biomed Mater Res A 2015;103:2449–59.

[198] Zhang Y, Fan W, Ma Z, Wu C, Fang W, Liu G, et al. The effects of pore architecture in silk fibroin scaffolds on the growth and differentiation of mesenchymal stem cells expressing BMP7. Acta Biomater 2010;6:3021–8.

[199] Kim H-J, Lee J-H, Im G-I. Chondrogenesis using mesenchymal stem cells and PCL scaffolds. J Biomed Mater Res A 2010;92:659–66.

[200] Cheng GZ, Folch E, Brik R, Gangadharan S, Mallur P, Wilson JH, et al. Three-dimensional Modeled T-tube Design and Insertion in a Patient With Tracheal Dehiscence. Chest 2015;148:e106–8.

[201] Al Kadah B, Papaspyrou G, Schneider M, Schick B. Novel modification of voice prosthesis. Eur Arch Otorhinolaryngol 2016;273:697–702.

[202] Noirez L, Musani AI, Laroumagne S, Astoul P, Dutau H. Montgomery T-tube Migration: A Rare and Life-threatening Complication. J Bronchology Interv Pulmonol 2015;22:e14–5.

[203] Young VN, Zullo TG, Rosen CA. Analysis of laryngeal framework surgery: 10-year follow-up to a national survey. Laryngoscope 2010;120:1602–8.

[204] Ahmed M, Hamilton G, Seifalian AM. Viscoelastic behaviour of a small calibre vascular graft made from a POSS-nanocomposite. Conf Proc . Annu Int Conf IEEE Eng Med Biol Soc IEEE Eng Med Biol Soc Annu Conf 2010;2010:251–4.

[205] Pillsbury TE, Kothera CS, Wereley NM. Effect of bladder wall thickness on miniature pneumatic artificial muscle performance. Bioinspir Biomim 2015;10:055006.

[206] Won-Hyeong Park, Tae-Heon Yang, Yongjae Yoo, Seungmoon Choi, Sang-Youn

Kim. Flexible and bendable vibrotactile actuator using electro-conductive polyurethane. 2015 IEEE World Haptics Conf., IEEE; 2015, p. 165–70.

[207] Feng B, Jinkang Z, Zhen W, Jianxi L, Jiang C, Jian L, et al. The effect of pore size on tissue ingrowth and neovascularization in porous bioceramics of controlled architecture in vivo. Biomed Mater 2011;6:015007.

[208] Bigham WJ, Stanley P, Cahill JM, Curran RW, Perry AC. Fibrovascular ingrowth in porous ocular implants: the effect of material composition, porosity, growth factors, and coatings. Ophthal Plast Reconstr Surg 1999;15:317–25.

[209] Solouk A, Cousins BG, Mirahmadi F, Mirzadeh H, Nadoushan MRJ, Shokrgozar MA, et al. Biomimetic modified clinical-grade POSS-PCU nanocomposite polymer for bypass graft applications: a preliminary assessment of endothelial cell adhesion and haemocompatibility. Mater Sci Eng C Mater Biol Appl 2015;46:400–8.

Appendix A

The analyses of POSS leachate by ethanol rinse of casted and microporous ($NaHCO_3$) POSS-PCU materials (BLL Reference : 09-0038-15 and 09-0039-15).

Certificate of Analysis

University College London
Centre for Nanotechnology & Regenerative Medicine
Division of Surgery & Interventional Science
Royal Free London NHS Foundation Trust Hospital
9th Floor, Room 304
Pond Street
London NW3 2QG

Report Ref: 1509-0019-01
Date issued: 29 October 2015
Job Ref: 1509-0019

For the attention of Dr Brian Cousins

Analysis of Polymer based sample extracts by GCMS and ICPOES

Samples Received: 2 September 2015

Analysis Started: 6 September 2015 Analysis Completed: 7 October 2015

BLL Reference	Sample Reference
09-0036-15	1. POSS enhanced ethylene diethylene glycol succinate solid elastomer
09-0037-15	2. POSS enhanced ethylene diethylene glycol succinate foam elastomer
09-0038-15	3. POSS enhanced polycarbonate (urea) urethane solid polymer
09-0039-15*	4. POSS enhanced polycarbonate (urea) urethane porous polymer
09-0040-15	5. POSS (Polyoligomeric silsesquioxane) powder

*Sample was dried between tissue paper and left to air dry before weighing.

Approximately 1g of samples 1 to 4 was weighed into a vial to which 5.0mL of absolute ethanol was added. After 45 seconds (samples 1 and 2) or 5 minutes (samples 3 and 4) the test item was removed from the solvent and placed in another vial.
A 1000ppm solution of sample 5 in absolute ethanol was also prepared.
The ethanol extracts/solutions were then tested for volatile and semi-volatile components by GCMS and for metals by ICPMS.

GCMS analysis

10µg of d8 toluene was added to 1.0mL of each of the ethanolic solutions which were then analysed using the following conditions:

Instrument: Varian 2200 GCMSMS (BL65D)
Column: CP-select 624 60m x 0.32mm 1.8µm film
Carrier: Helium 1.0mL/min
Temp program: 40°C (5min) to 250°C at 10°C/min
Injection: 1µL in split mode
Quantitation ions (m/z): RIC

There were no responses other than ethanol and the internal standard observed in the GCMS analysis.

ICPOES analysis

1.0mL of ethanol (blank) and all of the remaining ethanolic solution for samples 1 to 4 (nominally 4mL) was quantitatively transferred to a platinum crucible and evaporated to dryness. 0.1mL of sample 5 solution was similarly treated.

1g of lithium borate was added to each of the residues which were then fused at 1000°C for 15 minutes. After cooling the melts were transferred to PTFE beakers using 20mL of conc nitric acid, 80mL of purified water including 1.0mL of 100ppm Yttrium internal standard was also added. Once dissolved solutions were transferred to polypropylene tubes for ICP analysis. Extractable silicon results, corrected for a process blank (nominally equivalent to 65µg/g), are tabulated below.

BLL Reference	Silicon
09-0036-15	43µg/g
09-003715	65µg/g
09-0038-15	<10µg/g
09-0039-15	12µg/g
09-0040-15	13.4, 13.3%w/w*

*This is effectively an assay but the method used is probably not best suited for this level of silicon.

Analysed in accordance with Butterworth Laboratories Limited in house SOPs IM65D and IM66D.

Michael North
Project Manager

David Bell
Head of Projects
Issued for and on behalf of
Butterworth Laboratories Ltd

Encl. Raw Data Pack

Appendix B

Effect of sterilisation on HBEC's viability and proliferation

HBECs were seeded and grown on 30%, 50% and M70% $NaHCO_3$ microporous POSS-PCU using autoclave as a sterilisation technique. The results showed HBECs did not maintain their viability on material. In addition, the viability decreased over time course and were not significantly different from blank on day 11-14 ($P > 0.05$). This result supported the use of ethanol cleanse in *in vitro* culture experiments.

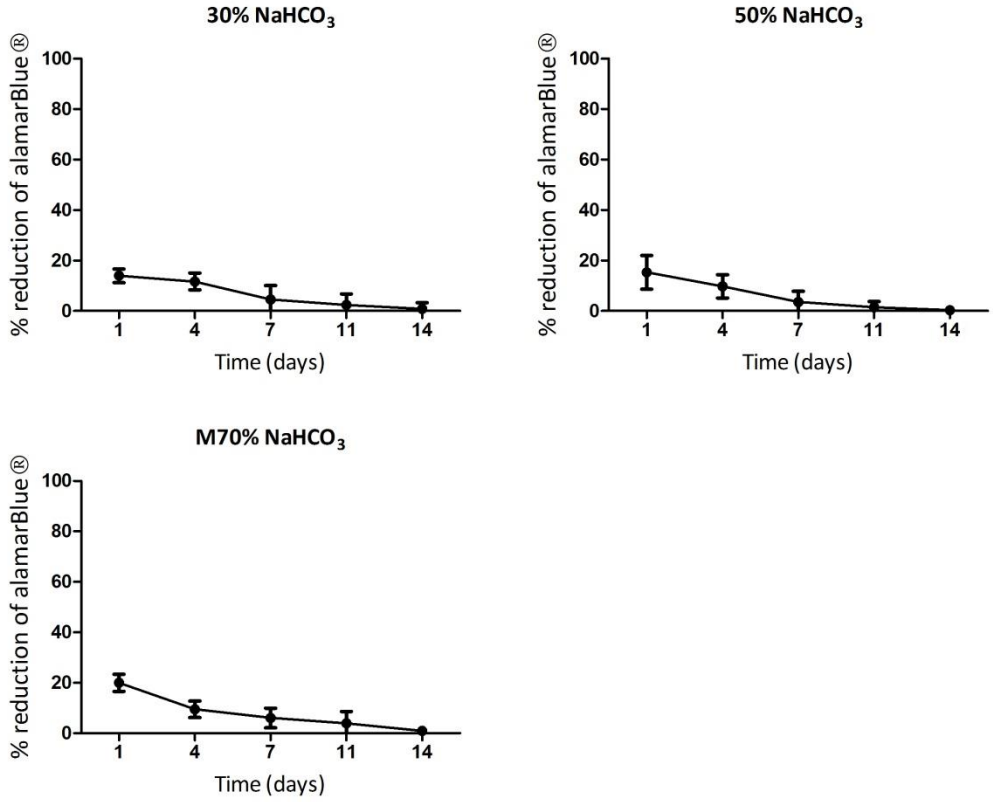

Appendix C

Initial seeding density is crucial for observing the cell growth. Selecting the right density can help determine the optimal level of growth which is comparable between samples. The cell viability assay (alamarBlue®) was employed to determine in this step with different initial seeding densities of HBECs on 24-well TCP plate (5×10^3, 1×10^4, 5×10^4, and 1×10^5 cells per well).

The initial seeding of 1×10^5 cells/well was probably too high because the cell grew fast from day 1 -11 and drop from day 11-14 which might be the death phase of the cell population. The initial seeding of 5×10^4 cells/well exhibited the pattern covered much full range of growth phase during day 1 – 14. In addition, at day 14 the growth reached about the maximum and plateau out of growth level but not entered a dead phase. However, the initial seeding of 5×10^3 and 1×10^4 cells/well demonstrated the early growth phase with slow acceleration and did not reach the maximum point after 14 days. In conclusion, the 5×10^4 cells/well presented the optimal pattern of cell growth, reached the maximum growth at the end of observing time and had distinctive alamarBlue® measurement at each time points. This cell concentration was chosen for cell growth of *in vitro* experiment for both HBEC and BM-MSC on POSS-PCU materials.

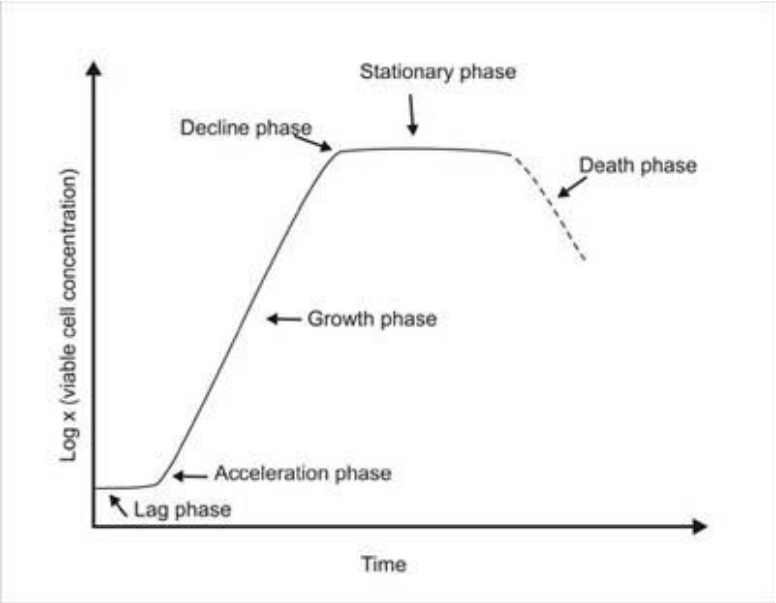

Figure 1 Typical cell growth pattern, illustrating lag phase, growth phase, stationary phase and death phase.

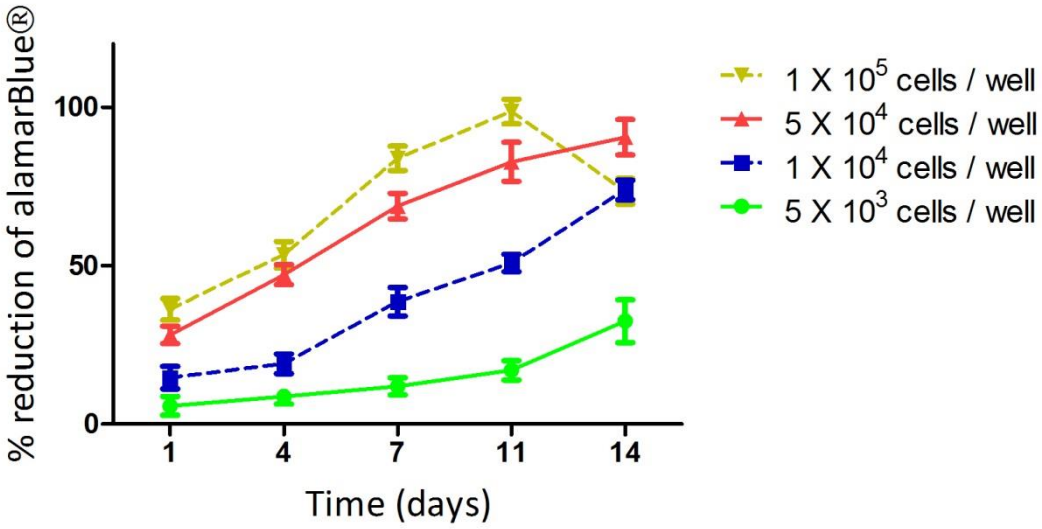

Figure 2 Growth pattern of HBECs over 14 days on TCP with different initial seeding densities.

Publications

Crowley C, Klanrit P, Butler CR, Varanou A, Platé M, Hynds RE, Chambers RC, Seifalian AM, Birchall MA, Janes SM, 2016. Surface modification of a POSS-nanocomposite material to enhance cellular integration of a synthetic bioscaffold. *Biomaterials*, 83, pp.283–293.

Teoh, G.Z., Klanrit P, Kasimatis M, Seifalian AM, 2015. Role of nanotechnology in development of artificial organs. *Minerva Medica*, 105(1)(OCTOBER 2014), pp.17–33.

Klanrit P, Loh W, Darbyshire A, Cousins BG, Birchall M, Seifalian AM, 2013. Development of 3D tissue engineered larynx scaffold using POSS-nanocomposite materials. *Current Opinion in Biotechnology*. 24: S47-S47.

Conferences

Klanrit P, Loh W, Darbyshire A, Cousins BG, Birchall M, Seifalian AM, 2014. Development of 3D tissue engineered larynx scaffold using POSS-nanocomposite materials. Health Challenge Thailand Conference, London, UK

Klanrit P, Loh W, Darbyshire A, Cousins BG, Birchall M, Seifalian AM, 2013. Development of 3D tissue engineered larynx scaffold using POSS-nanocomposite materials. European Biotechnology Conference, Bratislava, Slovak Republic

Klanrit P, Loh W, Darbyshire A, Cousins BG, Birchall M, Seifalian AM, 2012. Development of 3D tissue engineered larynx scaffold using POSS-nanocomposite materials. The UK Society for Biomaterials Conference, Nottingham, UK